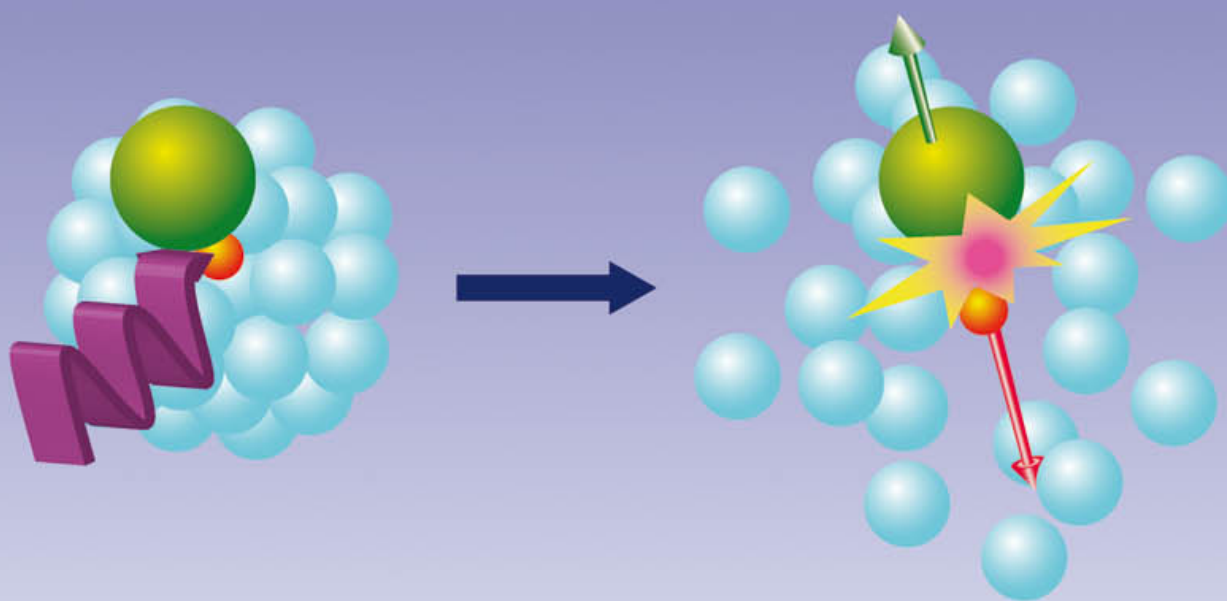


MOLECULAR DYNAMICS IN FREE CLUSTERS AND NANOPARTICLES STUDIED IN MOLECULAR BEAMS

Michal Fárník





**INSTITUTE OF
CHEMICAL TECHNOLOGY
PRAGUE**

J. Heyrovský Institute of Physical Chemistry, v.v.i.
Academy of Sciences of the Czech Republic

**MOLECULAR DYNAMICS
IN FREE CLUSTERS AND NANOPARTICLES
STUDIED IN MOLECULAR BEAMS**

DSc. Thesis in Physical Chemistry
by Michal Fárník

ICT Prague Press
2011

Reviewer: Prof. RNDr. Petr Klán, Ph.D.
RNDr. Zdenek Havlas, DrSc.

First published in 2011

Published by the Institute of Chemical Technology, Prague,

ICT Prague Press
Technická 5
166 28 Praha 6
Czech Republic

Printed in the Czech Republic

ISBN 978-80-7080-781-1

Copyright © 2011 by Michal Fárník

*Laß die Moleküle rasen
was sie auch zusammenknobeln!
Laß das Tüfteln, laß das Hobeln
heilig halte die Ekstasen!*

Christian Morgenstern: *Alle Galgenlieder*
Insel Verlag Wiesbaden, 1972

To my family

Acknowledgements

The work presented in this Thesis would not be possible without the contribution support and encouragement of many colleagues and friends, whom I wish to express my sincere thanks. Where do I start? Perhaps five years ago in 2005, when I was donated the generous gift of our present experimental apparatus by Udo Buck. I was returning from several long term –altogether ten years– postdoctoral stays abroad back to the J. Heyrovský Institute of Physical Chemistry in Prague, and Udo presented me with one of his molecular beam machines from Göttingen. This really helped me to have a head start with my own research in Prague. Indeed, I am also grateful to Udo for all I have learned from him during the three years, when I have worked in his laboratory at the Max-Planck Institute in Göttingen as a postdoc, and this learning still continues during our mutual visits till today –and I learn a lot not only in terms of science.

Speaking about postdoctoral stays, I should also mention also all my other mentors, whom I have worked with during the ten years abroad: J. Peter Toennies at the Max-Planck Institute in Göttingen, David J. Nesbitt at the Joint Institute for Laboratory Astrophysics in Boulder, Colorado, and Martin A. Suhm at the Institut für Physikalische Chemie, GA Universität in Göttingen. I have a great respect for all of them as leading scientists in their respective fields and the interaction with them have shaped my own scientific career.

My scientific work actually started in the laboratory of Zdeněk Herman at the J. Heyrovský Institute of Physical Chemistry, which I have joined already as a beginning student at the Faculty of Mathematics and Physics of the Charles University. Zdeněk was an example for me: I respected his great scientific achievements as well as admired his many other talents and

his personal attitude to me as a student. And not only that, he has also initiated my recent return from abroad to Prague, and has strongly supported me during the transition period. I probably would have never returned to the J. Heyrovský Institute and continued my scientific career here without Zdeněk's contribution and support. I am very grateful to him for everything he has done for me.

When I landed in Prague with the Herculean task to assemble together all alone a huge molecular beam machine, which I brought from Göttingen all in pieces, I would probably soon get insane without the help of the workshop staff under the leadership of Lojza Kulhánek. They helped me to arrange my new lab, to lift the hundreds of kilograms of stainless steel when assembling the machine, etc.. And also the financial, moral and other support of the people in the J. Heyrovský Institute management at that time has to be greatly acknowledged.

I was very lucky when my first postdoc Viktoriya Poterya joined me in the lab. After almost a year of struggling alone with the machine I was accompanied by the most reliable, responsible, and hard working person I could imagine, and she was highly motivated to work on the project. Thanks to her contribution we put the rest of the demanding setup together and started the first measurements in another couple of months. In the five years, Viktoriya became an indispensable member of our group and I am really grateful to her for everything she is doing for our lab and the group.

My return actually seemed to be paved by good luck. Petr Slavíček returned from his stay in the USA soon after my arrival to Prague, and he started to work at the Institute of Chemical Technology. Since he was doing the theoretical calculations interpreting the results of our experiments already in Göttingen, we have immediately started to collaborate again. Peter's extensive knowledge and chemical intuition and –for a theoretician– an exceptional understanding of the experiment helps us immensely to interpret our results and design the new experiments. My gratitude belongs to him also for his contribution to the present results. Recently, in the last two years, our group has grown, and I would like to thank all the colleagues for making our lab a place, where it is a pleasure and fun (most of the time) to work, and for all their contributions to the present work. I am grateful

in particular to Ondřej Votava, Juraj Fedor, Andriy Pysanenko and the students, who worked on their diploma thesis here or passed through our lab on various occasions. Finally, since this thesis also contains part of my work still from Göttingen the contribution of Hendrik Nahler, the PhD student whom I have worked with on this project, should not be omitted.

Last but not least I would have never managed to do all this work without the cordial and comforting support of my family. I am very grateful to Monika, Tom and Karolínka for everything they are doing for me every day.¹

¹All this work would be also impossible without a financial support. At this point I should mention the Alexander von Humboldt Foundation, which supported most of my previous research stays in Germany and more recently helped to support our cooperation with Udo Buck in Göttingen. My return to the J. Heyrovský Institute was facilitated by the award of the J. E. Purkyně Fellowship of the Academy of Sciences of the Czech Republic, which supported my first five years here. Besides, several grants supported our research within the past five years, namely: project No.: 203/06/1290 and 203-09-0422 of the Grant Agency of the Czech Republic, project No.: KAN 400400651 of the Grant Agency of the ASCR, and European project No.: 235414, an Intra-European Fellowship of J. Fedor in the framework of FP7 Marie Currie Actions.

Abstract

In this Thesis I have summarized our recent research of free clusters and nanoparticles generated by the molecular beam technique in vacuum and investigated by various laser spectroscopic and mass spectrometric methods. The clusters and nanoparticles are of great fundamental interest, since they can provide the link between the individual molecules and the bulk material composed of these molecules by investigating physical and chemical properties as a function of cluster size, ultimately resulting in understanding the transition from the molecule, to the bulk. The work in the field of clusters and nanoparticles in general is relevant to solid state, molecular, atomic and even nuclear physics and chemistry and has practical implications for many areas, e.g., nanoelectronics, surface science, catalysis, environmental studies, biology or even medicine. Besides, the free molecular clusters generated in molecular beams in vacuum poses unique properties, which promote their use for investigations of molecules and processes in complex environments at a detailed molecular level. In this Thesis four main research topics are presented: 1) Photofragmentation in model systems, i.e. hydrogen halides in rare gas clusters; 2) Clusters and nanoparticles of atmospheric relevance; 3) Biologically relevant processes studied in clusters; 4) Novel molecules of rare gas atoms generated in clusters.

The Thesis is based on sixteen recent publications in peer-reviewed international journals. My independent original research started in 2005, when I moved a unique molecular beam experimental apparatus from the Max-Planck Institute in Göttingen to the J. Heyrovský Institute of Physical Chemistry in Prague and founded a new laboratory and experimental *group of Molecular and Cluster Dynamics*, and started a new area of research in the Czech Republic. The focus is, therefore, on the original research ac-

completed within the last 5 years in our laboratory. However, the present research stemmed from my previous work in Göttingen, therefore, some of this earlier work is outlined in the Thesis as well.

First, to open the Thesis, a brief history of molecular beams and cluster research, and the general motivation for our particular studies is outlined in the *Introduction*. The second chapter *Experiment* is devoted to the description of the apparatus, and the experimental methods are briefly overviewed. The experiment is quite complex and includes several unique and up-to-date methods. The molecular beam techniques are used to generate beams of free molecules, clusters and nanoparticles of various sizes in vacuum. The species in the beams are interrogated by scattering with atoms from a secondary molecular beam, or by electron ionization, or by interactions with UV-photons causing photodissociation and/or photoionization. Various mass-spectrometric methods (quadrupole and time-of-flight mass spectrometers) and energy distribution measurements are implemented to analyze the ongoing processes. Non-trivial laser techniques are employed to generate tunable UV laser beams of high-intensities.

The chapter *Results* of the Thesis outlines the general outcome of our studies which is organized in four sections. The first one *Photodissociation of hydrogen halides in rare gas clusters* summarizes some of our earlier results on the photodissociation of various hydrogen halides (HX, X=Cl,Br,I) in rare gas (Ar and Ne) clusters. These systems provided a detailed understanding of the photodissociation in the cluster environments. Important phenomena, such as *caging* and *cage exit* of the dissociated fragments, have been observed. These model systems facilitated the understanding of the more complicated species, such as the hydrogen halides in water clusters or functional units of biomolecules in clusters, which are discussed in the following sections.

The section *Atmospherically relevant clusters* summarizes our results on photochemistry of hydrogen halides on ice nanoparticles and pure water clusters photodissociation. Such species play a key role in the ozone depletion process in atmospheric chemistry. Our studies brought the first experimental evidence for the neutral hydronium radical H_3O , which is generated in $\text{HX}\cdot(\text{H}_2\text{O})_n$ species upon UV excitation. The way to the generation of the H_3O radical leads via the acidic dissociation in the ground state to the

zwitterionic species $X^- \cdot H_3O^+ \cdot (H_2O)_{n-1}$. Possible consequences for the atmospheric chemistry models are briefly discussed. The hydronium radical seems to play a central role in the photochemistry of the aqueous systems, which is essential not only to the atmospheric chemistry but also to the other important areas such as the radiation damage of biomolecules.

The section *Biomolecules in clusters* is related to the important issue of photostability of biomolecules. Clusters of small heteroaromatic ring molecules (pyrrole, imidazole, pyrazole) were investigated, which constitute the essential functional blocks and the UV active chromophores in the larger biomolecules. The solvent molecules have a profound effect on the photochemistry of these molecules. Various mechanisms of the solvent induced photostability were revealed, such as closing the dissociation channels by electronic interactions, or stabilization by hydrogen transfer in the excited states.

In the section *Novel rare gas molecules*, the hydride compounds of the type H-Xe-Y (Y is an electronegative atom or group) containing rare gas atom are investigated. These species are stable molecules with partly ionic and partly covalent bonding character. In our experiments they are produced free in the gas phase by photodissociation of the precursor molecules HY on large rare gas Xe-clusters.

The Thesis close with a chapter summarizing some of the general results of our research, and especially with a brief overview of some of the future experiments which were opened for investigation by the introduction of this vital new field of research in our laboratory.

Fárník, M.: Molecular dynamics in free clusters and nanoparticles studied in molecular beams; VŠCHT Praha: Praha, 2011. ISBN 978-80-7080-781-1.
Kniha je k dispozici v elektronické formě na stránkách vydavatelství VŠCHT Praha, <http://vydavatelstvi.vscht.cz>, E-mail: vydavatelstvi@vscht.cz, Tel.: (+420) 220 443 211

Contents

1	Preface	3
2	Introduction	5
2.1	Molecular beams and clusters	5
2.2	Clusters and their relevance	8
2.2.1	Atmospheric chemistry	12
2.2.2	Biomolecules in clusters	15
2.2.3	Clusters as nano-cryo-reactors	17
3	Experiment	21
3.1	General description	21
3.2	Expansions and beams	24
3.3	Scattering, size selection	31
3.4	Photodissociation	35
3.4.1	Willey-McLaren Time-of-Flight Spectrometer	38
3.4.2	Photodissociation of a molecule in cluster	40
3.5	Laser system	45
4	Results	48
4.1	HX in rare gas clusters	48
4.1.1	Photodissociation of hydrogen halides on argon clusters	49
4.1.2	Photodissociation of HBr and HCl in neon clusters . .	53
4.2	Atmospherically relevant clusters	56
4.2.1	Hydrogen halides on water clusters	56
4.2.2	Pure water clusters	62
4.3	Biomolecules in clusters	65

<i>CONTENTS</i>	<i>CONTENTS</i>
4.4 Novel rare gas molecules	73
5 Conclusions and outlook	78
6 Bibliography	85
A List of abbreviations	95
B Thesis publications	96

Chapter 1

Preface

To open this Thesis, the molecular beam research in the context of our local physical-chemical community will be briefly outlined and our own cluster research will be introduced. The molecular beams were introduced in the Czech Republic by Z. Herman in the late 1960s at the J. Heyrovský Institute of Physical Chemistry, ASCR. His apparatus EVAII was one of the first, and at the beginning of 1970s one of the few, in the world for studying the ion molecular reactions in crossed-beams. My first personal encounter with the molecular beam technique and molecular dynamics was in the laboratory of Z. Herman during my diploma and subsequently Ph.D. work (1987-95). Then I was introduced to the clusters -namely large superfluid helium nanodroplets- as a postdoc in the laboratory of J.P. Toennies at the Max-Planck-Institut für Dynamik und Selbstorganisation, Göttingen, Germany (1995-98). I learned some laser spectroscopy in the laboratory of D.J. Nesbitt at the Joint Institute of Laboratory Astrophysics, Boulder, Colorado (1998-2001), where I was studying also spectroscopy of small molecular clusters. The work covered in the present Thesis started when I came for my third postdoc position to the MPI in Göttingen, to the group of U. Buck (2002-2004). Here one of the projects I was involved in, was the study of photodissociation in cluster environments – namely hydrogen halide molecules in rare gas clusters – with the present molecular beam apparatus.

In 2005 my own project started by moving the cluster beam apparatus from Göttingen to Prague with the aim to build a new laboratory and to

CHAPTER 1. PREFACE

introduce a new research area here. Thus the molecular beams started by Z. Herman in 1960s, which were traditionally the leading basic research in physical chemistry in this country, have been extended with our new laboratory to the field of clusters and laser chemistry. It ought to be mentioned, that the present cluster-beam apparatus is not only unique in the Czech Republic but hosts several features unique worldwide, e.g., neutral cluster size selection.

Our present research summarized in this Thesis stemmed from my previous work with U. Buck in Göttingen. Therefore some of this earlier work will be outlined here. However, the focus is on my original research which started in 2005, when the apparatus was moved to Prague and the new laboratory was founded. This includes in the first place the new areas, to which we have extended the previous work, namely (i) photodissociation of nanoparticles relevant in *atmospheric chemistry* (e.g. hydrogen halide molecules on ice nanoparticles), and (ii) photochemistry of small *biomolecules* in cluster environments.

Chapter 2

Introduction

2.1 Molecular beams and clusters: A tool for understanding chemistry at the molecular level

Even in the simplest of chemical reactions many elementary processes take place. Dozens of reactions and other processes between molecules can occur in parallel. To understand the details of the chemistry at the molecular level is certainly a scientific challenge. The situation of a chemist struggling to unravel the mystery of a chemical process from the initial reactants and the final products has been compared with that *“of a spectator of a drastically shortened version of a classical drama - Hamlet say - where he or she is only shown the opening scenes of the first act and the last scene of the finale. The main characters are introduced, then the curtain falls for change of scenery and as it rises again we see on the scene floor a considerable number of dead bodies and a few survivors. Not an easy task for the inexperienced to unravel what actually took place in between”* [1].

When physicists developed atomic and molecular beam techniques [2, 3, 4], they presented chemists a unique and extremely useful tool for investigating elementary chemical processes [5, 6]. For the first time chemists could observe and gain fundamental insights into the mechanism and dynamics of elementary chemical reactions in crossed-beam scattering experiments, i.e.,

the collision of two molecules and the resulting exchange of atoms, independent of secondary processes [7, 8]. In 1986 D.R. Herschbach and Y.T. Lee received the Nobel Prize in chemistry together with J.C. Polanyi for their outstanding contribution towards “*understanding the dynamics of chemical elementary processes*”, which were studied experimentally in the crossed molecular beams. Combination of molecular beams with lasers allowed, not only to study reactions between individual molecules, but also reactions between molecules in prepared individual quantum states while probing the quantum states of the products, i.e., paving the way to the ideal chemist-purist world of well defined state-to-state reactions. Further development of the laser techniques to short (femtosecond) pulses in combination with molecular beams allowed direct tracking of chemical reactions in real time. For this development another Nobel Prize was awarded in 1999 to A.H. Zewail.¹

All these developments represented a huge leap forwards in detailed understanding of chemistry at the molecular level. Yet, a question can be posed by a hard-core macroscopic chemist: Do we really learn something about the bulk chemistry once we void the studied system of its environment? The major advantage of the molecular beams, i.e., the possibility to study the reaction independent of secondary processes, may become the major flaw of the method in the eyes of a chemical engineer. His chemistry happens in the bulk where the processes are strongly influenced by the solvent molecules.

By the way of example, let us consider the acidic dissociation of hydrogen halide HX (X=Cl or Br) molecule in water to halide anion and proton. Indeed, the way we usually write this reaction: $\text{HX} + \text{H}_2\text{O} \rightarrow \text{X}^- + \text{H}_3\text{O}^+$, it actually never happens. A single HX molecule cannot react with a single water molecule this way. A collective action of hydrogen bonds of several water molecules is necessary to break the H–X bond. Thus a crossed-beam study of HX with H₂O would yield absolutely no products. Similar conclusions were also drawn for another very reactive system: Na+H₂O. No products were observed in crossed molecular beam studies [9]. And yet we learn, and

¹A number of Nobel Prize awards was connected with the molecular beam methods, which underlines their importance: O. Stern (1943), I. I. Rabi (1944), P. Kusch (1955), and recently J. B. Fenn have received the Nobel Prize in 2002 for the electrospray ionization method, which stem from the molecular beams as well.

often eye-witness already in freshmen's chemistry courses, how reactive this system is.

The question arises: Can we study the elementary processes in the presence of solvent molecules without increasing the complexity of the system so that we would have to recede from the molecular level understanding of the studied processes? Is there a middle ground between the macroscopic bulk-chemistry and the individual molecule-molecule elementary collisions? The answer to these questions is the *cluster*.

Clusters are weakly bound aggregates of molecules which can be generated in molecular beams. We can study elementary chemical and physical processes, in them, thus investigating the processes with the molecule in an environment. The Cluster Isolated Chemical Reaction (CICR) method was advocated in late 1990s [10], in which the elementary processes between molecules were studied on large mainly rare-gas clusters. In addition, the clusters can, in principle, allow observation of the solvent effects on the studied process by adding the solvent molecules subsequently one-by-one. By the way of example, for the above mentioned acidic dissociation of HBr in water, experiments with $\text{HBr}(\text{H}_2\text{O})_n$ clusters revealed that for $n=5$ the so called zwitterionic structure $\text{H}_3\text{O}^+(\text{H}_2\text{O})_{n-1}\text{Br}^-$ was generated, i.e., that the acidic dissociation occurred [11, 12]. Similarly, the reaction $\text{Na}+\text{H}_2\text{O}$ was studied in $\text{Na}_m(\text{H}_2\text{O})_n$ clusters [13].

The topicality of molecular beams combined with laser techniques and clusters has been underlined above. This is the subject of the present Thesis: the investigation of molecular dynamics in clusters generated in molecular beams and probed by various laser techniques; in particular photodissociation and photoionization. The part of our research covered in this Thesis can be divided essentially into four areas:

- (1) Photodissociation of hydrogen halide molecules on rare gas clusters. They provide model systems for investigations of the general question: How does the solvent influence the photodissociation process? Processes, such as *fragment caging* can be studied in these systems.
- (2) Photochemistry of nanoparticles relevant in atmospheric chemistry, e.g., in the ozone depletion process. This includes namely photodissociation of hydrogen halide molecules on ice nanoparticles $\text{HX}\cdot(\text{H}_2\text{O})_n$ ($\text{X}=\text{Br},\text{Cl}$) and

photodissociation in pure $(\text{H}_2\text{O})_n$ clusters.

(3) Photodissociation of basic constituents of biomolecules in cluster environments. The photolysis of small heteroaromatic molecules as pyrrole, imidazole and pyrazole was investigated in clusters, with the aim to study the effect of the solvent on the photostability of biomolecules in general.

(4) The studies of novel rare gas compounds generated by photodissociation of precursor molecules in rare gas clusters. This is one of the original projects from Göttingen continued in our laboratory in Prague, where new results have been obtained. Investigation of the noble gas compounds is interesting and important from the fundamental point of view, since they substantially enrich our understanding of the chemical bonding.

Besides several other projects have been pursued in our laboratory in Prague, e.g., fragmentation of rare gas clusters after ionization, ion-imaging of photodissociation dynamics in molecules and small clusters, etc., however, they are not treated in this Thesis to keep the focus on the three major topics above. In the following section the four topics above will be briefly introduced.

2.2 Clusters and their relevance to the fundamental research, atmospheric chemistry and biology

The term *molecular clusters* denotes aggregates of molecules ranging from dimers to conglomerates of thousands or even more constituents, bound together by weak van der Waals interactions or by hydrogen bonds etc. These interactions are typically of the order of ~ 0.1 eV and less, i.e., more than an order of magnitude weaker than the covalent chemical bonds in the constituent molecules which are several eV. Since the typical dimensions of the larger clusters consisting roughly of 10 - 10^3 molecules are of the order of nanometers, they are often called *nanoparticles*. Work in the field of cluster and nanoparticles in general is relevant to solid state, molecular, atomic and even nuclear physics and chemistry and has practical implications for many areas, e.g., nanoelectronics, surface science, catalysis, environmental studies,

biology or even medicine [14, 15].

More specifically, in this Thesis we will be concerned with free clusters and nanoparticles generated in vacuum in molecular beams [16, 6]. Essentially three motivations can be put forward for such cluster investigations:

- (1) the fundamental understanding of bulk properties based on the properties of the individual constituent molecules;
- (2) the unique properties of clusters, which promote their use as *nanolaboratories* for investigations of various physical and chemical processes at a detailed molecular level;
- (3) the practical role which the clusters and nanoparticles play in nature, e.g., in atmospheric chemistry or astrochemistry.

The first point was one of the original motivations for cluster studies in molecular beams. Clusters can provide the link between properties of an individual molecule and the properties of the bulk material composed of these molecules by investigating physical and chemical properties as a function of the cluster size, ultimately resulting in understanding the transition from the molecule, to the bulk.

In addition, the clusters possess many unique properties. Just to mention a few, they exhibit a large number of (i) isomeric structures, (ii) internal degrees of freedom, and (iii) closely spaced energy levels. These make them a very efficient heat bath and they can cool down in vacuum by evaporation of their constituents from the surface to very low internal temperatures $T_C \sim 0.1-100$ K. Besides, the surface-to-volume ratio in clusters is large, while the volume molecules quickly converge to the bulk behaviour at the same time. Another peculiarity of the molecular clusters is the dual character of bonding: strong intramolecular bonds ($\sim 1-10$ eV) vs. weak intermolecular interactions (~ 0.1 eV). All these properties have recently promoted their use as *nanolaboratories* for investigations of various processes. For example large He_n -clusters ($n \geq 10^3$), so called *He-nanodroplets*, provide ultra-cold He (0.37 K) superfluid, i.e., non-perturbing, matrices for spectroscopy of molecules [17]. Even complex spectra of large biomolecules could be resolved in He-droplets due to their very low temperature attained by the molecule [18].

The photodissociation of molecules in rare-gas clusters, which was stud-

ied previously with the experiment presented in this Thesis, may serve as another example [19] of how the clusters can be exploited as *nanolaboratories* for studying the photochemical processes in solvent environment. The understanding of photochemical processes in condensed media is one of the current challenges in chemical physics both for fundamental and technological reasons. A molecular level understanding is difficult to achieve due to the many-body nature of the interactions leading to inseparable dynamics on a wide range of time and length scales. A photodissociation process of a diatomic HX molecule is schematically represented in Fig 2.1. In the gas

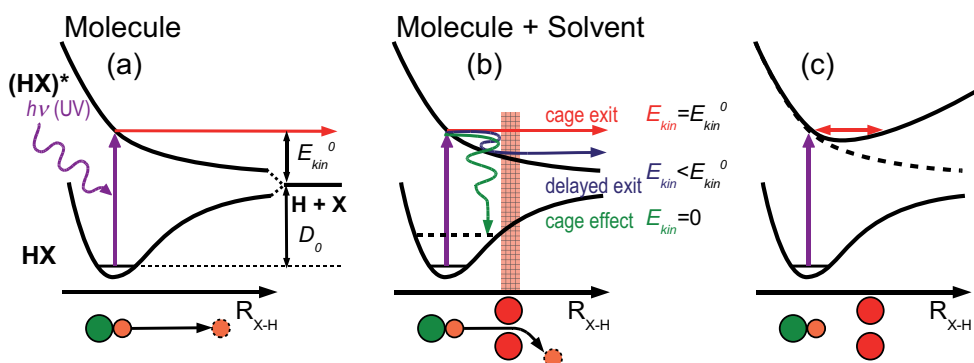


Figure 2.1: Schematic representation of photodissociation of an isolated HX molecule (a), and the possible effects of the solvent molecules on the photodissociation process: mechanical (b) and electronic interaction (c).

phase the isolated molecule is promoted by the UV radiation to an excited (HX)* PES which is repulsive and the system evolves on this surface unperturbed by other interactions so that the hydrogen atom departs with the kinetic energy $E_{kin} = h\nu - D_0$ ($h\nu$ is the UV-photon energy and D_0 is the HX dissociation limit in the particular electronic state, and the heavy X-atom is assumed to remain at rest after the photodissociation due to its much higher mass $m_X \gg m_H$ in the first approximation), Fig 2.1 (a). The solvent molecules surrounding the HX molecule in the condensed phase can be represented in the simplified picture by a wall in the way of the departing H-fragment, Fig 2.1 (b). However, in this representation the wall would be partly transparent and some fragments could pass through and leave with their E_{kin} unchanged. Some fragments can lose part of their kinetic energy

in inelastic collisions with the solvent cage molecules but they still leave the cage with somewhat lower energy. Other fragments, on the other hand, can lose their energy entirely and the HX molecule can recombine, possibly in some higher excited state. To overcome the simplification of this “wall” approach one should take into account the electronic structure of the solvent molecules and their interaction with the HX molecule which may change the PESs substantially. Thus the dissociative PES of the excited state (HX)* of an isolated molecule can be changed into a bound state by the presence of the solvent species, Fig 2.1 (c).² In other words, some photodissociation channels of the bare molecule may be closed in the bulk and some new ones may open by the presence of the solvent. The situation is even more complicated by the possibility of chemical reactions between the departing fragment and the solvent molecules. It is extremely challenging to study all these processes at the molecular level in the bulk. At this point the free clusters as *flying nano-laboratories* can help.

When the molecule is photolyzed in a cluster the initial dynamics of the process is essentially the same as in the condensed phase, since the molecule is surrounded by the solvent. Nevertheless, while in the condensed phase the fragments usually do not leave the bulk and are, therefore, often lost from detection, the clusters decay during the process and the escaping fragments can be detected. Thus, in the cluster experiments, observables can be measured not accessible in the bulk studies, e.g., the kinetic energy of the fragments after the photodissociation. This energy carries the information about the fragment interaction with the solvent cage after the photodissociation. Besides, investigating the process as a function of the cluster size, i.e., as a function of the number of solvent molecules, brings the information about the role of the solvent in the photodissociation. Last but not least, the finite size of the clusters allows theoretical treatments at a level of theory which would be too demanding for the non-periodic condensed matter. Altogether detailed information about the dynamics of the process in the molecule-solvent system can be gained from such studies, as will be shown in this Thesis.

²An example of such a change of PES from a dissociative to a bound state by the presence of a solvent molecule will be discussed in Sec. 4.3 in photodissociation of pyrrole.

Finally, the third motivation for cluster studies revealed above were practical implications which some clusters and nanoparticles have in the nature. By the way of example the ice nanoparticles play an important role in the interstellar space, where the density of chemical species and temperatures are too low for chemistry and the microscopic particles can accumulate the impinging molecules for a very long time and provide the necessary catalytic surfaces for their chemistry to occur. In addition, water clusters and ice nanoparticles are also key players in atmospheric chemistry. This example will be further detailed in the following section. Subsequently two other major areas of our cluster research covered in this Thesis, will be briefly introduced.

2.2.1 Atmospheric chemistry

Stratospheric ice particles play a key role in the *ozone depletion* process. Many details of the ozone chemistry in the stratosphere still elude the very detailed understanding. Yet, it has been well established already in 1980s, soon after the striking discovery of the ozone hole above Antarctica, that the chemistry leading to the ozone depletion in the stratosphere is not a pure gas-phase chemistry but a heterogeneous chemistry involving reactions and processes on the surface and in the bulk of ice particles in the polar stratospheric clouds (PSCs) [20, 21, 22, 23, 24]. The stratosphere, which is generally very dry, is not easily prone to cloud formation. Therefore, the PSCs can only form in the extremely cold conditions of the polar winter stratosphere. These cloud particles provide the necessary heterogeneous surfaces for the fast chemistry in the stratosphere. Above Antarctica the PSCs generation and evolution is assisted by other atmospheric conditions such as lower temperatures and polar vortex (huge masses of cold air circling near poles).

Many different reactions were proposed to proceed in the course of the heterogeneous chemistry assisted by the ice particles in PSCs. Essentially these reactions lead to conversion of so called *reservoir species* (e.g., HCl, HBr, ClONO₂) relatively harmless to ozone to the *active species* (e.g., Cl₂, Br₂, BrCl, HOCl, HOBr), which can be readily photolyzed by the sun UV

radiation and release halogen radicals that destroy ozone directly in catalytic cycles [25]. The active species are generated in the PSCs in these reactions during the cold polar winter and their photolysis starts releasing the halogen radicals in the Antarctic spring when the sun radiation reaches the Antarctic region. The molecular precursors for the above mentioned reservoir species are freons: chlorofluorocarbon (CFC) molecules, e.g., CCl_2F_2 . The ozone depletion chemistry is illustrated by a simplified cartoon in Fig. 2.2.

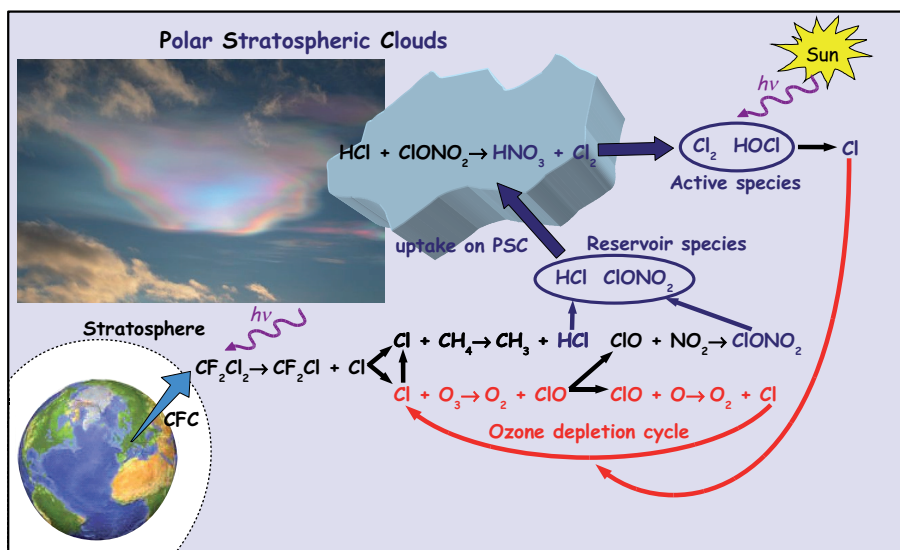


Figure 2.2: A simplified schematic cartoon of the ozone depletion chemistry.

More recently alternative reaction models have been proposed, which lead to halogen radical generation directly from these CFCs, bypassing the necessity of generating the reservoir species from CFCs [26, 27]. Nevertheless, the key role of PSCs is preserved in these models, since the essential step is a dissociative attachment of the *solvated electron* generated by cosmic radiation in PSC particles to the CFC molecules adsorbed on the particle surface [28].

From the above it is obvious that the chemistry and photochemistry of the ice particles in the PSCs with the adsorbed pollutant molecules such as hydrogen halides play a key role in the ozone depletion process. The ice nanoparticles (large water clusters), which can be generated in the molecular beams in our apparatus with hydrogen halide molecules attached to them can

mimic the stratospheric particles in the laboratory conditions. Interacting these species with UV laser beams can then reveal their photochemistry.

In our studies we were also trying to address another more fundamental question, however, closely related to the above PSC particle chemistry. It is the issue of hydrogen halide acidic dissociation. It has been pointed out in the previous Sec. 2.1 that the acidic dissociation cannot occur between HCl and a single water molecule but at least four water molecules are necessary. This conclusion followed from numerous theoretical studies, which obtained the zwitterionic structure $\text{Cl}^-\cdot(\text{H}_2\text{O})_{n-1}\cdot\text{H}_3\text{O}^+$ as the energy minimum for water tetramer $n=4$ with HCl molecule. An experimental evidence has been provided for the acidic dissociation of HBr in water cluster with 5 water molecules [11, 12]. On the other hand, investigations of $(\text{HCl})_m(\text{H}_2\text{O})_n$ clusters with Fourier-transform infrared (FTIR) vibrational spectroscopy in supersonic expansions [29, 30, 31] did not bring any evidence for covalently bound HCl molecules in species larger than $m=1$ and $n=2$, which might indicate an onset of acidic dissociation for HCl already in water trimer $n=3$. At a closer look it becomes obvious that the question of the onset of acidic dissociation is a more complex issue.

While from the point of view of the theoretical calculations the acidic dissociation occurs for the cluster size where the zwitterionic structure represents the energy minimum deeper than the structure with covalently bound molecules, in the experiment the dynamical passage must be considered from the covalently bound molecule deposited on the water cluster to the ionic structure. This is clearly a function of the cluster temperature [32, 33]. Therefore, even on the bulk ice surface, where the acidic dissociation could be expected, undissociated covalently bound molecules were observed at low temperatures. Experimentally a transition between covalently bound and acidically dissociated HCl molecules on bulk ice was measured between 80 K and 130 K [34].

Therefore, a fundamental question arises: Are the HCl molecules on the ice nanoparticles in our molecular beam covalently bound or acidically dissociated? Since the water cluster temperature in our size region $n \approx 10^2$ - 10^3 is not exactly known and values between 70 K and 200 K were reported (see Sec. 3.2), the acidic dissociation of HCl can in turn provide further exper-

imental evidence for the cluster temperature. From a more practical point of view the important question is: Are the HCl molecules on PSC particles covalently bound or ionized? An answer to this question is, indeed, essential for the chemistry considered in the stratospheric models, which will differ significantly if HCl or H_3O^+ and Cl^- are involved in the corresponding reactions. These questions were addressed by our studies of ice nanoparticles with embedded hydrogen halide molecules in the molecular beams discussed in this Thesis in Sec. 4.2.

2.2.2 Biomolecules in clusters

Biological systems involve rather complex molecules. The understanding of chemistry and physics in these species at the molecular level is correspondingly complicated. Therefore, often smaller functional units of the larger biomolecules are investigated in the gas phase. Fig. 2.3 illustrates the *bottom-up approach* in studies of biomolecules: if we want to understand the photochemistry of the larger biomolecules, we start from the essential building blocks of these molecules. Thus we start with pyrrole, which is a building block of the porphyrin ring. The porphyrin ring is a part of many biomolecules such as hemoglobin or chlorophyll. Pyrrole is not only part of these molecules, but it is also the UV-active chromophore, i.e., the unit where the UV photon is absorbed and the photochemistry is initiated. Therefore, many studies were devoted to the photochemistry of pyrrole molecule in the gas phase [35, 36, 37, 38, 39, 40, 41, 42]. However, it turns out that the photoinduced processes are often controlled by the environment of the chromophores. This can be demonstrated on the example of nucleic acid photochemistry [43, 44]. Therefore, also here the clusters can provide model systems. Increasing the complexity of the studied systems by adding various solvents to the simple molecules such as pyrrole can allow for answering the essential questions as: Are the molecules intrinsically photostable or is the photostability provided via the solvation? Do specific interactions (e.g., hydrogen bonds) play a defining role in the photochemistry of these molecules in biological systems?

Hydrogen bond is very important bond in biological matter. The most

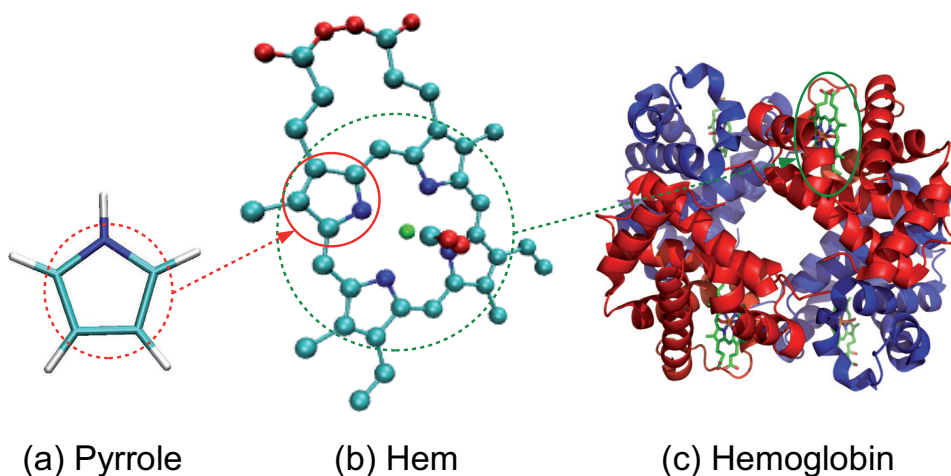


Figure 2.3: Pyrrole molecule as a basic functional unit of biomolecules illustrating the *bottom-up approach*: the pyrrole molecule (a) is a building block of porphyrins, which are the essential units of biomolecules such as hem (b), which in turn is a basic functional unit of hemoglobin (c).

prominent examples of its significance in biology are the pairing of base pairs in nucleic acids, molecular recognition or enzyme catalysis. All these examples are related to essential conditions of life. For this reason, hydrogen bonding phenomena became a subject of extensive studies. Experimental studies of hydrogen bonding in the ground state are relatively straightforward, e.g., using vibrational spectroscopy, which provides a very detailed information about this type of bonding [45, 46, 47].

Experimental investigation of hydrogen bonding in the excited state is more complicated. While photochemistry of systems with intramolecular hydrogen bonds was studied for a relatively long time (e.g., in a context of sunscreen protection or fluorescence spectroscopy), photochemistry of intermolecular hydrogen bond has become only recently a major research subject [48]. There are interesting questions to be addressed: Is there any photochemistry specific for hydrogen bonded systems? And if the answer is yes, is the different photochemistry related to biophysically relevant processes? The answer to the first question is affirmative, photoinduced processes are controlled by the ground state structure and the $X-H\cdots Y$ structural mo-

tif implies ultrafast excited state hydrogen (or proton) transfer as a typical reaction of hydrogen bonded systems. The hydrogen bond was suggested to be a key component in protecting nucleic acids against radiation damage [49, 50, 51].

Since the absorbed photon triggers ultrafast dynamical processes, various time resolved experiments, based on photoabsorption, fluorescence or photoionization can be used to study the excited state dynamics [52]. The dynamical processes occur often on the edge of the time resolution of the respective experiments. In our studies, we concentrate on the experiments in the energy domain. In particular we detect the kinetic energy distribution of the atomic fragments released from the studied system. The natural choice for the study of hydrogen bonded systems is to detect the kinetic energy of the hydrogen atoms. If the detected hydrogen atom was released from the molecule participating in the hydrogen bonding, we obtain information about the character of this bond both in the ground and in the excited states. The results of our studies of small biomolecules in clusters will be presented in Sec. 4.3.

2.2.3 Clusters as nano-cryo-reactors

It has been mentioned above that due to their many unique properties the free clusters in molecular beams can be exploited as *flying nanolaboratories* for investigating embedded species and processes. In this Thesis a particularly interesting example will be discussed in Sec. 4.4, where the clusters are exploited as *flying nano-cryo-reactors* or *flying nano-matrices* for generating novel rare-gas molecules in the gas phase and orienting them in electric fields.

The closed-shell electronic configuration of the noble-gas atoms in their ground state leads to their chemical inertness. Therefore, the discovery of chemical compounds of rare gas elements surprised chemists in early 1960s. These noble-gas compounds constitute some of the most unusual examples of chemical bonding, therefore, their exploration unravels new bonding mechanisms and expands our understanding of chemical bond [53]. One particular branch of the development in the noble-gas chemistry concerns formation of compounds of the type of H-Rg-Y, where Rg is a rare gas atom and Y is an

electronegative atom or group. It has been suggested that there is a strong partial ionic character to these compounds $[\text{H-Rg}]^{\sigma+}-\text{Y}^{\sigma-}$. However, the role of the covalent bonding in these systems is also essential. They are usually quite stable being prevented from $\text{HRgY} \rightarrow \text{HY} + \text{Rg}$ decomposition by a high barrier, and from the three body decay $\text{HRgY} \rightarrow \text{H} + \text{Y} + \text{Rg}$ by the reaction endoergicity.

Experimentally, these species are usually produced by dissociation of the HY molecules adsorbed in the rare gas matrices. The precursor molecules can be either UV photolyzed or dissociated by electron bombardment. Then the matrix is annealed by heating, typically from about 10 K to 40 K, to make the hydrogen mobile and recombine to the H-Rg-Y molecule. In 2005 over 20 such molecules prepared in matrices were reviewed in Ref. [54] and their number is ever increasing. However, only three rare gas molecules have been generated in the gas phase so far: HXeI, HXeCl and HXeCCH, and they were all prepared on the present experimental apparatus [55, 56, 57, 58].

In our cluster experiments the molecules are produced by the photolysis of HY precursor molecules on rare gas clusters (Xe_n clusters in particular). Thus the clusters serve as *reactors* for HRgY synthesis. In addition the cluster experiments provide several unique insights. First, an interesting issue is the HRgY formation mechanism. In the matrix experiments the molecules are generated by *delayed mechanism* including annealing and H-atom migration after the HY photolysis in the matrix. Yet, since these experiments themselves are very long-range in time, an intermediate steps including direct formation of HRgY on a much shorter time-scale cannot be excluded from the observations. In fact, since the HRgY molecules are generally very strong absorbers, the UV radiation used to photolyze the precursor HY molecule photodissociates also the HRgY molecules readily. In other words, the HRgY molecules produced by the *direct mechanism* would be dissociated by the same radiation which generated them and excluded from the IR detection.

On the other hand, in the cluster experiments only molecules produced by the *direct formation mechanism* after HY photodissociation can be observed. No annealing of the cluster is possible and the clusters decay during the process of HY photodissociation and immediate HRgY generation, so that

the HRgY molecule remains isolated in the vacuum after the whole process is finished. A schematic cartoon of the HXeY molecule generation in the gas phase is shown in Fig. 2.4.

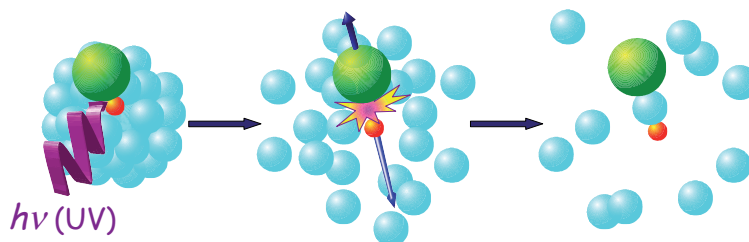


Figure 2.4: A schematic cartoon of the HXeY molecule generation in the gas phase by the HY precursor photodissociation on Xe_n cluster. First the HY precursor is photolyzed and the cluster begins to decay. The H-fragment is scattered from a Xe atom back to recombine with Y fragment with another Xe atom inserted to generate the HXeY molecule.

The second unique feature of our experiment is the preparation of the HRgY molecules *aligned and oriented* in the vacuum. Molecular alignment and orientation is a fascinating issue and a relatively young research field. In principal, by using an intense laser pulse it is possible to replace the random angular distribution of a gas-phase molecules by a distribution that is strongly aligned, that is, to create a situation where the molecules, still in the gas phase, are oriented in space, with their axes along the polarization vector of the laser [59]. There are numerous applications of this alignment effect, both in fundamental studies and in applications in material processing and laser-molecule interaction. By the way of example, in the molecular beam research of elementary chemical processes, outlined in this introduction, an ultimate answer about the molecular mechanism of a chemical reaction can be obtained by colliding the reactants in an oriented fashion.

The first theoretical paper by B. Friedrich and D. Herschbach describing laser-induced molecular alignment appeared in 1995 [59], but it was not until 1999 that the effect was first seen experimentally [60, 61]. The experiment in Göttingen detecting the HXeI molecule in 2001 was one among the first experiments to demonstrate the alignment of a molecule in the com-

bined laser and electrostatic fields [55] and was soon followed by a further elegant proof of the molecular orientation [56, 62]. It should be noted that the cold temperature of the cluster together with its evaporation during the HRgY generation process, which further cools the HRgY molecule are essential for the observation of the oriented states of the HRgY molecule, since the molecule must be generated in its lowest state -so called *pendulum state* [59]. This makes our clusters the so called *cryo-reactors*. These experiments will be further discussed in Sec. 4.4.

Chapter 3

Experiment

3.1 General description of the experiment

The experiments covered in this thesis were all carried out on an molecular beam apparatus for studies of photodissociation of molecules in cluster environments [19]. The apparatus was built and originally used in the group of U. Buck at the Max-Planck-Institute for Dynamics and Selforganization in Göttingen. I joined this group in 2002 and started to work on this experiment. In 2005 I have moved the apparatus to the J. Heyrovský Institute in Prague. Some small modifications and additions were made to the setup in Prague, however, the apparatus remained essentially in the original configuration as described in some of the early publications [63, 64, 65]. A comprehensive account of the experimental apparatus in its last configuration in Göttingen can be found in the Ph.D. Thesis of H. N. Nahler [66].

The whole experiment encompasses a vacuum apparatus and laser system. In the vacuum apparatus the clusters are generated in molecular beams and they are further manipulated, analyzed and detected by various methods. The laser system serves to provide UV-light of various wavelengths for photodissociation and photoionization experiments. First, the general overall scheme of the experiment will be described. Then a brief account of the individual parts of the apparatus and methods will be given in the following sections.

The schematic picture of the present experiment with its essential parts

3.1. General description

CHAPTER 3. EXPERIMENT

is shown in Fig. 3.1. The clusters are produced by a supersonic expansion of the corresponding gas molecules through a nozzle into the vacuum. The supersonic expansions, molecular beam generation and cluster formation will be discussed in more details in Sec. 3.2.

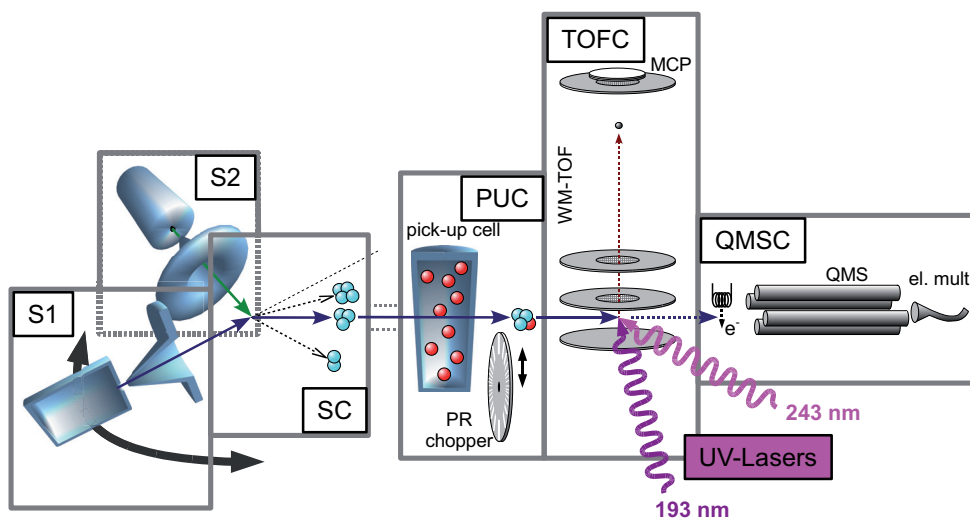


Figure 3.1: The schematic picture of the present experiment: S1–primary beam source chamber; S2–secondary beam source chamber; SC–scattering chamber; PUC–pick-up chamber hosting pick-up cell and pseudorandom (PR) chopper; TOFC–time-of-flight chamber with WM-TOF spectrometer, where laser beams interact with the molecular beam, and the fragments are detected by multichannel plate (MCP); QMSC–quadrupole chamber with QMS, where clusters are ionized by electrons and fragment mass spectra are recorded by electron multiplier.

After passing the skimmer, the neutral clusters can be size selected in elastic scattering with a perpendicular beam of He atoms produced in the secondary nozzle. The basic principle of the size selection method is indicated schematically in Fig. 3.1: the smaller (lighter) clusters are scattered to the larger laboratory angles than the larger (heavier) clusters. The whole assembly of the two source vacuum chambers attached to the scattering chamber can be rotated with respect to the rest of the apparatus as indicated in Fig. 3.1. Choosing an appropriate laboratory angle to which the clusters are scattered, clusters of the selected size n are allowed to proceed further

3.1. General description

through the apparatus. Actually, the angularly selected beam contains also clusters smaller than n and further methods can be employed to obtain a complete size selection of the neutral clusters¹. These methods will be described in more detail in Sec. 3.3. It is worth noting that the possibility to obtain explicit information about the neutral cluster size distribution is one of the unique features of our apparatus.

After the scattering chamber the clusters enter another vacuum chamber, where they can be doped with foreign molecules by passing through a pick-up cell filled with the foreign gas at a low pressure (see the Sec. 3.2 for details). This chamber is hosting a pseudo-random chopper, which together with the quadrupole mass filter and channeltron detector at the end of the apparatus enables to analyze the cluster velocities by a time-of-flight method. In addition, a velocity selector can be used to select clusters with a given narrow velocity interval (which corresponds to a certain cluster size as will be explained in Sec. 3.3) however, this option was not exploited in the experiments discussed in this Thesis.

Then the clusters enter the first detection chamber with a time-of-flight spectrometer of the Wiley-McLaren type (WMTOF) [67]. The molecules in the clusters are dissociated and ionized by the laser beams. The ionized fragments are extracted into the WMTOF field free region and detected at the end with a multichannel plate and their TOF spectra are recorded. The WMTOF can be operated as a mass spectrometer when the ions are extracted with a high electric field. However, in the photodissociation experiments it is rather operated in the so called *low field mode* with a small extraction field, where the kinetic energy distribution (KED) of a particular fragment (e.g., H-atom) can be measured (see Sec. 3.4.1).

The H-fragments are efficiently photoionized at 243.07 nm (5.1 eV) by a

¹It ought to be mentioned that, although the beams of fully size selected small neutral clusters can in principle be prepared by the scattering method, the cluster densities in these size selected beams were not sufficient for the photodissociation experiments. Therefore the scattering was employed to reveal the neutral cluster size distribution under the given expansion conditions, under which the experiments were performed in the direct cluster beam without the scattering. Thus, although the experiments were performed with clusters which were not size selected, the neutral cluster size distributions and consequently the mean cluster sizes were known.

resonance-enhanced multiphoton ionization (REMPI) process. The molecules in the clusters can be photodissociated previously either by photons of the same wavelength within the same laser pulse or by another laser pulse at 193 nm (6.4 eV). In the photoionization experiments the clusters and/or their fragments are ionized by a non-resonant absorption of several photons from any of the two lasers. These experiments are typically performed with one laser only (usually the 193 nm laser, which can provide higher photon fluxes to facilitate the multiphoton processes).

Alternatively the mass spectra can be recorded with a quadrupole in the last vacuum chamber. For this purpose the clusters are not interacted with the laser beams in the WMTOTF chamber but proceed into the QMS chamber, where they are ionized by electrons. The ionized fragments pass the quadrupole mass filter and are detected by a channeltron multiplier.

A more detailed description of the individual parts of the experiment will follow in the next few sections.

3.2 Supersonic expansions, molecular beams

Molecular beams are generated by *supersonic* – so called *free-jet* – expansions of molecules in the gas phase into the vacuum. The overview of the technique can be found in many reviews and textbooks, e.g., in Refs. [5, 6]. Generally, the gas expansion can be characterized by the Knudsen number $K_n = \lambda/d$, where λ is the mean free path of the molecules in the reservoir and d is the nozzle diameter. For $K_n \geq 1$ the molecules do not collide frequently in the nozzle vicinity and an effusive molecular beam is generated characterized by the broad Maxwell-Boltzmann distribution of molecular velocities, low intensity, and wide angular distribution. In this regime the expansion can be treated within the gas kinetic theory.

On the other hand, for $K_n \ll 1$ the supersonic expansions can be achieved resulting in fast molecular beams with narrow velocity distribution, high particle densities and small angular divergence. The condition $\lambda \ll d$ implies many collisions during the expansion establishing a local equilibrium at each point along the expansion, which can be then treated as an adiabatic process. The molecules, which are accelerated by the pressure difference, reach the

local sonic speed at the nozzle throat and further exceed it – therefore the term *supersonic expansion*. The continuous flow in the expansion in this regime can be described by flow dynamic and thermodynamic equations.

The free-jet expansion is illustrated schematically in Fig. 3.2. The in-

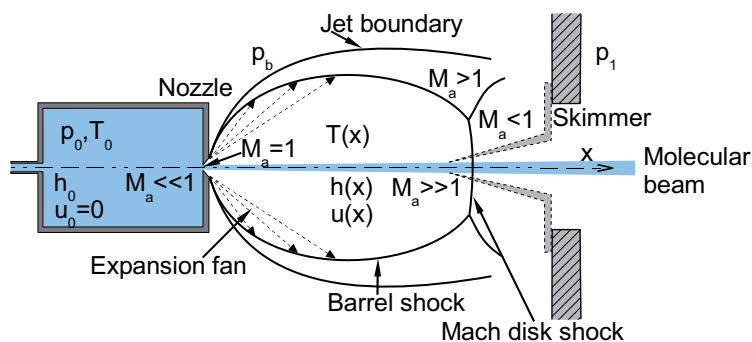


Figure 3.2: Schematic illustration of the supersonic expansion of a gas through a nozzle. The various regions of the free-jet expansion are labelled. The gas expands from the stagnation temperature T_0 and pressure p_0 through the nozzle into a background vacuum p_b . The various free-jet expansion regions are characterized by the Mach number M_a which is the ratio of the particle speed to the local speed of sound, i.e. $M_a \gg 1$ means that highly supersonic speeds are achieved. The molecular beam is formed by inserting a skimmer into the free-jet expansion before the Mach disk shock and the expansion enters another differentially pumped chamber. The skimmer interference with the expansion should be minimized by its shape and position.

ternal thermal energy of the gas is turned into the kinetic energy of the molecular flow with velocity u during the expansion. Assuming a one-dimensional flow in the direction x from the nozzle throat the total energy per molecule, which is the sum of the enthalpy $h(x)$ and the kinetic energy, i.e. $e(x)=h(x)+\frac{m}{2}u^2(x)$, has to be conserved along x . Thus

$$h_0 = \frac{m}{2}u^2(x) + h(x), \quad (3.1)$$

where h_0 is the enthalpy of the molecule in the source. The enthalpy is a function of temperature and for an ideal gas can be written as

$$h_0 - h = \int_T^{T_0} \frac{c_p}{N_a} dT' = \frac{c_p(T_0 - T)}{N_a}, \quad (3.2)$$

where N_a is the Avogadro constant and c_p is the molar heat capacity at a constant pressure, $c_p = N_a k_B \frac{\gamma}{\gamma-1}$, where k_B is the Boltzmann constant, and γ is the heat capacity ratio c_p/c_V ($\gamma=5/3$ for an ideal gas). The thermal motion of the molecules in the beam is given by the local temperature $T(x)$ which is cooled down during the expansion. If the entire enthalpy is transformed into the kinetic energy of the molecule the terminal temperature will be $T = T_\infty = 0$ after the expansion process is finished. In this case Eqs. 3.1 and 3.2 yield for the terminal velocity

$$u = u_\infty = \sqrt{\frac{2k_B T_0}{m} \frac{\gamma}{\gamma-1}}. \quad (3.3)$$

In reality the molecules maintain a certain rest thermal velocity $\alpha = \sqrt{\frac{2k_B T}{m}}$ corresponding to a finite final temperature T . The molecular cooling, i.e. the quality of the expansion can be characterized by the *speed ratio* $S = u/\alpha$. It can be shown that the speed ratio can be determined experimentally as

$$S \approx 2\sqrt{\ln 2} \frac{u_e}{\Delta u_e}, \quad (3.4)$$

where u_e is the experimentally determined velocity of the molecules and Δu_e is the full width at half maximum (FWHM) of the measured velocity distribution. Typically the speed ratio reaches values of 10 to 100, i.e., the thermal speed of the molecules is one or two orders of magnitude smaller than the beam speed. Despite many approximations in the derivation of Eq. 3.3, the measured beam velocities agree surprisingly well with u_∞ especially for rare gas expansions. By the way of example the calculated terminal velocity for He and Ar expansions at room temperature (300 K) $u = 1767 \text{ ms}^{-1}$ and 559 ms^{-1} , respectively, usually agree with the measured velocities within a few percent.

Due to the assumption $T=0$ the terminal velocity u_∞ should be the upper limit. However, in the cluster beams the condensation energy released upon molecule clustering can accelerate the species and even faster beams than the calculated u_∞ can be obtained. It should be noted that the above derivation of u_∞ assumed c_p being temperature independent, which is a rough approximation. By the way of example for He, which is usually considered to be closest to the ideal gas behaviour, c_p changes by factor of four in the temperature range between 3 K and 300 K. A more rigorous treatment of the

supersonic expansions can be found in the above mentioned textbooks [5, 6] and in the recent publications [68, 69].

The molecules cool down in the expansion cooling the various degrees of freedom at various rates depending on the energy transfer collision cross sections for the various energy modes. Therefore the different energy modes of the molecules can be characterized by different temperatures. The translational temperature of the random molecular motion α around the beam velocity u can correspond to very low temperatures $T_{tr} \sim 1-10$ K. The rotational relaxation leads to very low temperatures typically $T_{rot} \sim 10$ K. This strong cooling is largely exploited in various rotational and ro-vibrational spectroscopies. On the other hand, vibrational relaxation requires typically 10^4 collisions, while in usual expansions the molecules undergo 10^2-10^3 collisions, leading to only moderate vibrational cooling and consequently the vibrational modes usually freeze out in the expansion without converting their energy into the directional velocity of the beam. The low temperatures, the long interaction time between molecules moving in the same direction with the same velocity, and the numerous collisions in the expansion can lead to the cluster generation in the beam.

Molecular clusters are often produced in *seeded expansions*. The molecules are added in small concentrations ($\leq 10\%$) to the expansion of a carrier gas, typically rare gas such as He or Ar. To calculate the beam velocity for such expansions, Eq. 3.3 can be modified by using a weighted average mass $m = C_M \cdot m_M + (1 - C_M) \cdot m_B$, where C_M is the relative concentration of molecules M , m_M is their mass, and m_B is the mass of carrier (buffer) gas. As long as the concentration of molecules is small, the expansion parameters, i.e., the velocity u and speed ratio S , are mostly determined by the carrier gas. Thus the heavy molecules coexpanded with helium can reach high speeds and velocity ratios. Helium also does not tend to generate clusters with the molecules due to its very weak interactions and pure molecular clusters are generated. Argon, due to its higher mass, can carry away more energy from the system in three-body collisions, i.e. the clustering of molecules in Ar expansions is more efficient. This results in larger clusters generated in Ar than in He under the same expansion conditions. However, the somewhat stronger interaction of argon with the molecules can lead to the generation

of mixed clusters. By the way of example, pure HBr clusters were produced in our experiments with 5% mixture of HBr in Ar in a range of pressures (1-6 bar) and nozzle temperatures around 300 K. Nevertheless at low enough HBr concentrations ($\leq 1\%$) and nozzle temperatures 170-230 K argon clusters were generated with HBr molecules or small $(\text{HBr})_m$ clusters embedded inside the larger Ar_n clusters. The differences between He and Ar expansions were exploited in our experiments with clusters of small biomolecules discussed in Sec. 4.3.

The clusters generated in free jets exhibit a certain size distribution. If small clusters are produced, e.g., in He-expansions under normal conditions², the size distributions usually assume an exponential shape, the molecular beam being dominated by the monomers and falling off exponentially towards larger cluster sizes. Examples of such distributions are the clusters of biomolecules produced in helium expansions discussed in Sec. 4.3. To determine the neutral cluster size distributions of the small clusters the scattering method described in the next Sec. 3.3 was employed.

A typical example of the larger clusters treated here are the rare gas clusters. Their size distribution can be characterized mathematically by a log-normal distribution, the width of which roughly corresponds to its mean value [71]. The mean cluster size can be determined from the expansion pressure p_0 and temperature T_0 according to the empirical formula (Hagena's scaling law) [72, 73, 74, 75]:

$$\bar{n} = K \cdot \left(\frac{\Gamma^*}{1000} \right)^\zeta, \quad (3.5)$$

where $K = 38.4$ and $\zeta = 1.64$ were determined from diffractive He atom scattering on large Ar_n clusters [75]. The dimensionless parameter Γ^* introduced by Hagena [73] allows to compare various expansions independent of nozzle and gas parameters:

$$\Gamma^* = \frac{p_0[\text{mbar}] \cdot d_e[\mu\text{m}]^{0.85}}{T_0[\text{K}]^{2.2875}} \cdot K_c, \quad (3.6)$$

²It should be mentioned that under high enough pressures (several tens bars) and low enough temperatures (typically around 10 K and below) even helium can generate large clusters of 10^3 - 10^8 atoms, so called He nanodroplets [70].

where K_c is characteristic constant of the expanding gas (e.g., $K_c=1646 \text{ K}^{2.2875} \text{ mbar}^{-1} \mu\text{m}^{0.85}$ for Ar) and d_e is the equivalent nozzle diameter, which is for the present nozzles of conical shape with diameter d and opening angle α_D :

$$d_e = 0.736 \cdot \frac{d}{\tan(\alpha_D/2)}. \quad (3.7)$$

For example, in the present experiments under typical expansion conditions $p_0=3 \text{ bar}$ and $T_0=210 \text{ K}$ the argon expansion through the typical nozzle of $d=60 \mu\text{m}$ diameter and $\alpha_D=30^\circ$ opening angle results in the mean Ar_n cluster size $\bar{n}=100$.

The other example of the large clusters discussed in this Thesis are the water clusters (ice nanoparticles). These can be produced by pure or Ar-seeded expansion of water vapour in a special cluster source with a heated reservoir attached directly to the nozzle inside the vacuum chamber. The reservoir can be filled with water from outside the vacuum and heated to a temperature T_R ($\sim 300\text{-}470 \text{ K}$) to generate sufficient water vapour pressure expanded through the nozzle, which is heated independently to a temperature $T_0 \geq T_R$ to prevent condensation in the nozzle. The size distributions of large water clusters $\bar{n}=10\text{-}1750$ have been studied previously in the group of U. Buck with the present water cluster source [76]. Their size distributions were measured directly by fragmentation free methods, namely by doping with Na atoms followed by single photon ionization [77]. The resulting average sizes could be again correlated with the source parameters based on Eq. 3.5. The resulting parameters are available for water and ammonia clusters in Refs. [76, 77].

Highly relevant general question is the one of the internal cluster temperatures, yet it is difficult to access experimentally. Two approaches have been exploited so far: (1) electron diffraction, which reflects the thermal motion of the particles forming the cluster [78, 79]; (2) ro-vibrational spectroscopy of a molecule embedded in the cluster. The later method works only for very weakly interacting large helium clusters, which turned out to be superfluid and thus not hindering the motion of the molecule. Therefore rotationally resolved spectra of, e.g., SF_6 and OCS molecules were obtained in helium nanodroplets and their rotational temperature was determined to

be 0.37 K [17]. This is probably the most accurately determined cluster temperature. For the other rare gas clusters the temperatures determined by the first method range from approximately 10 K for Ne_n to 80 K for Xe_n with some dependence on the cluster size [78, 79]. For water clusters, where the temperature is crucial for the issue of hydrogen halide acidic dissociation discussed in this thesis, still some ambiguity exists. The electron diffraction yielded the temperature of 180 ± 20 K for $(\text{H}_2\text{O})_n$, $n \leq 200$ [80]. Besides the cluster temperatures can be estimated based on model calculations. A relaxation model calculations delivered temperatures of approximately 70 K and 190 K for $(\text{H}_2\text{O})_9$ [81]. An estimate based on the same model results in temperatures in the range 100-130 K for our clusters of several hundreds water molecules [82]. Some discussion of cluster temperatures can be found in the review [10].

It has been mentioned above that the coexpansion (e.g., HBr with Ar) can lead to the clusters with foreign molecules embedded inside. To prepare mixed clusters with molecules or small host clusters adsorbed on the surface of the larger clusters the so-called pick-up technique introduced by Scoles and coworkers [83] is applied. The cluster is passed through a small scattering cell filled with the molecular vapour with a variable pressure (in the present case the beam path in the cell is 5 cm long and the pressure is typically in the range of 10^{-2} mbar). The number of captured molecules depends sensitively on this pressure and follows a Poisson distribution [84]. By a suitable choice of the pick-up pressure, one can arrange conditions at which only one or a few molecules are adsorbed on the surface of the cluster. The probability of the molecule to penetrate inside the cluster depends on the parameters of the local interactions between the deposited molecule and the cluster molecules. By the way of example, it has been shown by a series calculations [85] that, e.g., the HBr molecule deposited on Ar_n in the pick-up process stays near the surface in the first and second shells. Similarly, if more than one molecule is coadsorbed on the cluster, they can coagulate to generate small clusters on the cluster, again depending on the nature of intermolecular interactions. The water clusters with hydrogen halide molecules treated in Sec. 4.2 were prepared by the pick-up process, and also the large rare gas clusters with adsorbed HY molecules for preparation of the HRgY molecules discussed in

Sec. 4.4.

3.3 Scattering experiment, neutral cluster size selection

One of the original motivations for cluster studies was to investigate an evolution of a certain property or phenomena with the cluster size in order to track the evolution from a single molecule to the bulk. As easy as it may sound it is actually experimentally extremely challenging because of the difficulty to obtain *neutral* clusters of a given *single size*. Indeed, it is relatively easy to size select charged clusters with mass spectrometry methods. Yet, the electric charge on a cluster can change substantially its properties with respect to the corresponding neutral species. One way to size-select neutral clusters is the scattering method introduced in 1984 by Buck and Meyer [86] and described in detail in Refs. [87, 88, 89]. The scattering analysis provides a unique correlation between the detected cluster fragment ion and its neutral precursors, independent of the cluster size distribution in the primary beam and the fragmentation process in the ion source [87]. The method relies on the specific kinematic behavior of clusters with different sizes scattered from a target beam. This is illustrated by the Newton diagram in velocity space, Fig. 3.3.

Let us assume a beam of molecules M colliding at right angle with a beam of He atoms. As outlined in the previous section, all the molecules attain in the expansion approximately the same velocity \vec{v}_M . The secondary He-beam velocity is denoted by the velocity vector \vec{v}_{He} . The particles collide with the relative velocity $\vec{g} = \vec{v}_{He} - \vec{v}_M$. The center-of-mass (CM) of the system moves with the velocity \vec{c} :

$$\vec{c} = \frac{m_M \vec{v}_M + m_{He} \vec{v}_{He}}{m}, \quad (3.8)$$

where $m = m_M + m_{He}$. For an observer moving with the CM of the system the particles move on the straight line defined by the vector \vec{g} towards the observer with CM velocities, which for the molecule M are

$$\vec{u}_M = \vec{g} \cdot \frac{m_{He}}{m}, \quad \vec{u}_{He} = -\vec{g} \cdot \frac{m_M}{m}. \quad (3.9)$$

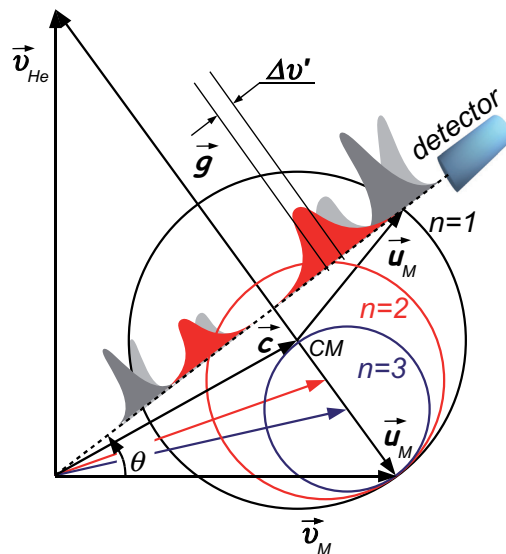


Figure 3.3: Schematic Newton diagram for scattering of M_n clusters with He-atom beam: \vec{v}_M is the molecular beam velocity; \vec{v}_{He} is the secondary He-beam velocity; \vec{g} is the collision velocity; \vec{c} is the velocity of the center of mass (CM); u_M is the velocity of the molecule in the CM system. The circles denote correspond to the elastically scattered molecules ($n = 1$), dimers ($n = 2$), and trimers ($n = 3$). A TOF spectrum (velocity distribution) measured at a particular laboratory angle Θ is schematically shown, and a selected velocity region is indicated corresponding to the selection of only dimers from the beam.

For the elastically scattered molecules the speed u_M remains unchanged and only its direction can change. Therefore they are found scattered in the velocity space on a circle (labelled by $n=1$ in Fig. 3.3) with its center at the end of the CM-velocity vector \vec{c} and the radius u_M . This is so called *Newton sphere*, in this case projected onto the circle in the collision plane.

For different clusters M_n in the beam the velocity \vec{v}_M is the same but the CM velocity changes with n due to the change of mass: m_M is replaced with $n \cdot m_M$ in Eq. 3.8. The center of the scattering circle shifts correspondingly and its radius decreases for larger n , as illustrated for $n= 2$ and 3 in Fig. 3.3. Thus each cluster M_n could be scattered in the laboratory (LAB) system only within a certain angular range. The tangent to the corresponding circle

determines the maximum LAB scattering angle Θ_n to which clusters of the size n can be deflected. Setting the detector to a larger scattering angle $\Theta > \Theta_{n+1}$ implies that only clusters with sizes smaller than $n + 1$ can reach the detector.

Thus the angular selection serves as a *low pass filter*, removing the larger clusters from the beam at a particular LAB angle. To achieve a complete size selection requires to set a *high pass filter* to remove the smaller clusters. This can be done in the detection by the quadropole mass filter. Setting the quadrupole to an ionized cluster fragment mass larger than M_{n-1} (e.g., the protonated fragments $M_{n-1}\text{H}^+$ are usually detected in case of hydrogen bonded clusters) ensures that only the signal from neutral M_n clusters of the particular size n is detected. Indeed, this method leads to detection of one particular neutral cluster size and can be used, e.g., in the depletion spectroscopy of size selected clusters [47, 90, 91, 92], however, it does not produce a cluster beam of one particular size. The beam which is selected by the scattering angle contains also the monomers and small clusters according to the original cluster size distribution up to the selected size n .

Generation of a beam of completely size selected clusters can be achieved by complementing the scattering method with a velocity selection [65]. The principle of the method can be seen again from the Newton diagram in Fig. 3.3. At a particular laboratory angle Θ the different cluster sizes scattered to that angle will possess different LAB velocities. If a TOF (velocity) distribution is measured under the given angle it will exhibit peaks at times (velocities) corresponding to the various clusters sizes. A velocity selector can be employed to cut out from this distribution a narrow portion of velocities which correspond to a single cluster size, as indicated in Fig. 3.3. In this way a cluster beam of only one single size is transmitted through the selector. However, it ought to be mentioned that the particle density in such size-selected beam is too low for the photodissociation experiments presented here. Therefore, usually, the neutral size distribution is determined by the scattering experiment and the photodissociation experiment is performed directly in the primary beam with the entire distribution.

To recover the neutral cluster size distribution from the measured mass spectra, the probability f_{nk} for the neutral cluster of size n to fragment to

an ion of size k , $M_n \rightarrow M_k^+$, is needed. It can be determined as

$$f_{nk} = N_{nk} / \sum_{k=1}^n N_{nk}, \quad (3.10)$$

where N_{nk} is the intensity of the neutral cluster of size n detected at the mass corresponding to the ion fragment M_k^+ . Hence to calculate the fragmentation probability one has to measure the intensity N_{nk} . The intensity is a complicated function

$$N_{nk}(\Theta) = A\rho_n\sigma_n(\Theta)C_n f_{nk}, \quad (3.11)$$

where ρ_n is the density of neutral clusters of size n in the beam, σ_n is the differential scattering cross section with the target (He) beam in the LAB system, C_n is the total ionization cross section, and the constant A contains all the other scattering characteristics not relevant to the cluster size separation.

In our experiment two types of measurements are usually performed. First, the angular distribution for the sequence of ionic fragments $k=1, 2, \dots$ is measured. The intensity of the detected signal S_k at a given angle Θ is the sum of the contributions from all the neutral precursors which can be scattered to that angle.

$$S_k(\Theta) = \sum_{n=k}^{n_{max}(\Theta)} N_{nk}(\Theta). \quad (3.12)$$

The second type of measurements are TOF spectra measurements in which a pseudorandom chopper is used in conjunction with the quadrupole mass spectrometer to measure the time dependent signal of a particular ion mass, i.e. the velocity distribution. As can be seen from Fig. 3.3, the neutral clusters with sizes allowed at a given scattering angle ($n \leq n_{max}(\Theta)$) arrive with different velocities depending on their size. By measuring the TOF distributions the relative integrated intensities X_{nk} can be determined

$$X_{nk}(\Theta) = N_{nk}(\Theta) / \sum_{n=k}^{n_{max}(\Theta)} N_{nk}(\Theta), \quad (3.13)$$

where the sum in the denominator represents an integral of the measured TOF spectrum over the final LAB velocity \vec{v} . Using Eqs (3.12) and (3.13)

the fragmentation probabilities can be calculated as follows

$$f_{nk} = S_k X_{nk} / \sum_{k=1}^n S_k X_{nk}. \quad (3.14)$$

where the normalization condition is given by $\sum_{k=1}^n f_{nk} = 1$. Here f_{nk} is expressed in terms of two measurable quantities: S_k obtained from the angular distributions and X_{nk} from the analysis of the normalized TOF spectra.

This method to determine the neutral cluster size distribution has also been exploited recently in experiments where the fragmentation of clusters after ionization was determined in our laboratory [89, 93, 94]. However, these experiments are not subject of this thesis. It should be also noted that the scattering method for the size selection can be employed only for small clusters (roughly $n \leq 10$, depending on the species), which can be resolved angularly. For the large clusters the neutral cluster size distributions were determined by other methods, e.g., a non-destructive ionization methods and mass spectrometry [77, 76] mentioned in Sec 3.2.

3.4 Photodissociation experiment

In this section first the general physics of the photodissociation process will be briefly outlined. Then the WMTOF spectrometer will be described in Sec. 3.4.1 as a tool for the photodissociation experiments, and finally in Sec. 3.4.2 the principles of the experiment will be explained on an example of the photodissociation of the HBr molecules and clusters.

The basic idea of photodissociation has been mentioned in the introduction Sec. 2.2. Here, the photodissociation is illustrated on the example of the HBr molecule. Fig. 3.4 shows schematically the potentials involved in the photodissociation process: the ground state $X^1\Sigma_0^+$, and the repulsive excited electronic states $A^1\Pi_1$, $a^3\Pi_1$ and $a^3\Pi_0^+$.³ The $A^1\Pi_1$ and $a^3\Pi_1$ states correlate with the Br atom in the ground $^2P_{3/2}$ state in the dissociation limit, while

³It should be mentioned that altogether 12 electronically excited states are involved in the photodissociation processes of hydrogen halides in general. For HBr only the 3 excited states discussed above can be excited directly from the electronic ground state due to the selection rules for electronic dipole transition.

the $a^3\Pi_0^+$ potential leads to the spin-orbit excited state $\text{Br}^*(^2P_{1/2})$. The excitation $X^1\Sigma_0^+ \rightarrow a^3\Pi_0^+$ is a parallel transition, while the transitions to the $A^1\Pi_1$ and $a^3\Pi_1$ states are perpendicular⁴. The underlying mechanism of HBr photodissociation has been studied and understood in detail [95, 96, 97] also with the present apparatus [98]. At 243 nm used in our experiment the dissociation to the Br ground state proceeds through the excitation to the $A^1\Pi_1$ state which is a perpendicular transition, and the excited Br^* state can be populated in a parallel transition via the $a^3\Pi_0^+$ state.

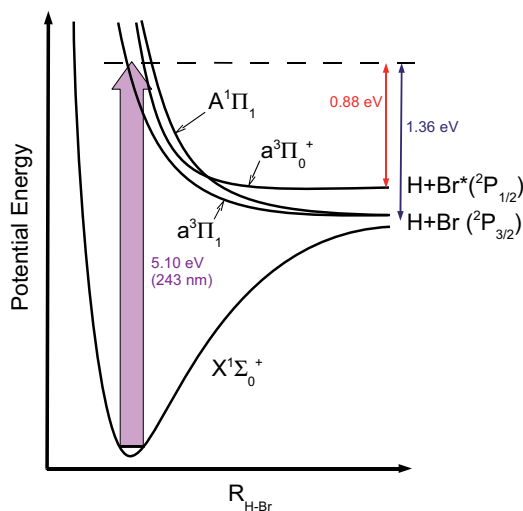


Figure 3.4: PESs involved in photodissociation of the HBr molecules. The vertical excitation with 243 nm (5.10 eV) is shown by the broad vertical arrow. The excited states $a^3\Pi_1$ and $A^1\Pi_1$ correlate with the ground state $\text{Br}(^2P_{3/2})$ in the dissociation limit, while the dissociation in $a^3\Pi_0^+$ state leads to the spin-orbit excited state $\text{Br}^*(^2P_{1/2})$. In the former process 0.88 eV excess energy is released into the relative kinetic energy of the fragments, while in the latter one it is 1.36 eV.

The kinetic energy of the H fragment $E_{kin}(H)$ measured in our experiment

⁴In principle parallel (perpendicular) transition means that the transition dipole moment of the molecule is parallel (perpendicular) to the molecular axis. In other words, the parallel (perpendicular) transition can be excited with a linearly polarized light oriented with the polarization electric field \vec{E}_L vector parallel (perpendicular) to the molecular axis.

can be interpreted in terms of the energy balance equation

$$h\nu + E_{int}(HBr) = D_0 + E_{int}(Br) + E_{kin}(Br) + E_{kin}(H), \quad (3.15)$$

where the laser energy $h\nu$ and the dissociation energy $D_0(HBr) = 3.745$ eV are known. The Br fragment kinetic energy $E_{kin}(Br)$ follows from the conservation of momentum. The HBr molecule dissociates to the Br atom either in the ground $^2P_{3/2}$ or the excited $^2P_{1/2}$ state with the excitation energy $E_{int}(Br)$ of 0.475 eV. The electronic excitation of the Br atom is reflected by the energy loss of the H atom. On the other hand an initial internal excitation of the HBr molecule $E_{int}(HBr)$ is reflected as a kinetic energy gain of the H fragment. Thus at the wavelength of our laser 243 nm (5.10 eV) the photodissociation from the $v=0$ vibrational level of the ground electronic state will yield H atoms with $E_{kin}(H) = 1.34$ eV and 0.87 eV corresponding to the generation of Br atom in the ground or excited state, respectively.⁵ An example of such H-fragment kinetic energy distribution after HBr photodissociation will be presented in Sec. 3.4.2, where the influence of cluster environments on this distribution will be discussed.

Besides the fragment kinetic energy, additional information, which can in principle be obtained from our experiment, is the H-fragment angular distribution. The distribution $I(\theta)$ is a product of $\vec{E}_L - \vec{\mu} - \vec{v}$ vector correlation, where \vec{E}_L is the electric field vector of the linearly polarized laser, $\vec{\mu}$ is the transition dipole moment for the excitation driven by the laser field, and \vec{v} is the resulting fragment velocity. For diatomic molecules $\vec{\mu}$ can be either parallel or perpendicular to the molecular axis. If the photodissociation is fast compared to the molecular rotation $\tau_{dis} \ll \tau_{rot}$, the fragment velocity vector \vec{v} lies in the molecular axis. This situation is illustrated in Fig. 3.5. It can be shown that the resulting fragment angular distribution is given by

$$I(\theta) = \frac{\sigma_0}{4\pi} (1 + \beta P_2(\cos \theta)), \quad (3.16)$$

where σ_0 is the photodissociation cross section and $P(x) = 1/2(3x^2 - 1)$ is the second order Legendre polynomial. The anisotropy parameter β as-

⁵The total energy, $E_{tot} = 1.36$ eV and 0.88 eV, released in the photodissociation process is partitioned between the kinetic energy of H and Br fragments. Thus, considering the momentum conservation, the kinetic energy of H-fragment is $E_{kin}(H) = E_{tot} \times \frac{m_{Br}}{m_H + m_{Br}}$.

sumes values between -1 and +2 for perpendicular and parallel transitions, respectively. Fig. 3.5 shows the corresponding $I(\theta)$ distributions.

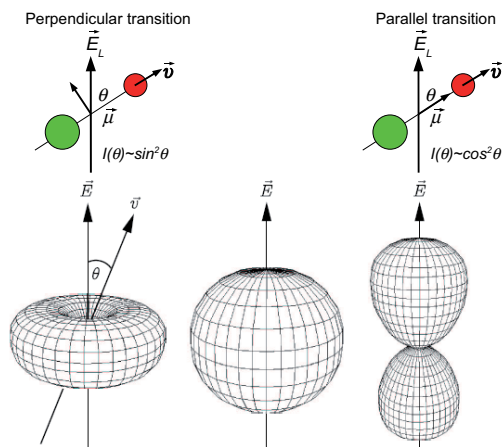


Figure 3.5: Top panel: illustration of the \vec{E}_L - $\vec{\mu}$ - \vec{v} vector correlation (\vec{E}_L -laser electric field vector, $\vec{\mu}$ -transition dipole moment, \vec{v} -fragment velocity). Lower panel: the fragment angular distributions for a perpendicular transition ($I(\theta) \propto \sin^2 \theta$, $\beta = -1$, left), parallel transition ($I(\theta) \propto \cos^2 \theta$, $\beta = +2$, right), and isotropic distribution ($\beta = 0$, center).

Before HBr photodissociation in cluster will be discussed in Sec. 3.4.2, our experimental tool –the WMTOF spectrometer– will be briefly described in the next section.

3.4.1 Willey-McLaren Time-of-Flight Spectrometer

The photodissociation, which is the major experiment on our apparatus, is performed in the time-of-flight spectrometer of the Wiley-McLaren type. Besides, the spectrometer is also used for the photoionization and subsequent TOF mass spectrometry experiment. Therefore, the WMTOF spectrometer will be briefly described here before going into the details of the photodissociation measurements.

Fig. 3.6 shows schematically the design of the two-stage TOF spectrometer according to Wiley and McLaren [67]. The basic principle is that the ions produced at the distance s_0 from the extraction plate are accelerated

3.4. Photodissociation

by the electric potentials U_s and U_d into the field free region and arrive to the detector at different times according to either their different *masses* or different *initial kinetic energies*, depending on the mode of operation of the spectrometer. In so called *high field mode* it works as the mass spectrometer, while in the *low field mode* the initial kinetic energies of the particles are measured.

The spectrometer resolution is given by $t/\Delta t$, where Δt is the FWHM of the peak of ions arriving around time t . It is limited among other factors also by the finite ionization volume. The basic idea of the Wiley-McLaren design is the space focusing: the particles, which are ionized at a distance further away from the first extraction plate start at somewhat higher potential than the particles ionized closer to the first extraction plate. The former ions are thus accelerated by the field to a higher velocity with which they enter the drift region. Therefore, the faster ions will overtake the slower ones at some point along the flight path. If they meet exactly at the detector position they arrive at the same time and the time difference due to the finite initial ionization displacement will be zero, $\Delta t=0$. This space focusing condition can be fulfilled at the detector position for the given spectrometer geometry by tuning the extraction potentials U_s and U_d . Operating the TOF with the set of voltages satisfying this condition maximizes its resolution. The other factors leading to the finite resolution are the finite ionization- and detection-time and the velocity distribution of the fragments before the ionization. This later factor is actually the observable, which is measured in the low-field mode.

The solution of the equation of motion of an ion in the electric fields of the TOF spectrometer can be found, e.g., in the original Ref. [67] and for our particular geometry also in [66]. In the high-field mode (extraction voltage of typically $\sim 200 \text{ Vcm}^{-1}$) the WMTOF is used as the mass spectrometer and the arrival time of an ion is $t \propto \sqrt{m}$.

In the low-field mode with a small extraction electric field ($\sim 1\text{-}10 \text{ Vcm}^{-1}$) the ions with the same initial velocities pointing in the opposite directions \vec{v}_i and $-\vec{v}_i$ arrive at the detector at different times displaced by τ , which is called turn-around time. In the middle between them arrive the ions with initially zero velocity. This will be further illustrated on an example of HBr

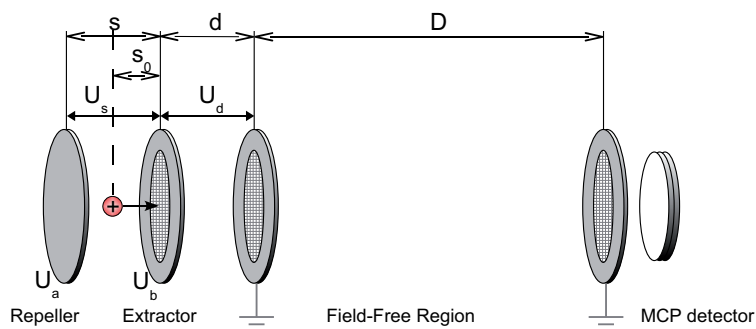


Figure 3.6: Schematic illustration of the two-stage TOF spectrometer according to Wiley and McLaren [67]. The particle ionized in the middle s_0 between Repeller and Extractor is first extracted by the potential difference U_s and then accelerated by U_d into the field free region (D) and its arrival time at the MCP detector is recorded.

photodissociation in the next section.

3.4.2 Photodissociation of a molecule in cluster

To understand the spectra resulting from the photodissociation of a molecule in the cluster, first the photolysis of a free molecule will be analyzed. At the beginning of Sec. 3.4 the physical principles of the photodissociation of HBr were outlined. These processes occurring in the WMTOF extraction region are illustrated in Fig. 3.7. With *linearly* polarized light only the molecules are dissociated, which are *aligned* so that their transition moment is close to *parallel* to the laser polarization direction. Thus with the laser polarization parallel to the WMTOF axis (0°) only the H-fragments can be detected originating from excitation of dissociative states with the transition moment parallel to the molecular bond. The molecules are dissociated in two opposite orientations with the H-atom pointing towards and away from the detector. The former H-fragments will arrive earlier into the detector than the latter ones, which have to be turned around first by the extraction field⁶.

⁶It should be noted that after the molecule photodissociation the H-fragment has to be ionized in order to be detected. Both photodissociation and photoionization processes take place almost at the same time (within the laser pulse duration of ~ 10 ns) and in the

This results in two peaks in the TOF spectrum as indicated schematically in Figure 3.7. The time distance τ (*turn-around time*) between these peaks corresponds to the energy released in the dissociation process. The dissocia-

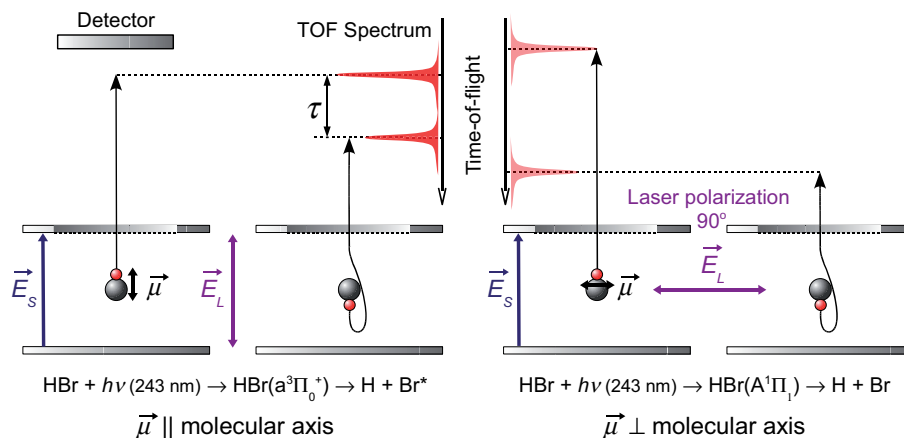


Figure 3.7: Schematic illustration of the HBr molecule photodissociation process in the WMTOF spectrometer and the corresponding TOF spectra generation. The excitation into the $a^3\Pi_0^+$ electronic state with the transition moment parallel to the molecular axis proceeds with the laser polarization 0° . The molecule is dissociated with the H atom pointing towards the detector resulting in the earlier arriving fragments, or with the H atom oriented in the opposite direction resulting in the late fragments. The peaks of early and late arriving fragments are separated by the turn-around time τ corresponding to the energy released in the photodissociation. The excitation into the $A^1\Pi_1$ state is a perpendicular transition and, therefore, the fragments are detected when it proceeds with the laser polarization 90° . Since this state correlates to the Br ground spin-orbit state, more energy is released in the dissociation process resulting in a larger time separation of the TOF peaks τ .

tive states with the transition moment perpendicular to the molecular bond can be also dissociated by the 0° polarized laser, but the initial fragment velocities will carry them out of the detector acceptance angle. Analogically for the laser polarization perpendicular to the WMTOF axis (90°) only the fragments originating from excitations with the transition moment perpendicular to the molecular bond can be detected.

same place (in the tight laser focus of $\sim 10 \mu\text{m}$ diameter).

With the 243 nm laser the former case of 0° polarization corresponds to the excitation of the $a^3\Pi_0^+$ leading to the population of Br^* state, as outlined at the beginning of Sec. 3.4. On the other hand the 90° polarized light excites the $A^1\Pi_1$ state yielding the ground state Br. In the former case of Br^* population less energy is released, therefore, the peaks in the TOF spectrum are closer together than in the later case.

Now the photodissociation of the HBr molecule in the cluster environment can be discussed. The kinetic energy of the H fragment $E_{kin}(H)$ will be given by energy balance similar to the Eq. 3.16 for the single molecule

$$h\nu + E_{int}(\text{HBr}) = D_0 + E_{int}(\text{Br}) + E_{kin}(\text{Br}) + E_{kin}(H) + E_{clu}. \quad (3.17)$$

The influence of the cluster is included by the term E_{clu} , which expresses a continuous energy loss of the H atom caused by collisions and capturing processes by the cluster cage. Thus we can distinguish essentially three cases of photofragment behavior in the cluster: (i) The H-atom leaves the cluster after the photolysis without losing any energy in interactions with the cage atoms, i.e. $E_{clu} = 0$ (*direct cage exit*). In this case the corresponding peaks occur in the TOF spectrum on the sides at arrival times corresponding to the maximum energy available for the fragment. (ii) In the other extreme case the H fragment can lose all of its kinetic energy in the collisions with the cage atoms, i.e. $E_{kin}(H) = 0$ (*cage effect*). The corresponding peak appears at the center of the TOF spectrum. (iii) Finally, in an intermediate case the fragment loses part of its energy in collisions and escapes the cage (*delayed cage exit*). In this case the signal appears on the shoulders of the TOF spectrum between the exit peaks and the central zero kinetic energy peak.

All these contributions can be seen in Fig. 3.8, which shows the measured TOF spectra from photodissociation of $(\text{HBr})_n$ $\bar{n} \approx 10$ clusters. Peaks corresponding to the direct exit on the sides are indicated by arrows. The spectrum exhibits the zero kinetic energy peak at the centre and some intensity in between corresponding to the delayed fragments.

In the data analysis process the measured TOF spectrum is usually converted to the kinetic energy distribution (KED) of the fragment H atoms. The analysis involves the complete Monte-Carlo (MC) simulation of the par-

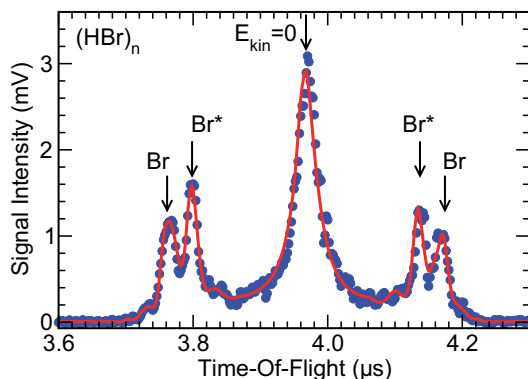


Figure 3.8: H-fragment TOF spectrum from $(\text{HBr})_n$ $\bar{n} \approx 10$ clusters produced in expansion of 5% HBr in Ar at pressure $p_0=1.5$ bar and nozzle temperature $T_0=258$ K measured at 243 nm wavelength with 2.9 mJ/pulse 0° polarization. Peaks of the direct cage exit corresponding to the ground Br and excited Br^* state fragments are indicated. The middle peak corresponds to the zero kinetic energy fragments $E_{kin} = 0$ eV.

ticle trajectories, which is carried out, considering the molecular beam data, the photodissociation process parameters, the WMTOF geometry, the finite interaction volume, and the detector electronic response. The way how the simulation is done is described in detail in Refs. [66, 98, 99]. It is worth noting that in our experimental arrangement, the detection probability is extremely enhanced at the small kinetic energies so that we are in particular sensitive to the caged atoms [99]. This can be seen in Fig. 3.9 where the H-fragment KED from $(\text{HBr})_n$ $\bar{n} \approx 10$ clusters is shown, obtained by the TOF \rightarrow KED conversion of the spectrum in Fig. 3.8. Clearly the strong zero kinetic energy peak in the middle of the TOF spectrum transforms to a very small maximum at $E_{kin}(H) = 0$ in the KED spectrum. The direct cage exit peaks appear in the KED at energies $E_{kin}(H) = 1.34$ and 0.87 eV derived at the beginning of Sec. 3.4.

It can be also noted that some intensity appears at energies exceeding the maximum available energy. From Eq. 3.17 it follows that these fragments have to originate from initially vibrationally excited HBr molecules. The mechanism of vibrational excitation of a molecule by frustrated dissociation

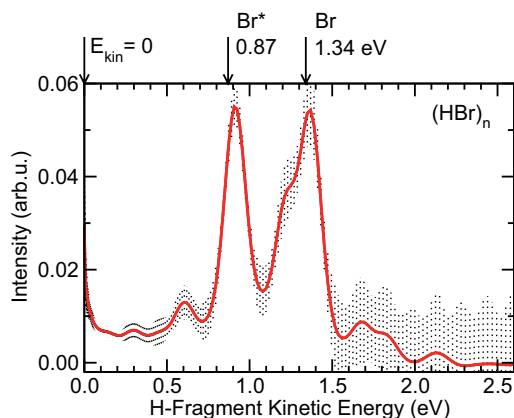


Figure 3.9: H-fragment KED from $(\text{HBr})_n$ $\bar{n} \approx 10$ clusters obtained from the TOF spectrum in Fig. 3.8. Peaks of the direct cage exit and the zero kinetic energy peak are indicated. The dotted area indicates the 90% confidence interval of the fit.

in clusters has recently been revealed in our experiment with photodissociation of acetylene molecules in various clusters [100]. It has been found that the C_2H_2 molecules can be initially excited into a dissociative state but caged by the cluster and recombined to the electronic ground state, yet vibrationally excited. These vibrationally excited molecules were then photodissociated by the next photon yielding the faster fragments.

We have increased the average time delay between the subsequently arriving photons by decreasing the laser photon fluence and thus the excited molecule could dissipate more energy into the cluster before absorbing the dissociating photon, which led to less amount of the faster fragments. This is schematically illustrated in Fig. 3.10. It is interesting to note that this way, we are actually able to obtain information about the cluster dynamics in the time domain from the measurements in the energy domain (i.e. the measurements of the kinetic energy of the H-fragments). Indeed, such measurements cannot substitute the time-resolved experiments [101, 52] but can provide an interesting alternative to study the dynamics in clusters and are capable of delivering a complementary information.

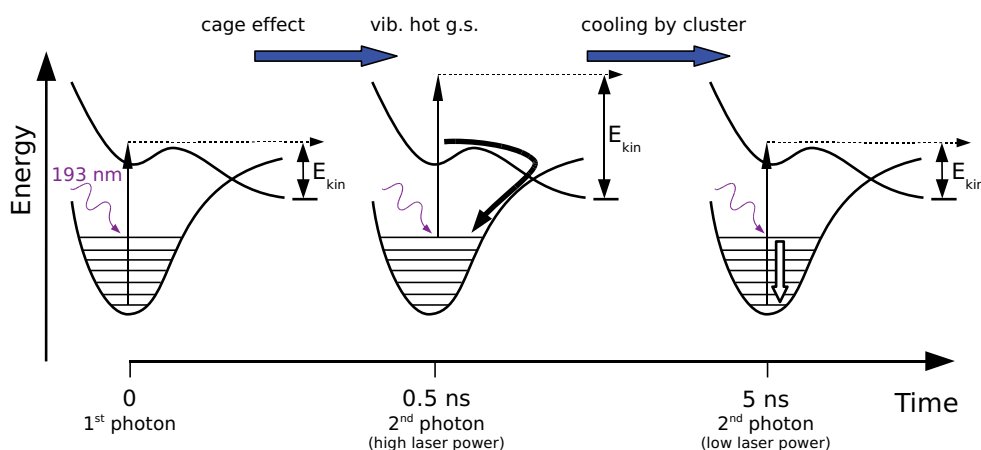


Figure 3.10: Schematic illustration of the photodissociation dynamics reflected by the fragment kinetic energy measurements: The molecule is promoted to an excited dissociative state but can be caged by the cluster environment and undergo a transition through a conical intersection to a vibrationally excited electronic ground state. The next arriving photon can excite the vibrationally hot molecule resulting in the fragments with higher kinetic energy E_{kin} . If the delay between the successive photons is increased by using lower laser intensities, the vibrational relaxation of the molecule by cluster cooling can result in less energetic fragments. (Adopted from photodissociation measurements of C_2H_2 in clusters [100].)

3.5 Laser system

From the point of view of the employed laser systems, essentially two kinds of experiments are performed: (i) one color experiments, where the wavelength of 243 nm is used to photodissociate the molecules and subsequently to photoionize the H-fragment by resonance enhanced multiphoton ionization (REMPI) in a 2+1 excitation scheme⁷; (ii) two color experiments in which the molecules are photodissociated at 193 nm and the H-fragments are subsequently photoionized with the 243 nm laser.

The wavelength of 243 nm is generated by mixing the 1064 nm funda-

⁷The simultaneous two-photon excitation with 243.06 nm wavelength corresponds to the $1s \rightarrow 2s$ transition in the H atom and the additional third photon then brings the electron from the 2s level into the ionization continuum resulting in the proton H^+ .

3.5. Laser system

CHAPTER 3. EXPERIMENT

mental of a Nd:YAG laser (Quanta Ray GCR-5) with the frequency doubled output of a dye laser (LAS, LDL 20505) operated at 630.3 nm, and pumped by the second harmonic of the Nd:YAG laser, i.e. 532 nm (see Fig. 3.11). The laser pulses are repeated at a frequency of 10 Hz with a pulse length of 5 ns. The laser beam is focused into the detector chamber by a 400 mm quartz lens onto a spot of 14 μm radius in the intersection point of the cluster beam and the WMTOF axis. The laser beam and the WMTOF axis are perpendicular to each other. The typical laser energies range between 2–4 mJ/pulse resulting in laser intensities at the focal spot of the order of 10^{10} Wcm^{-2} which translates into a typical photon flux of the order of $10^{28} \text{ s}^{-1}\text{cm}^{-2}$. The polarization of the linearly polarized laser light can be turned parallel (0° polarization angle) or perpendicular (90° polarization angle) with respect to the WMTOF axis by passing the beam through a series of 90° turning prisms. It ought to be mentioned that the present laser system can in principle be tuned in the UV range between 217 nm and 437 nm by tuning the dye laser wavelength and exchanging the various mixing crystals in the WEX. However, this option was not exploited in the present experiments, where the hydrogen fragments were detected exclusively.

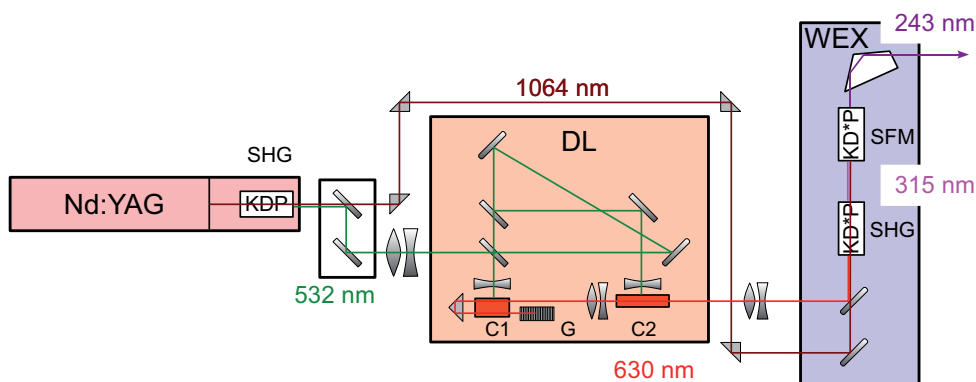


Figure 3.11: Schematic picture of the tunable UV laser system. Nd:YAG laser produces 1064 nm radiation, which is frequency doubled (SHG) in a nonlinear KDP crystal to 532 nm. By this wavelength the dye laser (DL) is pumped producing 630 nm. In the wavelength extender (WEX) the 630 nm is frequency doubled to 315 nm, which is then added with the original 1064 nm (SFM) resulting in 243 nm.

3.5. Laser system

The 193 nm laser light is produced by an ArF/F₂-Excimer laser (Lambda-Physics: LFP 202). The emitted light is unpolarized, and it can be polarized using a thin film polarizer (TFP). It is sent into the detector chamber perpendicularly to both, the cluster beam and the WMTOF axis. The angle between the 193 nm and 243 nm laser beams is 17.5° in the plane encompassing the molecular beam. The rotation of the TFP about the laser beam axis allows to change the laser light polarization from 0° to 90° polarization angle with respect to the WMTOF axis. The laser beam is focused into the chamber by a 366 mm LiF lens. To determine the spot size of the laser beam which is in principle rectangular, the laser beam shape was measured at various positions along the beam and the spot area at the intersection point with the molecular beam was calculated from these measurements. This area is approximately 10⁻⁴ cm⁻². The laser energy can be varied up to 200 mJ/pulse of unpolarized light at the laser output with the pulse duration of approximately 20 ns, i.e. at the highest energy the corresponding unpolarized laser intensity interacting with the molecular beam is 10¹⁰ Wcm⁻², which corresponds to the photon flux of 10²⁸ s⁻¹cm⁻². The use of TFP lowers the intensity by more than an order of magnitude.

Critical to the two-color experiments is the beam overlap in time and space. The time synchronization of the two laser beams is achieved by triggering the excimer laser by the Nd:YAG laser pulses via a pulse delay generator (Stanford Research: DG 535). Experimentally challenging is the spatial overlap of the two laser beams focussed to a tight spot with the intersection point of the cluster beam and the WMTOF axis. The overlap was adjusted with the intensity, and the symmetric shape of a time-of-flight (TOF) spectrum of the test HBr/Ar_n system.

Chapter 4

Results

4.1 Photodissociation of hydrogen halides in rare gas clusters

In this first Result section some of the studies will be presented, which were performed with the present apparatus still in Göttingen. They concerned the photodissociation of hydrogen halides on the surface and in the interior of the rare gas clusters. The clusters of rare gas atoms as a non-reactive and relatively weakly interacting medium represent a structureless and chemically inert solvent archetype, in which the photodissociation is studied. These studies were mostly motivated as studies of model systems for future investigations of atmospherically relevant processes such as the photodissociation of hydrogen halides on ice nanoparticles discussed in Sec. 4.2. However, it ought to be emphasized that a number of interesting and important phenomena was discovered in these model rare gas systems, and their detailed understanding gained by this research enabled the understanding of the new phenomena observed in the systems with more practical relevance such as the ice nanoparticles of atmospheric importance or clusters of model biomolecules, studied in our laboratory in Prague. Some of the major results obtained in the rare gas systems will be summarized in the following subsections and further details can be found in the corresponding publications outlined in Appendix B.

4.1.1 Photodissociation of hydrogen halides on argon clusters

Before presenting the results of the hydrogen halide photodissociation on Ar_n clusters it is useful to recall the photodissociation of the bare molecules. In Sec. 3.4 we have already illustrated the hydrogen halide dissociation on the case of HBr. Fig. 3.4 shows the potential energy curves of the excited states relevant for the photodissociation.

In the general case of HX molecule photodissociation the involved excited states are in principle the same. The excited states $a^3\Pi_1$ and $A^1\Pi_1$ correlate with the ground state $X(^2P_{3/2})$ in the dissociation limit, while the dissociation in $a^3\Pi_0^+$ state leads to the spin-orbit excited state $X(^2P_{1/2})$.¹ The energetics is, indeed, different for the different hydrogen halides, and so is the transition dependence on the laser polarization and the branching ratio for the excited and ground spin-orbit state population $R = [X^*]/[X]$.

For the HI molecule the $^3\Pi_1$ and $^1\Pi_1$ correlating with the ground state I are populated by a perpendicular transition ($\beta = -1.0$), while the $^3\Pi_0^+$ state leading to the spin-orbit excited state I^* is reached in a parallel transition ($\beta^* = 2.0$). Thus HI exhibits a strict separation with the parallel transition to the excited and perpendicular transition to the ground spin-orbit state. It turns out that at the wavelength of 243 nm these transitions occur with roughly equal probabilities, i.e. that the branching ratio is about $R \approx 1$. At 193 nm excitation wavelength the absorption due to the $^3\Pi_1$ and $^3\Pi_0^+$ states dies out so that only the excitation to the $^1\Pi_1$ state remains, which is a pure perpendicular transition leading to the ground spin-orbit state of iodine.

In case of HCl molecule only the $^1\Pi_1$ state is excited directly in a perpendicular transition ($\beta = -1.0$) from the ground state, which would lead to the population of the ground Cl state exclusively. However, during the dissociation process the other dissociative states ($^3\Pi_1$, $^3\Sigma_1^+$) are populated via non-adiabatic spin-orbit couplings resulting in the population of the excited Cl^* state. At 193 nm the branching ratio $R \approx 0.69$ was measured and anisotropy factors $\beta = -1.01$ and $\beta^* = -0.94$.

¹In principle for HI also another dissociative state $t^3\Sigma_1^+$ leading to the excited I^* fragment can be populated at wavelengths below 200 nm

HBr represents an intermediate case where the excitation depends on the wavelength. The excitation at 243 nm has been briefly discussed in Sec. 3.4. The dissociation to the Br ground state proceeds through the excitation to the $^1\Pi_1$ state which is perpendicular ($\beta_{243nm} = -0.96$), and the excited Br* state can be populated in a parallel transition via the $^3\Pi_0^+$ state ($\beta_{243nm}^* = 1.96$). At the shorter wavelengths the excited Br* state can be populated via a perpendicular transition caused by coupling into the $^3\Sigma_1^+$ state. This results in $\beta_{193nm}^* \approx 0.00$. The branching ratio remains $R \approx 0.15-0.20$ over the entire wavelength region, i.e. mainly the ground state Br fragments are produced.

One of the essential questions asked in the experiments below was, how this complex photodissociation behaviour of the HX molecules outlined above is influenced by the clusters.

Photodissociation of HI on Ar_n

Hydrogen iodide HI molecules were deposited on Ar_n clusters, with an average size $\bar{n} \approx 139$, and photodissociated at 243 nm. The experiment was carried out for different laser polarizations 0° and 90° . The measured H-fragment KEDs exhibited a strong fraction of completely caged fragments at zero kinetic energy and pronounced peaks at the unperturbed cage exit positions corresponding to both spin-orbit channels leading to I and I*. Surprisingly, these peaks are present in almost the same intensity in the spectra obtained with both laser polarizations. As outlined above, at this wavelength the bare HI molecule exhibits a strict state separation, with a parallel transition to I* and perpendicular transitions to the ground state I.

Theoretical molecular dynamics simulations were employed to elucidate the experimental results. The HI dopant landing on the surface of the argon cluster during the pick-up process was simulated resulting in occupation of a substitutional position on the cluster surface. The HI molecule is oriented with the H atom pointing into the cluster interior. Therefore, part of the H-fragments after the photodissociation penetrates deep into the cluster and is caged. However, the libration motion of the HI molecule yields some fragments scattered elastically from the Ar atoms of the cluster surface leading to

4.1. *HX in rare gas clusters*

the cage exit fragments. The scrambling of the intensities resulting from the perpendicular and parallel transitions is explained by the scattering, which can direct into the detector even the fragments from the molecules dissociated with the “wrong” orientation (i.e. the orientation, which would lead to the loss of the H-fragment from the detection in the case of a bare molecule dissociation, however, the scattering with the cluster atoms can redirect these fragments into the detector). The simulations reproduced the experimental spectra remarkably well.

Further details of these experiments and calculations can be found in Ref. [102].

Photodissociation of HCl on and in Ar_n

Photodissociation in Ar_n clusters doped with HCl molecules in the pickup process was studied, in the mean cluster size region $\bar{n} \approx 140\text{--}1000$. The molecules were excited at 193 nm. The KEDs of the H-fragments are completely dominated by the peaks at zero kinetic energy corresponding to the fragment caging. The spectra did not exhibit any significant intensity at the energies of the direct cage exit. These results were explained by accompanied theoretical calculations, which showed that the HCl molecule was deeply buried in a substitutional position in the outer shell of the Ar-cluster. The HCl orientation was with the H atom pointing directly into the cluster interior. Therefore, the H-fragments enter the cluster after the photodissociation and lose their energy in the collisions with the Ar atoms and remain caged with zero kinetic energy.

In addition, the experiments were performed also with HCl molecules embedded in the Ar_n clusters. These species were produced by coexpansion of a diluted HCl/Ar mixture. Depending on the mixture concentration small $(\text{HCl})_m$ clusters inside larger Ar_n complexes were produced. In these experiments additional peak at approximately 2 eV appeared in the KED spectra in addition to the zero kinetic energy peak. This high energy peak corresponded to the unperturbed cage exit fragments. The peak corresponding to the cage effect increased in intensity with respect to the cage exit peak with the increasing cluster size. All these observations were also elucidated by the

4.1. *HX in rare gas clusters*

simulations. The cage exit fragment in the case of HCl molecule embedded in the Ar_n cluster corresponds to the molecule dissociated in a favourable orientation in which the H-fragment can escape between the cluster atoms without losing energy in scattering with them. These experiments and calculations are detailed in Ref. [103].

Photodissociation HBr on Ar_n

Single HBr molecules deposited on the surface of large Ar_n clusters, $\bar{n} \approx 159$, in the pickup process were photodissociated at the wavelength of 193 nm. Dependence on the polarization of the photodissociation laser was investigated at 0° , 90° and 54.7° polarization.² The H-atom KED exhibited a zero energy peak corresponding to the caged fragments and an additional broad peak close to the direct cage exit position.

The analysis of the polarization dependence of the spectra showed that the photodissociation dynamics did not change from the one of a bare HBr molecule by placing it on the Ar cluster. Namely that both the ground and spin-orbit excited Br states are mainly populated by a perpendicular transition (to $^1\Pi_1$ state) with a small admixture of a parallel transition for Br^* population.

These experiments together with the results of $\text{HBr}\cdot\text{Ar}_n$ photodissociation at 243 nm measured previously [99, 85] were compared with molecular dynamics simulations, which accounts for the quantum libration delocalization of the H atom at the finite temperature of the HBr molecule of 27 K. These calculations yield a very good agreement with the observed spectra and reveal the physical mechanism of the excitation process. At both wavelengths the excitation proceeds through a perpendicular transition into the ground spin-orbit state. At 243 nm in the tail of the Franck-Condon overlap this remains practically the only channel. At 193 nm in the middle of the Franck-Condon region the population of the excited state seems larger than that of the ground state since the cage exit is mainly caused by slowed down H atoms. Further details can be found in Ref. [104].

²The polarization angle of 54.7° is equivalent to the action of an unpolarized light.

Comparison of photodissociation of HI, HBr and HCl on Ar_n

Since the above results for HI, HCl and HBr molecules were published in separate papers it is useful to provide a brief direct comparison of the main results here. The comparison is illustrated schematically in Fig. 4.1.

First, the comparison of a photodissociation of HBr and HCl molecules on Ar_n clusters at 193 nm is made. While the H-fragments from HBr molecules exhibited significant cage exit no evidence for such process was observed for HCl molecule, where only the caged atoms with near-zero kinetic energy were measured. This could be rationalized by the fact that the smaller HCl molecule fits better into a substitutional position on the Ar_n cluster surface, leading to the higher caging probability.

Second, the comparison between HBr and HI on Ar_n clusters at 243 nm reveals a very similar behaviour with both the ground X and the spin-orbit X^* states populated almost equally. While in the case of HBr both states are populated through a perpendicular transition, in the case of HI the ground state I is populated via a perpendicular transition and the excited state I^* population comes from a parallel transition. Besides, in HI the intensities corresponding to I and I^* populations are mixed by scattering processes from the surrounding Ar atoms of the cluster. This can be rationalized by libration motion and the larger size of the HI molecule, which does not fit into the substitutional position and sits more on the outside of the cluster surface, which in turn leads to the efficient H-fragment scattering.

4.1.2 Photodissociation of HBr and HCl in neon clusters: Are the neon clusters liquid or solid?

While the clusters of the heavier rare gas atoms beginning from Ar can be treated classically to some extent, helium clusters, on the other hand, exhibit properties such as superfluidity requiring a full quantum mechanical treatment [17, 70]. Neon cluster may represent a border case, where the classical treatment may be sufficient to describe some properties, while the quantum mechanics might be necessary for understanding of some other phenomena. Therefore, it was interesting to investigate the photodissociation process in neon clusters and compare it to the previous studies in the heavier rare gas

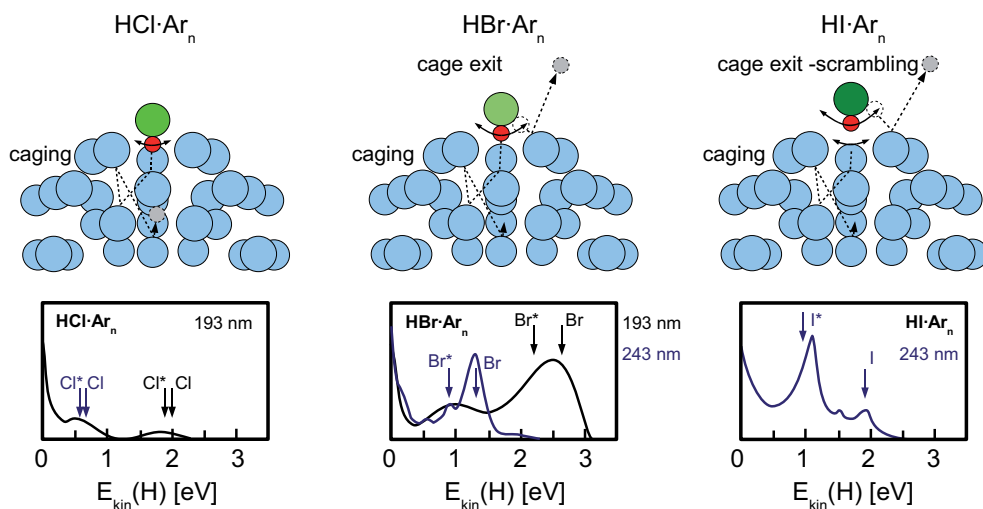


Figure 4.1: Schematic illustration of photodissociation of various hydrogen halides on Ar_n clusters. (a) HCl is buried deep in the substitutional position on the Ar_n cluster surface, leading to the caging of the H-fragment after the photodissociation. (b) HBr does not fit into the substitutional position completely, therefore, part of the fragments from librating HBr molecule can be elastically scattered from the surface and lead to the cage exit. (c) HI sits even more outside on the surface than HBr, therefore, the cage exit is even more pronounced and scrambling of the angular distributions from different polarizations occurs. At the bottom some representative KEDs are shown to illustrate these effects.

clusters, which were summarized for example in the review [19].

One of the intriguing results of the earlier investigations of photodissociation in Ne, Ar, Kr, and Xe clusters [19] was the dependence of the process on the initial site of the molecule in the cluster. The molecules could be either embedded in the cluster interior or deposited on the cluster surface. Experimentally, the surface or interior positions were prepared by a pick-up or coexpansion procedure, respectively, as outlined in Sec. 3.2. For the surface case, the H-fragment KEDs from HX (X= Br, I) dissociated on Ar_n, Kr_n and Xe_n exhibited similar features, but differed significantly from the KEDs produced by HX dissociation on Ne_n. This and further experimental evidence suggested that in case of neon the embedded molecules penetrated

into the cluster interior, which pointed to a liquid-like nature of neon clusters under the present experimental conditions, as opposed to the solid-like clusters of the heavier rare gases. Since the melting temperature depends strongly on the cluster size [105], a phase transition between solid-like and liquid-like behaviour should occur at some well-defined cluster size.

Therefore, in the present experiment the photodissociation of HBr and HCl on Ne clusters was studied as a function of the cluster size. The essential idea was that above the threshold size for solid-like cluster the dopant molecule was expected not to penetrate into the cluster interior and rather remain on the surface, which should then increase the fragment cage exit probability.

To extend the cluster size region of our cluster source a special cluster source assembly was designed and built which allowed cooling of the nozzle to lower temperatures down to 60 K, which were not attainable with our standard rare gas cluster source. With this modification the cluster size region between $\bar{n} \approx 100$ –1600 was covered.

Surprisingly, the experimental results exhibited no significant increase in the cage exit probability in the entire covered size region, which would be the manifestation of the transition to the solid-like surface state. However, this behaviour was justified by assuming that the outer surface shells remain liquid also for the larger clusters, which have frozen solid-like core. Thus the embedded molecule sinks deep into the surface layers, which then hinder the H atom dissociation fragment from leaving the cluster. This conclusion was based on the semiclassical molecular dynamics simulations that modelled the following aspects of the problem: (i) the landing of the dopant molecule during the pick-up process, (ii) the phase behaviour of the cluster, and (iii) the KEDs of the outgoing H-atoms. The theoretical calculations are in agreement with the experimental results and support the conclusion of the liquid-like neon cluster surface and dopant molecules buried deep in it. Further details can be found in Ref. [106].

4.2 Atmospherically relevant clusters

The motivation for the previous photodissociation experiments with hydrogen halide molecules on rare gas clusters in Göttingen was investigation of model systems for later studies of atmospherically relevant systems such as hydrogen halides on PSC particles, which play a key role in the ozone depletion process (see Sec. 2.2.1). Processes studied on large water clusters (ice nanoparticles) in the laboratory can actually mimic the processes on ice particles in the PSCs. Therefore, when the experiment was moved from Göttingen to the new laboratory in Prague, our major focus was to begin the studies of the large water clusters with hydrogen halide molecules $\text{HX}\cdot(\text{H}_2\text{O})_n$ ($\text{X}=\text{Cl},\text{Br}$) $\bar{n} \approx 10^2\text{-}10^3$. At the same time also pure $(\text{H}_2\text{O})_n$ clusters were investigated. The results were published in 4 papers listed in Appendix B. The general conclusions from them will be briefly outlined below and the interested reader is further referred to the corresponding publications for more details.

4.2.1 Hydrogen halides on water clusters

The question originally targeted by the photodissociation of hydrogen halide HX molecule on water clusters was, whether the hydrogen halide was covalently bound or ionically dissociated on the water cluster as introduced in chapter 2.2.1. The general idea of the experiment was essentially simple: If the molecule remained covalently bound on the cluster, it could be photodissociated by the laser radiation of the appropriate wavelength and the corresponding H fragment could be detected. If, on the other hand, the molecule was acidically dissociated to X^- and H_3O^+ the laser should not produce any hydrogen signal (provided that H_2O and H_3O^+ are not photolyzed at the applied wavelength). As is generally often the case in science, the interpretation of the experiment turned out to be much more complicated, and the observed H-fragment signal actually proved to be the experimental evidence for the acidic dissociation of the hydrogen halide on the cluster rather than for its covalently bound molecule, i.e., it turned out to be just the opposite of the original expectation. The major results will be briefly presented here and their analysis leading to the counterintuitive conclusion

above will be outlined.

The large water clusters of the mean cluster sizes $\bar{n} \approx 10^2$ - 10^3 were produced in the supersonic expansion, described in Sec. 3.2, and HX molecules were deposited on them in the pick-up cell so that on average the clusters contained a single HX molecule. These clusters were interacted with the 193 nm and 243 nm laser beams. The hydrogen fragments were REMPI ionized with the 243 nm laser radiation and their TOF spectra were recorded in the WMTOF low field mode. A relatively large H-fragment signal was observed in the experiment with $\text{HBr}\cdot(\text{H}_2\text{O})_n$.

Previously the H-fragment signals were measured from HBr molecules and clusters (see Sec. 3.4) [98], and from HBr on various rare gas clusters [99, 107, 103, 104] on the present experimental setup with the 243 nm laser only. However, in the experiment with HBr on water clusters the signal was only detected after the additional 193 nm excitation of the clusters.

The corresponding signal from pure $(\text{H}_2\text{O})_n$ clusters without HBr was more than an order of magnitude smaller than that from $\text{HBr}\cdot(\text{H}_2\text{O})_n$ suggesting that the H fragments originated from the HBr molecule on water cluster. To further confirm that the observed hydrogen signal did not originate from water, the experiment was performed with deuterated D_2O clusters. Deuterium was not detected in our experiment since the D-atom REMPI wavelength was outside the 0.04 nm bandwidth of our ionization laser. Besides the D^+ ion peak would occur at much longer flight times than the measured H^+ in the TOF spectra. Therefore, the somewhat lower H-fragment signal observed in the $\text{HBr}\cdot(\text{D}_2\text{O})_n$ experiment (see Fig. 4.3) should also originate from the HBr molecule.

Based on this observation we could conclude that in both experiments with normal and deuterated water clusters the observed H-fragment signal should originate from the covalently bound HBr. However, at this point also the experiment with DBr on $(\text{H}_2\text{O})_n$ clusters was performed. Indeed, no H-signal was expected in the experiment with $\text{DBr}\cdot(\text{H}_2\text{O})_n$.³ Yet a significant H-atom signal was measured from $\text{DBr}\cdot(\text{H}_2\text{O})_n$ system even larger than from $\text{HBr}\cdot(\text{D}_2\text{O})_n$.

³Note that deuterium was not detected and no significant signal was observed from $(\text{H}_2\text{O})_n$ clusters in the present experiments.

The puzzle of the strong H-fragment signal from the $\text{DBr}\cdot(\text{H}_2\text{O})_n$ clusters could be solved by postulating an H_3O radical molecule generated from HBr and H_2O molecules in the cluster. This idea followed from earlier theoretical predictions of H_3O species in similar systems by Domcke and Sobolewski. In a series of papers [108, 109, 110, 111, 112] they proposed theoretically the excitation of charge separated species such as the small zwitterionic clusters $\text{Cl}^-\cdot(\text{H}_2\text{O})_3\cdot\text{H}_3\text{O}^+$ to lead to the neutral H_3O radical. Fig. 4.2 depicts the suggested mechanism of the H_3O generation in our experiment: It starts with the acidic dissociation of the HBr molecule, forming a zwitterionic structure $\text{Br}^-\cdot\text{H}_3\text{O}^+\cdot(\text{H}_2\text{O})_{n-1}$, which is then excited by the 193 nm laser to an S_1 state of the charge-transfer-to-solvent (CTTS) character [109]. The system then relaxes into a biradical minimum with Br and H_3O neutral radicals, which can ultimately decay into water and the H atom detected [111, 108]. Several experimental findings and further arguments were found to support this mechanism and will be outlined below.

Double isotope substitution: The measurements with isotopic variants of HBr and H_2O provided a strong experimental evidence for the hypothesis that the detected H-atom originated from the H_3O species. On the right hand side of Fig. 4.3 the measured H-fragment TOF spectra from $\text{HBr}\cdot(\text{H}_2\text{O})_n$, $\text{DBr}\cdot(\text{H}_2\text{O})_n$ and $\text{HBr}\cdot(\text{D}_2\text{O})_n$ (top to bottom) are shown. The TOF spectra for the different isotope variations are identical in shape and their intensity ratio is 3.0:2.1:1.0. This ratio is in excellent agreement with the ratio of H atoms in H_3O , H_2DO and HD_2O species generated in the corresponding clusters by the above proposed mechanism as depicted schematically on the left hand side of Fig. 4.3. It ought to be mentioned that similar results were obtained also for HCl on water clusters and very recently also for HI.

The shape of the KED spectra: Further experimental evidence for the proposed H_3O generation mechanism was provided by the shape of the KED spectra. Left hand side of Fig. 4.4 shows the H-fragment KEDs from $\text{HBr}\cdot(\text{H}_2\text{O})_n$ (a) in comparison with $\text{HCl}\cdot(\text{H}_2\text{O})_n$ (b). In Fig. 4.4 (c) and (d) the H-fragment KEDs from $\text{HBr}\cdot\text{Ar}_n$ and $\text{HCl}\cdot\text{Ar}_n$ clusters, respectively, are shown for comparison. There are three important features of the spectra. First, the differences in KED shape between HBr and HCl on argon clusters

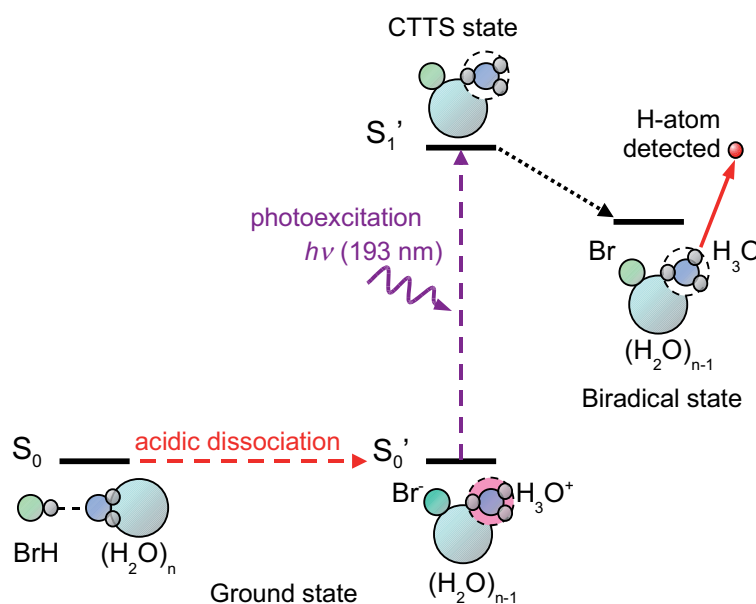


Figure 4.2: Proposed mechanism of the $\text{HBr}\cdot(\text{H}_2\text{O})_n$ cluster photochemistry: The acidic dissociation takes place in the ground state generating the zwitterionic species $\text{Br}^-\cdot\text{H}_3\text{O}^+\cdot(\text{H}_2\text{O})_{n-1}$, which is excited by the 193 nm laser radiation into the CTTS state and subsequently relaxes to the biradical state $\text{Br}\cdot\text{H}_3\text{O}\cdot(\text{H}_2\text{O})_{n-1}$. In this state the observed H-fragment is released from the H_3O radical.

reflect the differences in energetics between these two molecules. The arrows indicate the fragment energies corresponding to the direct cage exit. On the other hand, the KEDs from HBr and HCl on water clusters are both of the same shape (within the experimental error). This suggests that in the case of HBr and HCl on water the H-fragments originate from the same species, namely from the H_3O radical, rather than from the two different molecules.

Second, HBr and HCl on Ar clusters exhibit some fast H-atoms originating from the photodissociation HX molecule on the cluster and the direct exit of the H-fragment indicated by the arrows. On the other hand, the H-fragment KEDs from HBr and HCl on water clusters did not exhibit any fast fragments. The absence of these fast fragments in the KEDs from water clusters suggested that there was no direct photodissociation of HX on the water clusters.

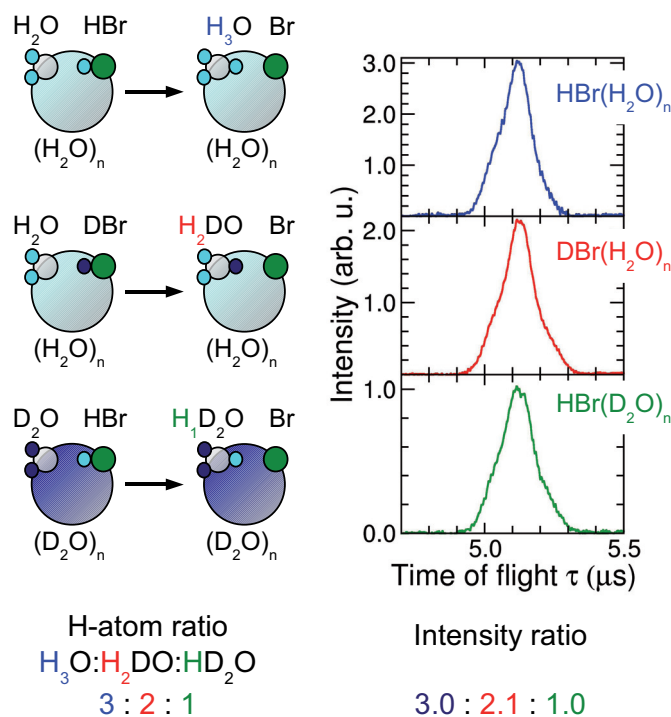


Figure 4.3: Photodissociation of HBr molecules on water clusters. Deuteration experiments pointing to the generation and dissociation of the H_3O radical. Right hand side shows the measured TOF spectra for the three differently deuterated species. Their H-fragment signal intensity ratio corresponds to the H atom ratio in the radical species of the H_3O type generated in the different clusters as illustrated on the left hand side.

Finally, the third noteworthy point is the energy extent of the KEDs on water clusters. The maximum observed kinetic energy of ~ 0.5 eV is quite in agreement with the theoretical calculations of the energetics for H-atom abstraction from H_3O in water clusters [112].

The intensity of the KED spectra: This argument supports the acidic dissociation in $\text{HX}\cdot(\text{H}_2\text{O})_n$ clusters in the ground state to the zwitterionic species. The ratio between the absorption cross sections of HBr and HCl molecules at 193 nm is $\sigma_{\text{HBr}}:\sigma_{\text{HCl}} \approx 25$ [113, 114]. In the first approximation, the total H-atom signal from the photodissociation of HX molecules

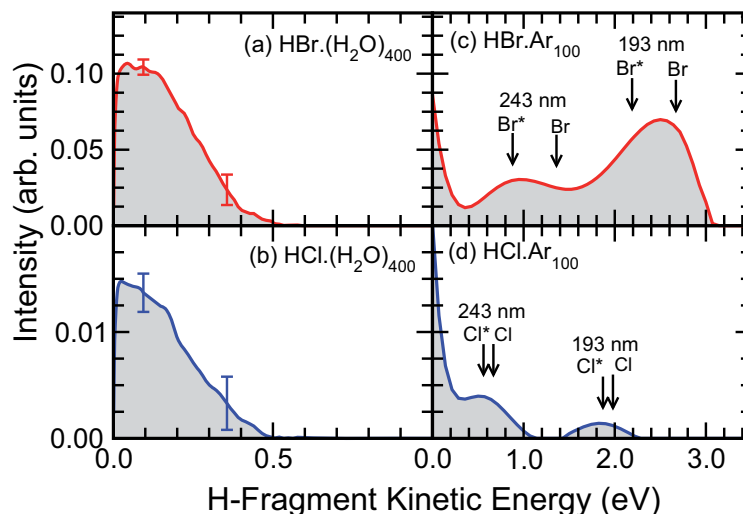


Figure 4.4: Photodissociation of HBr (top) and HCl (bottom) molecules on water (left) and argon (right) clusters.

is proportional to the absorption cross section. The ratio of the H-fragment intensity from the integrated KED spectra in Fig. 4.4 (c) and (d) from HBr and HCl on Ar cluster was 20 ± 5 quite in agreement with the ratio of the absorption cross sections. However, the intensity ratio from photodissociation of HBr and HCl on water clusters was significantly smaller 7.4 ± 1.0 , see Fig. 4.4 (a) and (b). This suggested again that the measured H-atom fragments did not originate directly from the HX molecules. Instead a process was operational on the water clusters, which changed significantly the absorption cross sections. This process was, indeed, proved to be the acidic dissociation. The proof was provided by the theoretical calculations of the cooperating theory group of P. Slavíček and the details can be found in the attached publication [115].

Essentially a significant red shift of the absorption spectra upon the acidic dissociation was calculated for small $HX \cdot (H_2O)_n$ clusters. This shift led a change of the cross section ratio at 193 nm so that it became significantly smaller for $n=4$, $\sigma(Br^-(H_2O)_3H_3O^+):\sigma(Cl^-(H_2O)_3H_3O^+) \approx 2-3$. This decrease in the ratio of absorption cross sections was in qualitative agreement with the experimental observation of the smaller integrated signal ratio.

All the above summarized experimental and theoretical evidence pointed consistently to the the proposed mechanism of the hydrogen halide dissociation on ice nanoparticles: The hydrogen halides undergo ionic dissociation in the ground state (at least to a significant extent) and generate charge-pairs. However, these ion pairs remain of a rather local nature on the time scale of our experiment ≈ 0.6 ms. The zwitterionic species are then excited to the CTTS states which relax to a biradical state where the H_3O molecular radical is generated. Subsequently H_3O dissociates to release the H-fragment which is then detected.

As a final note the possible *atmospheric implications* of the observed process should be mentioned. The direct photodissociation of HCl is usually neglected in the models calculating the Cl stratospheric budget. This is due to the small absorption cross section of HCl at the wavelengths above 200 nm, where the actinic flux from the sun radiation increases to significant levels. Therefore, the conversion of the reservoir species (HCl) to the active forms (Cl_2), which absorb at longer wavelengths around 300 nm, is considered in the stratospheric chemistry modelling. However, we have shown that the acidic dissociation shifts the electronic absorption spectrum to the red, so that it can be expected that the photolysis rate will be much enhanced when the hydrogen halide lands on an ice particle and generates the ion pair. To quantify this issue, we have calculated the photolysis rate using an actinic flux measured at the altitude of 50 km. The photolysis rate has increased by 4 orders of magnitude upon the HCl dissociation on $(\text{H}_2\text{O})_4$ cluster. It is worth noting that the dynamical calculations show that the Cl radical is released directly from the water cluster. Ice particles thus might catalyze the HCl photolysis in a way that can potentially play a non-negligible role in the stratospheric chlorine budget.

The results summarized briefly in this chapter have been published in Refs. [116, 117, 115].

4.2.2 Pure water clusters

In the course of the experiments with hydrogen halides adsorbed on water clusters small hydrogen fragment signal was observed from the pure water

clusters. This signal was more than an order of magnitude weaker than the corresponding signal from the water clusters with embedded hydrogen halide molecules. Therefore, it was subtracted as a background in the above experiments. However, by careful tuning of the experimental parameters (laser powers, WMTOT extraction voltages, etc.) we were able to measure this signal corresponding to the TOF spectra of H-fragments from pure water cluster photodissociation.

Photodissociation of pure $(\text{H}_2\text{O})_n$ nanoparticles of various mean sizes between $\bar{n} \approx 85$ and 670 was investigated at 243 nm and 193 nm. As an example, Fig. 4.5 shows the H-fragment KED from photodissociation of pure water clusters $(\text{H}_2\text{O})_n$ $\bar{n} \approx 670$ (top spectrum). The spectrum exhibited a slow component below approximately 0.5 eV quite similar to the KED from photodissociation of $\text{HBr}\cdot(\text{H}_2\text{O})_n$ clusters, shown below for comparison,⁴ and a low tail of faster fragments exceeding to about 1.5 eV. This bimodal character of the KED was preserved for other cluster sizes, however, the relative intensities of the two spectral components were changing. From their size dependence it was concluded that the faster fragments originated from the cluster surface, while the slow ones were generated in the cluster interior. The close similarity between the slow component of KED from pure $(\text{H}_2\text{O})_n$ clusters and the KED from $\text{HBr}\cdot(\text{H}_2\text{O})_n$ suggested that these fragments originated from H_3O radical formed also in pure $(\text{H}_2\text{O})_n$ clusters.

However, since the autoionization of pure water is rare,⁵ a mechanism of H_3O generation had to be proposed, different from the one operational in $\text{HX}\cdot(\text{H}_2\text{O})_n$ clusters above. Here we assume a direct H_2O photodissociation which in the cluster interior leads to an H fragment scattered from the neighbouring molecules being slowed down and eventually recombined in the reaction: $\text{H}_2\text{O} + \text{H} \rightarrow \text{H}_3\text{O}$. The H_3O subsequently dissociates in the reverse reaction yielding the slow H-fragments. Thus the temporal generation of the H_3O species serves as an efficient thermal bath for energy dissipation in the

⁴It ought to be mentioned that the spectrum from $\text{HBr}\cdot(\text{H}_2\text{O})_n$ system was more than an order of magnitude more intense than the one from $(\text{H}_2\text{O})_n$ under the same conditions otherwise.

⁵One ion pair is generated per 6×10^8 water molecules in a room temperature liquid water.

$(\text{H}_2\text{O})_n$ cluster.

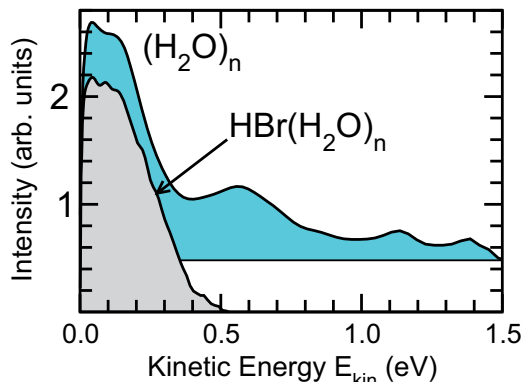


Figure 4.5: Comparison of H-fragment KEDs from photodissociation of pure water clusters $(\text{H}_2\text{O})_n$ $\bar{n} \approx 670$ (top spectrum) with $\text{HBr} \cdot (\text{H}_2\text{O})_n$ $\bar{n} \approx 500$ clusters (bottom).

It should be noted that a water molecule cannot be dissociated with a single 243 nm (5.1 eV) photon. Thus the observed H-fragments had to stem from two-photon dissociation in clusters, which was consistent with the higher photon fluxes ($\geq 10^{28} \text{ s}^{-1} \text{ cm}^{-2}$) used in these experiments. The experiment was also performed with 193 nm laser (6.4 eV). At this energy the direct photodissociation of water is possible, though the cross section remains very low. Correspondingly we observed a small additional signal of H-fragments with energies around 1.2 eV when 193 nm laser was added. This corresponds to the single photon dissociation of water.

High photon fluxes of the 193 nm radiation were used, however, there was no significant increase of the H-fragment intensity nor any indication of higher energy fragments originating from two photon processes. Therefore, we concluded that the two-photon excitation with the total energy of 12.8 eV leads to the ionization rather than to the photodissociation of the clusters. The competition between the dissociation and ionization in the two-photon excitation of water was justified by theoretical calculations of electronic structure for water molecule, $(\text{H}_2\text{O})_6$ cluster and a model of bulk water.

These results were published in Ref. [118].

4.3 Biomolecules in clusters

In this chapter we briefly outline the main results of our investigations of molecular clusters composed of small nitrogen-containing ring molecules: pyrrole (Py), imidazole (Im) and pyrazole (Pz). Their similar structures can be seen in Fig. 4.6. These molecules constitute elementary building blocks in the larger biological molecules. For example, the pyrrole structure is present in hemes and chlorophylls (see Sec 2.2.2), the imidazole structure can be found in purine or as the side chain of naturally occurring amino acid histidine. Pyrazole, on the other hand, is rare in nature, however, it produces clusters of different bonding motifs as mentioned below. Therefore, pyrazole was studied here for comparison purposes with the other two molecules.

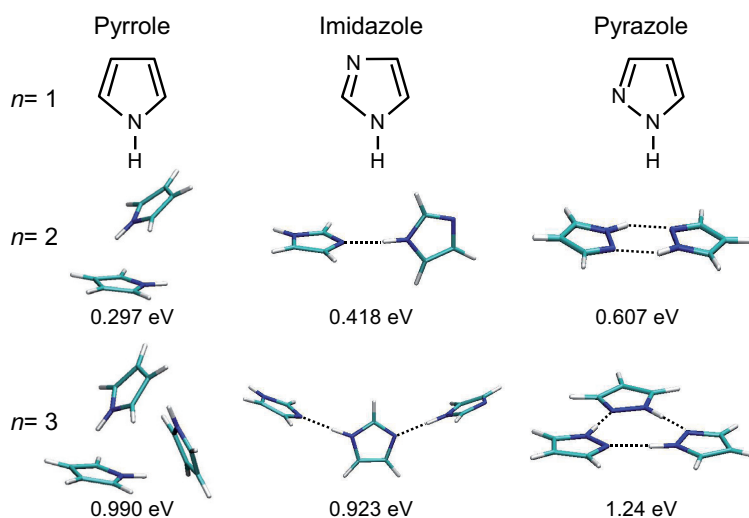


Figure 4.6: Structures and binding energies of the molecules and the different bonding motifs represented by the pyrrole, imidazole and pyrazole dimers and trimers.

Although all three molecules are structurally very similar their clusters are bound via quite different types of bonding as represented for the dimers and trimers in Fig. 4.6. In the pyrrole clusters the N-H bond of one molecule binds to the π electron cloud of the neighbouring molecular ring, the N-H $\cdots\pi$ bond. Imidazole molecules bind via a standard N-H \cdots N hydrogen bond, while the two pyrazole molecules in the dimer interact via a double

hydrogen bond. The general idea of our studies was to investigate, how these different bonding motifs influence the bond-breaking dynamics in clusters of these molecules upon excitation with UV photons or electrons. For example, it can be foreseen from the bonding motifs in Fig. 4.6 that in the case of imidazole and pyrazole one could expect hydrogen or proton migration in the excited state.

Before reviewing our results, we briefly summarize the UV photochemistry of an isolated nitrogen heterocycle in the gas phase, which was extensively studied both experimentally [119, 120, 121, 122] and theoretically [123, 124, 125, 126]. Figure 4.7 shows schematically cuts along the N-H stretching coordinate and the ring deformation coordinate through a general PES for such a system (based on the calculated PES for the pyrrole molecule [127]). The potential energy surfaces (PES) for all three molecules –pyrrole, imida-

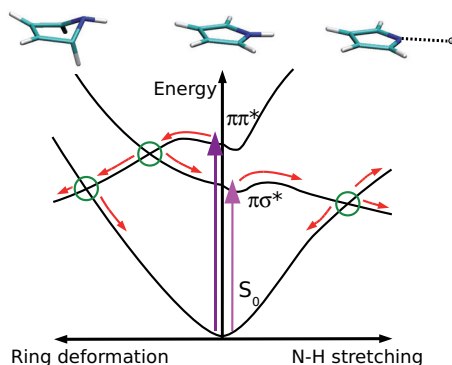


Figure 4.7: Schematic picture of general PES typical for the studied species based on *ab initio* calculations for pyrrole molecule. The cuts through PES along the N-H stretching and ring-deformation coordinates are shown as indicated by the schematic diagrams of pyrrole molecule at the top. The vertical arrows show the UV excitation and the red arrows indicate the possible dissociation pathways. Circles label the conical intersections CI $\pi\sigma^*/S_0$, $\pi\pi^*/\pi\sigma^*$ and $\pi\pi^*/S_0$.

zole, and pyrazole– posses qualitatively very similar features involving low lying excited states $\pi\sigma^*$ and $\pi\pi^*$ and conical intersections between them and between the ground state S_0 . Photochemical pathways in these compounds are controlled by an interplay between the dissociation channel on the $\pi\sigma^*$

state and ground state recovery via different mechanisms. Especially the role of the $\pi\sigma^*$ states in the photodissociation of these and similar molecules (e.g., phenol) has recently attracted much attention [119] due to their potential role played in the stabilization of larger biomolecules such as DNA [108].

The general picture of the photochemistry, which emerged from the numerous gas phase studies, is schematically represented in Fig. 4.8. Upon low energy excitation, the photodynamics is dominated by the $\pi\sigma^*$ state. This state is asymptotically dissociative (see Fig. 4.7) and as result, the hydrogen atom is released (hydrogen dissociation, HD, channel). At elongated N-H distances, the $\pi\sigma^*/S_0$ intersection occurs. It is, therefore, possible that frustrated dissociation (FD) takes place, and the molecular ground state is recreated. At higher photon energies, the $\pi\pi^*$ state is populated. A molecular ring distortion (MRD) reaction channel is opened. Subsequently, the molecule quenches into the vibrationally hot ground state where again the hydrogen atom can dissociate or other molecular fragments can be formed.

This dynamics leads to a bimodal character of the H-fragment KED spectra from the photodissociation of these molecules. These spectra measured for pyrrole molecule at 243 nm and 193 nm are schematically shown on the insets in Fig. 4.8. The relatively narrow peak of *fast fragments* (around 0.8 eV in the particular case of pyrrole) originates from the direct dissociation on the $\pi\sigma^*$ surface. The *slow fragments* exhibit a broad distribution peaking near zero. These fragments correspond to statistical decay of the vibrationally hot ground state molecule after the quenching of the $\pi\sigma^*$ or $\pi\pi^*$ state. This mechanism clearly justifies the higher relative contribution of the slow fragments at higher excitation energies (193 nm), where the $\pi\pi^*$ state is excited. Below, it will be shown how these spectra change upon complexation of the molecules in clusters and these changes will be rationalized based on theoretical calculations performed in the group of P. Slavíček, which were part of our joined publications.

We have investigated the photodissociation of Py, Im, and Pz clusters at two different wavelength 243 nm and 193 nm and for various cluster sizes. The mean cluster sizes were determined in the scattering experiment outlined generally in Sec. 3.3 and discussed in more detail for the particular systems in Refs. [128] and [129] for pyrrole and imidazole, respectively). Figure 4.9

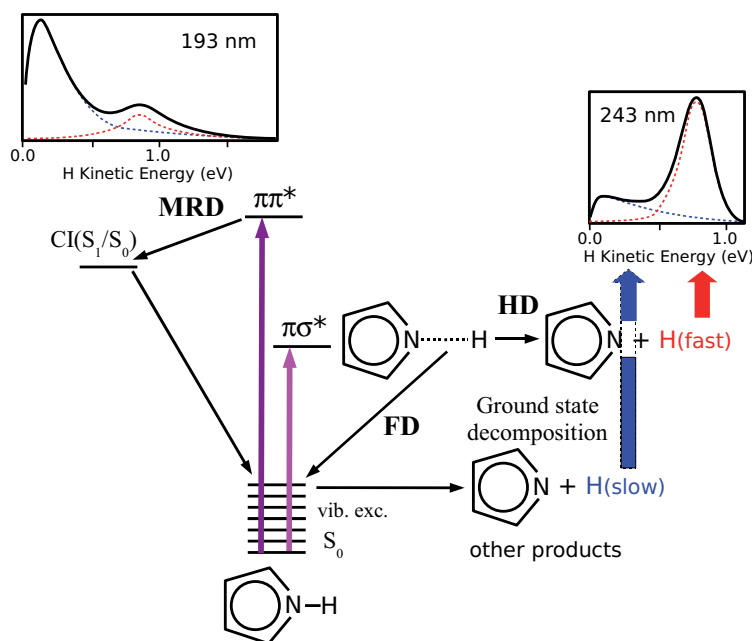


Figure 4.8: Schematic picture of photodissociation processes possible in the molecules (Py, Im, Pz). The excitation of $\pi\sigma^*$ state can lead to the direct hydrogen dissociation (HD) and fast H-atom production. Alternatively, frustrated dissociation (FD) can occur via a $\pi\sigma^*/S_0$ conical intersection at elongated N-H distances. At higher photon energies, the $\pi\pi^*$ state is populated and molecular ring distortion (MRD) can occur, quenching the molecule into the vibrationally hot ground state, where it can again dissociate yielding the slow H-fragments or other products.

shows examples of the measured H-fragment KEDs from Py (left panels (a) and (b)) and Im (right panels (c) and (d)) clusters at 243 nm. The top panels (a) and (c) correspond to the smaller clusters with the mean sizes of $\bar{n} \approx 3$ produced in expansions with He carrier gas. The bottom panels (b) and (d) correspond to the larger clusters generated in expansions with Ar. The mass spectrometric and scattering experiments in Ar expansions revealed mixed Py_nAr_m clusters with $\bar{n} \approx 4$ and $\bar{m} \approx 8$ for pyrrole, while pure Im_n clusters with $\bar{n} \geq 6$ were generated for imidazole. No measurable signal was observed at 243 nm for pyrazole. It should be mentioned that the KEDs

in Fig. 4.9 are normalized and the corresponding measured TOF spectra intensity exhibits a strong dependence on the mean cluster size, i.e. the signal decreases significantly with the increasing cluster size, as illustrated by the increasing error bars on the data in Fig. 4.9.

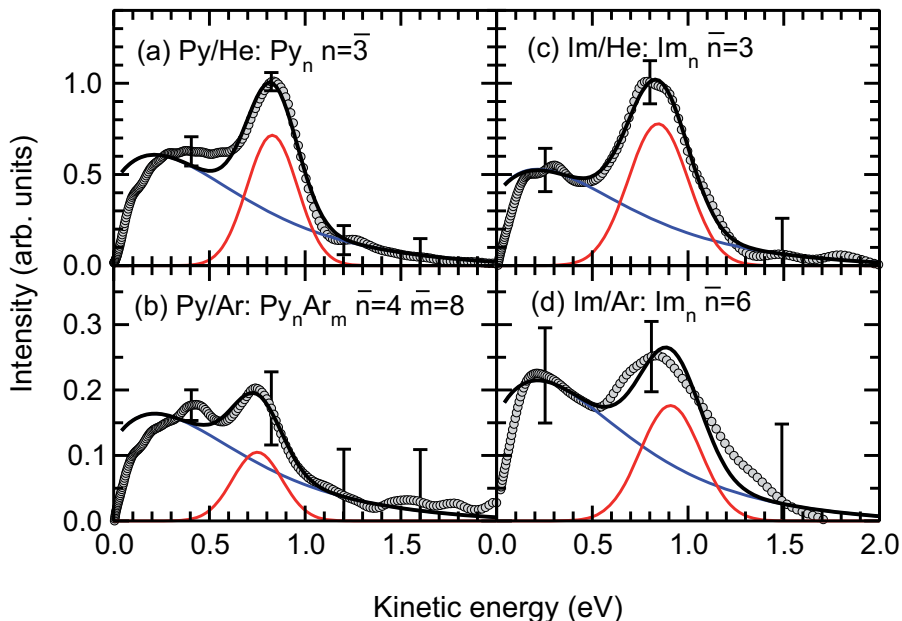


Figure 4.9: Measured KEDs of Py (left panels) and Im (right panels) clusters at 243 nm. The top panels correspond to the small clusters of the mean size $\bar{n} \approx 3$, while the bottom spectra correspond to mixed Py_nAr_m clusters with $\bar{n} \approx 4$ and $\bar{m} \approx 8$ (b) and pure Im_n clusters with $\bar{n} \approx 6$ (d). The spectra are analyzed for a *slow* (blue) and *fast* (red) component.

All the spectra in Fig. 4.9 exhibit a bimodal character with a narrower peak of *faster* fragments at approximately 0.8 eV, and a *slower* component with a broad distribution peaking below 0.4 eV. The spectra have been analyzed and deconvoluted to the contributions of the two components (red and blue lines in Fig. 4.9). The bimodal character of the spectra is very similar to the spectra measured for the bare pyrrole [37, 38, 36, 39, 130, 131] and imidazole [120] molecules. However, the relative ratio of the two components changes with the cluster size. The fast component decreases in intensity

relative to the slow one with the increasing mean cluster size. Besides, the overall intensities of the spectra decreases with the increasing cluster size as indicated by the larger relative size of the error bars. At 193 nm the fast fragment contribution in KEDs was very small already for the bare molecule (see the inset in Fig. 4.8), and the KEDs measured for clusters of the mean sizes mentioned above resembled the spectra of bare molecules. It is worth mentioning that at 193 nm also the spectra of H-fragments from the pyrazole clusters could be measured.

What is the reason for the decreasing contribution of the fast H-fragments with the increasing cluster size? In the case of pyrrole this question was elucidated by theoretical calculations of the PES of pyrrole molecule perturbed by the presence of a solvent. The calculations showed that the electronic interaction with the solvent led to a significant change in the PES along the N-H coordinate (shown in Fig. 4.10), while the PES along the molecular distortion coordinate remained essentially unchanged. The interaction with the solvent pushed the potential along the N-H coordinate higher in energy, which caused the conical intersection between the $\pi\sigma^*$ state and the ground state S_0 along this coordinate to disappear. This in turn closed the dissociation channel to the fast H-fragments. The reminiscence of the fast fragment peak in the KEDs from clusters could be due to the monomers and dimers (which have the free N-H bond too) in the beam. Actually, it is worth noting that the cluster distribution with $\bar{n}=3$, which has an exponential character, contains only less than half as many trimers as monomers.

Although the character and cluster size dependence of the KED spectra for imidazole was very similar as for pyrrole, the situation is somewhat different, enhanced by the possibility of hydrogen transfer process between the cluster units. The theoretical calculations of imidazole dimer confirmed that the hydrogen transfer occurred upon excitation. In addition, the calculations also showed the stabilizing effect of the hydrogen transfer process. Fig. 4.11 shows the calculated PESs for the imidazole dimer. The hydrogen transfer serves as an efficient dissipation channel for the excitation energy: the hydrogen is transferred from the hydrogen donor molecule to the acceptor one, however, at the transferred configuration the excited state PES has a conical intersection with the ground state S_0 , which provides a gradient back to the

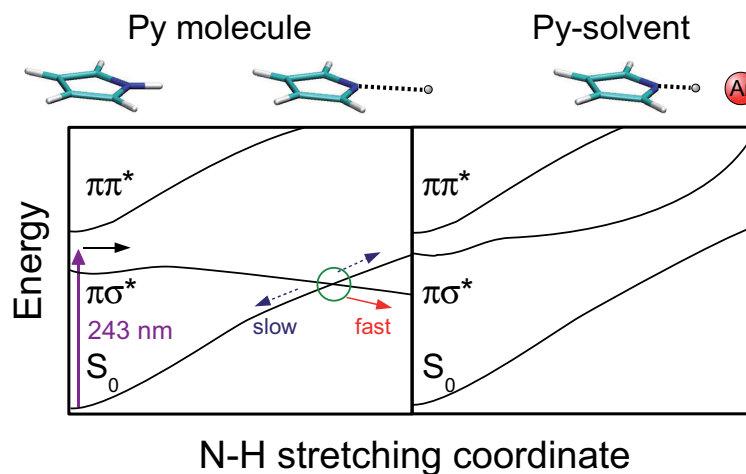


Figure 4.10: Schematic illustration of the influence of a solvent on photodissociation of pyrrole molecule: Left panel shows the PES for photodissociation of the bare molecule indicating the CI (green circle) between the repulsive $\pi\sigma^*$ state and the ground state S_0 leading to the production of the slow (blue arrow) and fast (red arrow) fragments. In the presence of an Ar atom as a prototype of a structureless solvent put into the dissociation pathway the CI along the N–H stretching coordinate disappears, i.e. this dissociation channel is closed. (Note that the slow fragments can be still produced along the other coordinates, e.g., the ring deformation coordinate, and by some other mechanisms discussed in the text).

original cluster configuration. Thus the hydrogen is transferred back to the original H-bond donor molecule, but it is then less prone to dissociation since the energy was dissipated in the other molecular unit.

The stabilizing effect of the hydrogen (or proton) transfer process was further confirmed experimentally in our mass spectrometric study of these clusters [129]. In these experiments the nonresonant multiphoton ionization by subsequently absorbed photons was investigated and compared to the electron ionization. While in electron ionization of pyrrole clusters Py_k^+ ionic fragments were observed, in the case of imidazole and pyrazole clusters the corresponding protonated ImH_k^+ and PzH_k^+ fragments, respectively, were detected. This provided an experimental evidence for the hydrogen (or proton) transfer in the later clusters.

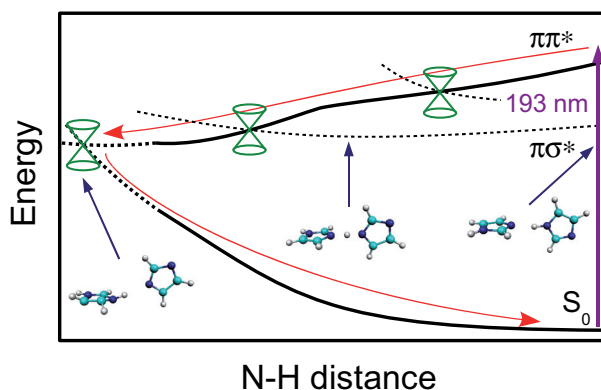


Figure 4.11: Schematic illustration of the photodissociation in imidazole dimer. After the excitation (vertical arrow) the PES gradient along the N–H \cdots N coordinate drives the hydrogen transfer from the hydrogen donor molecule to the acceptor one (red arrow). The conical intersection (green) at the transferred configuration funnels the system into the ground state S_0 , which provides a gradient back to the original cluster configuration. The energy is dissipated between the molecular units during this process and thus the dissociation is less probable. The calculated cluster configurations are indicated. The schematic PES is based on theoretical calculations.

The same was true for photoionization spectra, but very little Py^+ and essentially no Py_k^+ , $k \geq 2$, fragments were observed from the photoionization of the large pyrrole clusters. On the other hand, a significant amount of ImH_k^+ and PzH_k^+ fragments up to $k=5$ was detected from the photoionization of the large imidazole and pyrazole clusters. This again supported the higher photostability of the hydrogen-bonded imidazole and pyrazole clusters with respect to the pyrrole clusters bonded by the N–H $\cdots\pi$ bond. Further studies of similar systems can confirm if this conclusion could be generalized to the stabilizing effect of the hydrogen bond via hydrogen (or proton) transfer. This can help to further reveal the detailed molecular mechanism of photostability of biomolecules.

The results summarized in this section have been published in Refs. [127, 128, 132, 129].

4.4 Novel rare gas molecules

The investigation of noble-gas hydrides is a fascinating issue due to their role played in the fundamental understanding of chemical bonds as outlined in Sec. 2.2.3. Here we focus on the main results of our studies of these interesting species. Only three rare-gas molecules of the type H-Xe-Y have been generated in the gas phase so far: HXeI [55, 56], HXeCl [57] and HXeCCH [58]. This section is based on an article [57] about HXeCl, on a review [133] about the former two molecules generated still in Göttingen on the present apparatus, and on two new papers [58, 134] about HXeCCH recently prepared in our laboratory in Prague.

Experimentally these species were produced by photodissociation of precursor molecules HY on large Xe_n, $n \sim 10^2$ - 10^3 , clusters in the molecular beams, as outlined in Sec 2.2.3. In matrices, where these molecules are usually prepared, they are detected by vibrational IR spectroscopy. Due to their large dipole moments they are very strong absorbers and their light hydrogen vs. heavy rare-gas (H-Xe) vibrations exhibit typical frequencies. In the molecular beams their number density generated by the cluster photolysis is not sufficient for an IR spectroscopy. The molecules are detected by their alignment, which leaves a specific fingerprint on the measured H-fragment TOF spectra after the HRgY photodissociation, i.e. the asymmetry of the TOF spectra.

The details of the molecule generation and orientation are discussed, e.g., in the review [133]. Pictorially, the process is illustrated in Fig. 4.12. First the precursor HY molecule is dissociated and the H-fragment is scattered by the cluster cage and eventually recombines with an inserted Xe atom to the H-Xe-Y molecule. Generally these molecules have very large polarizability anisotropy $\Delta\alpha = \alpha_{\parallel} - \alpha_{\perp}$, where the polarizability α_{\parallel} along the principal molecular axis is much larger than the polarizability perpendicular to the molecular axis α_{\perp} . By the interaction of this polarizability anisotropy with the strong electric field $\vec{\epsilon}_L$ of the polarized laser radiation the molecule is forced to align in the direction of $\vec{\epsilon}_L$. Note that this *alignment* is not the *orientation* of the molecule yet. In the aligned state the molecule can still point with its hydrogen end in the direction towards the detector or in the

opposite direction (in the particular configuration depicted in Fig. 4.12).

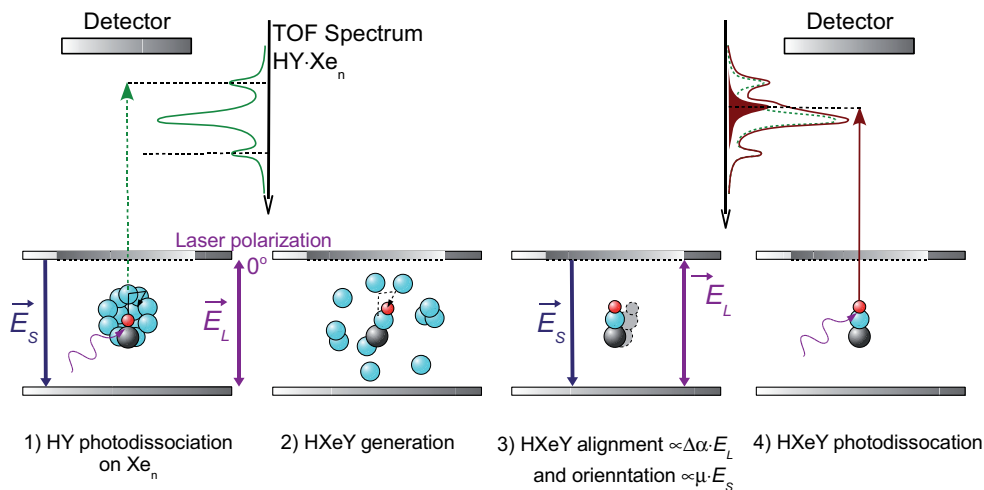


Figure 4.12: Schematic picture of the generation and orientation mechanism of an H-Xe-Y molecule by HY precursor photodissociation on Xe_n clusters: 1) HY molecule is photodissociated on the Xe_n cluster; 2) H fragment is backscattered from cluster atoms and recombines to HXeY molecule; 3) HXeY molecule is aligned in the strong laser field by the interaction of the laser electric field vector \vec{E}_L with the polarizability anisotropy of the molecule $\Delta\alpha$, and this alignment is turned into orientation by the interaction of the weak extraction field \vec{E}_S with the dipole moment $\vec{\mu}$ of the molecule; 4) the HXeY molecule is dissociated. The TOF spectrum of H-fragments from the oriented molecule exhibits only the peak of faster fragments (filled red peak), while the spectrum of randomly oriented HY molecule is symmetric (green line). The asymmetry of the measured total spectrum (red line) –which is a sum of the two spectra– is the experimental evidence for the HXeY molecule.

However, this alignment can be turned into the orientation by the electrostatic field \vec{e}_S used in the extraction region of the WMTOF spectrometer. In the combined parallel strong nonresonant laser field and the static electric field even a weak static field ($\sim 1 \text{ Vcm}^{-1}$) can induce a strong orientation due to the pseudo-first-order Stark effect [135, 136, 62]. The static field interacts with the permanent dipole moment $\vec{\mu}$ of the molecule and orients it with the H-atom towards the detector in the present geometry. The molecule is

trapped in the so called *pendular state* where the molecular axis undergoes a libration motion around the axis defined by the electric fields and the orientation can be characterized by the mean value of the orientation cosine $\langle \cos \theta_S \rangle$ of the polar angle θ_S between the molecular axis and the electrostatic field. Large values of orientation cosine close to unity mean very small angular amplitudes of the molecular axis librations in the field, i.e. the strong orientation.

The interaction between the laser field and the polarizability anisotropy results in a double-well potential (corresponding to the two orientations of the aligned molecule) supporting nearly degenerate tunnelling doublets of states with the opposite orientations. Therefore, the mixture of these states would exhibit only alignment, and not an orientation. Orientation can be achieved only if a single state of the doublet is selected. The cooling of the molecule due to the cluster evaporation leads to population of the lowest rotational state of the HXeY molecule which then correlates to the lowest pure state of the tunnelling doublet, and thus to the oriented molecule.

This orientation is reflected in the asymmetry of the measured TOF distributions of H fragments after a subsequent HRgY photodissociation. Generally, photodissociation of randomly oriented molecules yields a symmetric TOF spectrum since the fragments from the molecules oriented towards the detector have counterparts in fragments from molecules oriented in the opposite direction. The former fragments start after photodissociation with the initial velocity corresponding to the excess kinetic energy towards the detector and arrive earlier than the fragments with initially zero kinetic energy. On the other hand, the later fragments start with the velocity in the opposite direction and have to be turned around by the extraction field and arrive later than the zero kinetic energy fragments. Therefore, the TOF spectrum is symmetric with respect to the arrival time of the zero kinetic energy fragments (see also Sec. 3.4.2).⁶

⁶There is a slight asymmetry even in the TOF spectra of randomly oriented molecules due to slightly different acceptance angles of the detector for fragments starting towards the detector and away from it. This asymmetry is, however, considered in the evaluation procedure of our spectra and the present asymmetry due to the molecule orientation is more pronounced.

However, for the HXeY molecules preoriented with the H atom towards the detector only the early arriving part of the spectra is present while the slow fragments are missing entirely, i.e. the spectrum is asymmetric. The total measured spectrum is composed of the *symmetric* contribution from the H-fragments from the randomly oriented precursor HY and the *asymmetric* part from HXeY dissociation.⁷ Thus the resulting spectrum asymmetry is not overwhelming even for strongly oriented molecules yet it is significant. It should be mentioned that in the first observation of the HXeI molecules [55] the asymmetry of the observed spectrum was considered to be rather an experimental artefact. Only after very careful exclusion of all possible sources of experimental errors the persistent asymmetry was explained by the HXeI generation and dissociation. It is interesting to note that this new exciting field of cluster research originated as a byproduct of research aimed towards investigation of photodissociation of HI molecules in the cluster Xe_n environment.

It should be also mentioned that the orientation effect has been confirmed in an experiment with HXeI molecule [56], where the orientation of the extraction field was temporarily reversed. In this way the orientation of the HXeI molecule was also reversed and the H-fragment after its photodissociation started away from the detector (downwards in the present configuration). Indeed, to detect the ionized hydrogen fragment, it had to be accelerated up to the detector by turning the extraction field to its original orientation again after the photodissociation. By synchronizing properly the pulsed extraction field and laser pulses the asymmetry of the TOF spectra could be shifted to the other side from the zero kinetic energy peak, i.e. the photodissociation of the molecule oriented with the H-atom away from detector resulted only in the late arriving fragments.

The HXeI and HXeCl molecules were studied with the present experimental setup still in Göttingen and the studies are summarized in the review

⁷It ought to be mentioned that the orientation mechanism operates on any molecule with a polarizability anisotropy and a permanent dipole moment in the combined parallel static electric fields and the strong nonresonant laser fields, however, for most molecules, e.g., the precursor HY molecules, the resulting orientation cosine is essentially zero in the present fields, i.e. no orientation occurs.

4.4. Novel rare gas molecules

of the author [133]. The major conclusions from these experiments were the following: (1) The HXeI and HXeCl molecules could be prepared free in the gas phase by photodissociation of HI and HCl on Xe_n clusters. (2) Therefore, these molecules must have been generated by the direct mechanism. (3) These molecules could be oriented in the strong electric fields of laser combined with the weak static extraction fields, and they were detected by their orientation. (4) On the other hand the molecules HKrCl, HKrBr and HXeBr, which we were also searching for, either could not be generated or could not be detected by their orientation, i.e. their orientation cosine was too small to cause any significant asymmetry in the TOF spectra.

Further studies along these lines were performed after moving the experiment to Prague and the first evidence for organoxenon molecule HXeCCH in the gas phase was provided in our experiment. The molecule was produced by photodissociation of acetylene on Xe_n , $\bar{n} \approx 390$, clusters which were oriented and photodissociated subsequently. The measured TOF spectra were compared to H-fragment spectra from photodissociation of acetylene on Ar_n clusters, where an evidence for the generation of HArCCH molecule was not found. It is worth mentioning that this was an intriguing question to investigate, since the noble-gas compounds of the larger noble-gas atoms Kr and Xe are more stable due to the nature of bonding in these species (the outer electrons participating in the bonds are more shielded from the core in the heavier rare-gas atoms). Therefore, the only Ar compound observed so far experimentally in matrices was HArF [137] and the quest for Ar (and Ne and He) containing compounds continues. However, our spectra from C_2H_2/Ar_n system were symmetric providing no evidence for HArCCH. Besides the theoretical calculations [58] proved this molecule to be unstable.

Furthermore, our study of HXeCCH molecule was accompanied by theoretical calculations, which revealed the dynamics of its dissociation. Thus, in this case, data were provided by our experiment complementary to the IR vibrational spectroscopy of these species in matrices. These results are summarized in Refs. [58, 134].

Chapter 5

General Conclusions and Outlook

The particular conclusions of the experiments in the four fields reported in this Thesis –(1) rare gas clusters, (2) atmospheric nanoparticles, (3) biologically relevant clusters, and (4) novel rare gas molecules– have been outlined in the corresponding sections in the previous chapter. The major general conclusions across the fields will be briefly revealed in this chapter and the future directions of our research will be discussed.

In the early experiments with hydrogen halides molecules on rare gas clusters discussed in Sec. 4.1 we have obtained information about the photodissociation dynamics of these species in cluster environments. Processes as *fragment caging* and *cage exit* were analyzed and well understood. Besides, further interesting details about the studied systems were revealed, such as the observed liquid-like nature of the surface layer in neon clusters. These studies provided an excellent basis for the further investigations of e.g. atmospherically and biologically relevant systems developed in our laboratory in Prague.

Our experiments with hydrogen halides on ice nanoparticles in Sec. 4.2 showed that the UV excitation leads to the generation of H_3O neutral radical via acidic dissociation in the ground state. An evidence for the H_3O radical was also observed in the photodissociation of pure ice nanoparticles. This suggests that the H_3O plays a central role in the photochemistry of

CHAPTER 5. CONCLUSIONS AND OUTLOOK

aqueous systems, which can also have significant practical implications in the atmospheric chemistry and ozone depletion models.

Several future directions of research can be proposed from this point. An obvious one is the extension of our studies on systems including the other hydrogen halides HI and HF. Water clusters with HI can exhibit a lower lying CTTS state accessible already with the 243 nm laser. Thus the investigation of this system can further confirm the proposed excitation scenario at other energies. As a matter of fact, in the course of writing this Thesis, we have already started the experiments with HI and the preliminary results confirm the above scenario and also the lower lying CTTS band. On the other hand, HF is a weak acid and, therefore, no acidic dissociation should occur on the water clusters as suggested by our theoretical calculations [115]. It would be interesting to confirm experimentally the different behaviour of HF with respect to the other hydrogen halides. However, experiments with HF are difficult since hydrofluoric acid –though a weak acid– is very corrosive and difficult to handle and represents serious health hazards. Also straightforward is an extension of our experiments to the systems including other atmospheric molecules apart from hydrogen halides, e.g., HNO₃, H₂SO₄, OClO, etc. Again, these studies will be challenging experimentally since many of these species are potentially harmful to the apparatus and/or represent possible health hazards.

It has been mentioned in Sec. 2.2.1 that around 1999 a new mechanism has been advocated in the ozone depletion chemistry [26, 28, 27]. The *solvated electrons (aqueous electrons)* have been proposed to play the central role in this mechanism. Briefly, the solvated electrons are produced by cosmic radiation in the PSC particles and they attach directly to the CFCs on the particle surface. The dissociative attachment generates the corresponding negative ion in a dissociative state yielding the Cl⁻ anion immediately and further reactions lead to the Cl radical. This reaction chain bridges the step of producing the reservoir species (e.g., HCl) from CFCs, necessary in the original model [25] outlined in Sec. 2.2.1. Many experiments have been performed to test the aqueous electron hypothesis on bulk ice surfaces. By replacing HCl with CFCs (e.g., CF₂Cl₂) in our experiments with ice nanoparticles, we could observe the Cl generation in these species when e_{aq}^-

CHAPTER 5. CONCLUSIONS AND OUTLOOK

is produced by electron excitation of some species (e.g., I^-) doped in the ice clusters. For this purpose, our detection REMPI scheme has to be tuned from the hydrogen to Cl atom. There are several REMPI schemes for Cl ionization known from the literature and some of them are currently tested in our laboratory. Detecting other species than H atoms will open further possibilities for studying the other atmospherically relevant molecules on ice nanoparticles detecting fragments such as, e.g., Cl, NO, etc.

In Sec. 4.3 we have studied the effect of solvent molecules on photochemistry of small biomolecular units. It has been demonstrated that the presence of solvent molecules can change the photochemistry in various ways: (i) a photodissociation channel can be closed due to the electronic interaction between the studied biomolecule and the solvent, or (ii) the hydrogen or proton transfer in the excited state can be initiated in hydrogen bonded systems, which can lead to the excitation energy redistribution and dissipation. Both these effects can result in the solvent induced stabilization of the molecule in the cluster. Such cluster studies may provide a key to the molecular level understanding of stability of the larger biomolecules in their natural environments.

There are numerous molecules, which can be further studied to obtain a deeper insight into these issues. For example phenol, where the energetic ordering of the $\pi\sigma^*$ and $\pi\pi^*$ states is reversed with respect to the systems studied with our experiments so far. Further examples represent six-member aromatic ring molecules benzene, pyridine and pyrimidine, and their derivatives 4-aminopyrimidine and 4(1H)-pyrimidione, closely related to the nucleobases cytosine, thymine and uracil. Again, experimental challenges arise from the nature of many biomolecules, which are solids with relatively low vapour pressure, difficult to get into the gas phase. Another class of very interesting species is represented by mixed clusters, e.g., pyrrole··water [138], pyrrole··ammonia [139], phenol··ammonia [140, 141] or pyrrole··pyridine [142], where the hydrogen atom of the donor molecule can migrate to the acceptor molecule, and also new phenomena can occur, such as the proton migration along the molecular wire. Again already at the time of writing these Thesis some preliminary experiments have been performed on some of these new systems.

CHAPTER 5. CONCLUSIONS AND OUTLOOK

So far we have studied the above molecules in the environment of rare gas clusters as prototype of structureless model solvent, or in clusters with molecules of the same kind. Obviously, the systems closer to reality will be provided by embedding the biomolecules into their natural aqueous environment, i.e. into the water clusters. At this point the research of the biologically relevant molecules in a sense merges with the above research of atmospherically relevant species. Here the motif of *solvated electrons* appears again. It has been proposed that the radiation damage of DNA is actually caused by the e_{aq}^- generated in the aqueous solutions and attached to the DNA [143]. We can produce large water clusters with solvated electrons as proposed above for CFCs, and pick-up the biomolecules on them and observe the action of e_{aq}^- on the biomolecules.

The last issue treated in this Thesis are the rare gas molecules in Sec. 4.4. Here we have demonstrated that some of these interesting species can be generated in the gas phase by photolysis of precursor molecules on large rare gas clusters. Thus their stability and the direct generation mechanism have been proved. Besides, these molecules were oriented in the strong electric fields of laser combined with the weak electrostatic fields. Finally, also the photodissociation dynamics of these species has been studied. The huge discrepancy between the number of these species observed in matrixes (over 20) and in the gas phase (3) suggests many candidates for the future studies in our experiment.

On the other hand, these experiments belong to the most challenging ones on our apparatus. The rare gas molecules are detected by their orientation in the electric fields, which translates into the asymmetry of the measured TOF spectra. However, this asymmetry is usually seen as a very small effect superimposed on a much larger symmetric signal originating from the dissociation of the precursor molecules. In these experiments, possible experimental artefacts have to be carefully eliminated. One possible significant improvement of these experiments can be introduced by the imaging technique proposed below.

An exciting extension of our present research is the implementation of the so called *ion imaging*, *velocity mapping*, and *velocity slicing* techniques [144]. The primary observable in the photodissociation experiments above is the

CHAPTER 5. CONCLUSIONS AND OUTLOOK

velocity distribution of the photofragments, which provides information on both the energetics and spatial aspects of the studied processes. Traditionally this quantity has been obtained by measuring the arrival time of the fragments to a detector, i.e. by the time-of-flight technique, introduced in Sec. 3.4.1. However, this technique exhibits limited sensitivity by collecting only a small fraction of the fragments with the initial momentum directly towards and away from the detector. Even more importantly, it provides only one-dimensional cross section through the three-dimensional velocity map of the emerging molecular fragments. This severely limits the information, which can be extracted from the data. The ion imaging is a new method capable of providing the complete 3-D information about photofragment velocity distributions, which gradually becomes widely used in the studies of the dynamics of dissociation processes. Therefore, an extension of our present experiment with the ion imaging technique has been proposed.

Generally, in the imaging of a photodissociation process, the expanding Newton sphere of fragments is projected after a certain flight time onto a position sensitive detector -typically a large area multi-channel plate with a phosphorous screen, the image of which is recorded with a charge-coupled device (CCD) camera. The complete information about the fragment velocity obtained from the image, joined with a state-selective photoionization providing single quantum state specificity, yields a very detailed insight into the dynamics of the photodissociation process. The main advantage of the method for our experiment is the collection efficiency: while the TOF method harvests essentially only the fragments flying either directly to the detector or in the opposite direction and all the other fragments also carrying information about the studied process escape the detection, the imaging methods collects essentially all the fragments flying in any direction after the photodissociation. The spectra equivalent to the TOF spectra can be obtained by data processing as cuts through the measured images. Besides, any sort of asymmetry in the photodissociation process is immediately obvious directly from the image. Thus the method is ideally suited for the measurements of the oriented molecules, such as the rare gas hydrides discussed above.

The expected large increase of the detection sensitivity with the implementation of the imaging technique can be also exploited for experiments

CHAPTER 5. CONCLUSIONS AND OUTLOOK

with the *neutral size selected clusters*. It has been mentioned in Sec. 3.3 that our apparatus is capable of producing molecular beams of size selected neutral clusters, which is a worldwide unique feature. However, this feature cannot be fully exploited because of the limited cluster densities in the size selected beams not sufficient for the photodissociation experiments. The sensitivity increased by the imaging technique should allow for the photodissociation experiments with fully size selected neutral clusters. This way the effect of solvent molecules on photodissociation can be investigated by adding the solvent molecules one by one, which would be truly unique experiment, for which many researchers are longing.

For the purpose of introducing the new method in our experiment, first a new much simpler molecular beam apparatus is currently under construction in our laboratory, Fig. 5.1. It serves setting up and testing the imaging

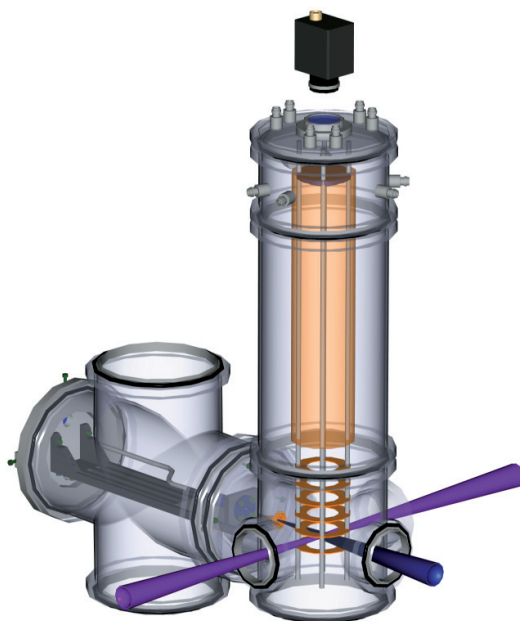


Figure 5.1: Schematic drawing of a new experimental apparatus for implementation of ion imaging, velocity mapping and velocity slicing methods in our group. The molecular beam (blue), UV laser beam (violet), and imaging detection system (gold) are mutually perpendicular.

system independently from our main cluster beam machine. Thus the de-

CHAPTER 5. CONCLUSIONS AND OUTLOOK

veloping of the system does not interfere with our current experiments. The new apparatus is designed so that it can be also used for other independent experiments with molecular beams and small clusters. Therefore, it further extends the experimental potential of our laboratory.

As a final remark, this Thesis summarize the major part of the new research, which has been started five years ago at the J. Heyrovský Institute of Physical Chemistry ASCR in Prague. It can be concluded that this research has opened a new interesting and vital field of studying photochemistry in free clusters and nanoparticles. The vitality of the present research is documented by the number of papers published within the last three years, some of which were part of this thesis. Yet, the field is still very young and this last chapter also illustrates the many possibilities and challenges for the future investigations in all the introduced areas.

Chapter 6

Bibliography

References

- [1] Forsén, S. In *Nobel Lectures, Chemistry 1981-1990*; Frängsmyr, T., Malmström, B. G., Eds.; World Scientific Publishing Co.: Singapore, **1992**.
- [2] Stern, O. *Z. Phys.* **1920**, *2*, 49.
- [3] Stern, O. *Z. Phys.* **1920**, *3*, 417.
- [4] Stern, O.; Gerlach, W. *Z. Phys.* **1922**, *9*, 349.
- [5] Scoles, G. *Atomic and Molecular Beam Methods*; Oxford: New York, **1988**.
- [6] Pauly, H. *Atom, Molecule and Cluster Beams*; Springer: Berlin, **2000**.
- [7] Bernstein, R. B. *Chemical Dynamics via Molecular Beam and Laser Techniques*; Oxford University Press: Oxford, **1982**.
- [8] Levine, R. D.; Bernstein, R. B. *Molecular Reaction Dynamics and Chemical Reactivity*; Oxford University Press: Oxford, **1982**.
- [9] Düren, R.; Lackschewitz, U.; Milošević, S.; Waldapfel, H.-J. *Chem. Phys.* **1990**, *140*, 199.

CHAPTER 6. BIBLIOGRAPHY

- [10] Mestdagh, J. M.; Gaveau, M. A.; Gée, C.; Sublemontier, O.; Visticot, J. P. *Int. Rev. Phys. Chem.* **1997**, *16*, 215.
- [11] Hurley, S. M.; Dermota, T. E.; Hydutsky, D. P.; Castleman, A. W. *Science* **2002**, *298*, 202.
- [12] Hurley, S. M.; Dermota, T. E.; Hydutsky, D. P.; Castleman, A. W. *J. Chem. Phys.* **2003**, *118*, 9272.
- [13] Buck, U.; Steinbach, C. *J. Phys. Chem. A* **1998**, *102*, 7333.
- [14] Castleman, A.; Keesee, R. *Science* **1988**, *241*, 36.
- [15] Jena, P.; Castleman, A. W. *Proc. Nat. Acad. Sci. USA* **2006**, *103*, 10560.
- [16] Haberland, H. *Clusters of Atoms and Molecules*; Springer: Berlin, **1994**.
- [17] Toennies, J. P.; Vilesov, A. F. *Angew. Chem. Int. Ed.* **2004**, *43*, 2622.
- [18] Dong, F.; Miller, R. E. *Science* **2002**, *298*, 1227.
- [19] Buck, U. *J. Phys. Chem. A* **2002**, *106*, 10049.
- [20] Molina, M. J.; Tso, T. L.; Molina, L. T.; Wang, F. C. Y. *Science* **1987**, *238*, 1253.
- [21] Tolbert, M. A.; Rossi, M. J.; Malhotra, R.; Golden, D. M. *Science* **1987**, *238*, 1258.
- [22] Tolbert, M. A.; Rossi, M. J.; Golden, D. M. *Geophys. Res. Lett.* **1988**, *15*, 847.
- [23] Leu, M.-T. *Geophys. Res. Lett.* **1988**, *15*, 17.
- [24] Peter, T. *Ann. Rev. Phys. Chem.* **1997**, *48*, 785.
- [25] Solomon, S.; Garcia, R. R.; Rowland, F. S.; Wuebbles, D. J. *Nature* **1986**, *321*, 755.

CHAPTER 6. BIBLIOGRAPHY

- [26] Lu, Q.-B.; Madey, T. E. *J. Chem. Phys.* **1999**, *111*, 2861.
- [27] Lu, Q.-B.; Sanche, L. *J. Chem. Phys.* **2004**, *120*, 2434.
- [28] Lu, Q.-B.; Sanche, L. *Phys. Rev. Lett.* **2001**, *87*, 078501.
- [29] Weimann, M.; Fárnik, M.; Suhm, M. A. *Phys. Chem. Chem. Phys.* **2002**, *4*, 3933.
- [30] Fárnik, M.; Weimann, M.; Suhm, M. A. *J. Chem. Phys.* **2003**, *118*, 10120.
- [31] Devlin, J. P.; Fárnik, M.; Suhm, M.; Buch, V. *J. Phys. Chem. A* **2005**, *109*, 955.
- [32] Devlin, J. P.; Uras, N.; Sadlej, J.; Buch, V. *May* **2002**, *417*, 269.
- [33] Buch, V.; Sadlej, J.; Aytemiz-Uras, N.; Devlin, J. P. *J. Phys. Chem. A* **2002**, *106*, 9374.
- [34] Kang, H.; Shin, T. H.; Park, S. C.; Kim, I. K.; Han, S. J. *J. Am. Chem. Soc.* **2000**, *122*, 9842.
- [35] Blank, D. A.; North, S. W.; Lee, Y. T. *Chem. Phys.* **1994**, *187*, 35.
- [36] Cronin, B.; Nix, M. G. D.; Qadiri, R. H.; Ashfold, M. N. R. *Phys. Chem. Chem. Phys.* **2004**, *6*, 5031.
- [37] Wei, J.; Kuczmann, A.; Riedel, J.; Renth, F.; Temps, F. *Phys. Chem. Chem. Phys.* **2003**, *5*, 315.
- [38] Wei, J.; Riedel, J.; Kuczmann, A.; Renth, F.; Temps, F. *Faraday Discuss.* **2004**, *127*, 267.
- [39] Papadakis, V.; Kitsopoulos, T. N. *Rev. Sci. Instrum.* **2006**, *77*, 083101.
- [40] Lippert, H.; Ritzel, H.-H.; Hertel, I. V.; Radloff, W. *Chem. Phys. Chem.* **2004**, *5*, 1423.
- [41] Barbatti, M.; Vazdar, M.; Aquino, A. J. A.; Eckert-Maksić, M.; Lischka, H. *J. Chem. Phys.* **2006**, *125*, 164323.

CHAPTER 6. BIBLIOGRAPHY

- [42] van den Brom, A. J.; Kapelios, M.; Kitsopoulos, T. N.; Nahler, N. H.; Cronin, B.; Ashfold, M. N. R. *Phys. Chem. Chem. Phys.* **2005**, *7*, 892.
- [43] Crespo-Hernandez, C. E.; Arce, R.; Ishikawa, Y.; Gorb, L.; Leszczynski, J.; Close, D. M. *J. Phys. Chem. A* **2004**, *108*, 6373.
- [44] Crespo-Hernandez, C. E.; Cohen, B.; Hare, P. M.; Kohler, B. *Chem. Rev.* **2004**, *104*, 1977.
- [45] Fárník, M.; Davis, S.; Nesbitt, D. J. *Faraday Discuss.* **2001**, *118*, 63.
- [46] Fárník, M.; Nesbitt, D. J. *J. Chem. Phys.* **2004**, *121*, 12386.
- [47] Fárník, M.; Steinbach, C.; Weimann, M.; Buck, U.; Borho, N.; Suhm, M. A. *Phys. Chem. Chem. Phys.* **2004**, *6*, 4614.
- [48] Sobolewski, A. L.; Domcke, W. G. *J. Phys. Chem. A* **2007**, *111*, 11725.
- [49] Schultz, T.; Samoylova, E.; Radloff, W.; Hertel, I. V.; Sobolewski, A. L.; Domcke, W. *Science* **2004**, *306*, 1765.
- [50] Markwick, P.; Doltsinis, N. *J. Chem. Phys.* **2007**, *126*, 175102.
- [51] Schwalb, N.; Temps, F. *J. Am. Chem. Soc.* **2007**, *129*, 9272.
- [52] Dermota, T. E.; Zhong, Q.; Castleman, A. W. *Chem. Rev.* **2004**, *104*, 1861–1886.
- [53] Gerber, R. B. *Annu. Rev. Phys. Chem.* **2004**, *55*, 55.
- [54] Pettersson, M.; Khriachtchev, L.; Lundell, J.; Räsänen, M. In *Inorganic Chemistry in Focus II*; Meyer, G., Naumann, D., Wesemann, L., Eds.; Wiley-VCH: Weinheim, **2005**; page 15.
- [55] Baumfalk, R.; Nahler, N. H.; Buck, U. *J. Phys. Chem.* **2001**, *114*, 4755.
- [56] Nahler, N. H.; Buck, U.; Bihary, Z.; Gerber, R. B.; Friedrich, B. *J. Chem. Phys.* **2003**, *119*, 224.
- [57] Nahler, N. H.; Fárník, M.; Buck, U. *Chem. Phys.* **2004**, *301*, 173.

CHAPTER 6. BIBLIOGRAPHY

- [58] Poterya, V.; Votava, O.; Fárník, M.; Ončák, M.; Slavíček, P.; Buck, U.; Friedrich, B. *J. Chem. Phys.* **2008**, *128*, 104313.
- [59] Friedrich, B.; Herschbach, D. *Phys. Rev. Lett.* **1995**, *74*, 4623.
- [60] Sakai, H.; Safvan, C.; Larsen, J.; K.M. Hiilligsø e, K. H.; Stapelfeldt, H. *J. Chem. Phys.* **1999**, *110*, 10235.
- [61] Larsen, J. J.; Hald, K.; Bjerre, N.; Stapelfeldt, H.; Seideman, T. *Phys. Rev. Lett.* **2000**, *85*, 2470.
- [62] Friedrich, B.; Nahler, N. H.; Buck, U. *J. Mod. Opt.* **2003**, *50*, 2677.
- [63] Baumfalk, R.; Buck, U.; Frischkorn, C.; Gandhi, S. R.; Lauenstein, C. *Ber. Bunsenges. Phys. Chem.* **1997**, *101*, 606.
- [64] Baumfalk, R.; Buck, U.; Frischkorn, C.; Gandhi, S. R.; Lauenstein, C. *Chem. Phys. Lett.* **1997**, *269*, 321.
- [65] Lohbrandt, P.; Galonska, R.; Kim, H. J.; Lauenstein, M. S. C.; Buck, U. In *Atomic and Molecular Beams. The State of the Art 2000*; Campargue, R., Ed.; Springer: Berlin, **2001**; page 623.
- [66] Nahler, N. H. *PhD Thesis, GA Universität Göttingen* **2002**.
- [67] Wiley, W. C.; McLaren, I. H. *Rev. Sci. Instrum.* **1955**, *26*, 1150.
- [68] Christen, W.; Rademann, K. *Phys. Rev. A* **2008**, *77*, 012702.
- [69] Christen, W.; Rademann, K. *Phys. Scripta* **2008**, *80*, 048127.
- [70] Toennies, J. P.; Vilesov, A. F.; Whaley, K. B. *Physics Today* **2001**, *2*, 31.
- [71] Póczik, I. *Z. Phys. D* **1991**, *20*, 395.
- [72] Hagena, O. F. *Surf. Sci.* **1981**, *106*, 101.
- [73] Hagena, O. F. *Z. Phys. D* **1987**, *4*, 291.
- [74] Hagena, O. F. *Rev. Sci. Instrum.* **1992**, *63*, 2374.

CHAPTER 6. BIBLIOGRAPHY

- [75] Buck, U.; Krohne, R. *J. Chem. Phys.* **1996**, *105*, 5408.
- [76] Bobbert, C.; Schütte, S.; Steinbach, C.; Buck, U. *Europ. Phys. J. D* **2002**, *19*, 183.
- [77] Schütte, S.; Buck, U. *Intern J. Mass Spectr.* **2002**, *220*, 183.
- [78] Farges, J.; de Feraudy, M. F.; Raoult, B.; Torchet, G. *Sur. Sci.* **1981**, *106*, 95.
- [79] Torchet, G.; Farges, J.; de Feraudy, M. F.; Raoult, B. In *The Chemical Physics of Atomic and Molecular Clusters*; Scoles, G., Ed.; North-Holland: Amsterdam, **1990**; page 513.
- [80] Torchet, G.; Schwartz, P.; Farges, J.; de Feraudy, M. F.; Raoult, B. *J. Chem. Phys.* **1983**, *79*, 6196.
- [81] Bruderemann, J.; Buck, U.; Buch, V. *J. Phys. Chem.* **2002**, *106*, 453.
- [82] private communication. Buck, U. **2007**.
- [83] Gough, T. E.; Mengel, M.; Rowntree, P. A.; Scoles, G. *J. Chem. Phys.* **1985**, *83*, 4958.
- [84] Behrens, M.; Fröchtenicht, R.; Hartmann, M.; Siebers, J. G.; Buck, U. *J. Chem. Phys.* **1999**, *111*, 2436.
- [85] Nahler, N. H.; Baumfalk, R.; Buck, U.; Vach, H.; Slavíček, P.; Jungwirth, P. *Phys. Chem. Chem. Phys.* **2003**, *5*, 3394.
- [86] Buck, U.; Meyer, H. *Phys. Rev. Lett.* **1984**, *52*, 109.
- [87] Buck, U.; Meyer, H. *J. Chem. Phys.* **1986**, *84*, 4854.
- [88] Buck, U. *J. Phys. Chem.* **1988**, *92*, 1023.
- [89] Steinbach, C.; Fárník, M.; Buck, U.; Brindle, C. A.; Janda, K. C. *J. Phys. Chem. A* **2006**, *110*, 9108.

CHAPTER 6. BIBLIOGRAPHY

- [90] Buck, U. In *Advances in Molecular Vibrations and Collision Dynamics*; Bowman, J. M., Bačić, Z., Eds.; JAI Press Inc.: Stanford, **1998**; page 127.
- [91] Buck, U.; Huisken, F. *Chem. Rev.* **2000**, *100*, 3863.
- [92] Fárník, M.; Weimann, M.; Steinbach, C.; Buck, U.; Borho, N.; Adler, T. B.; Suhm, M. A. *Phys. Chem. Chem. Phys.* **2006**, *8*, 1148–1158.
- [93] Poterya, V.; Fárník, M.; Buck, U.; Bonhommeau, D.; Halberstadt, N. *Int. J. Mass Spec.* **2009**, *280*, 78.
- [94] Janeček, I.; Cintavá, S.; Hrivňák, D.; Kalus, R.; Fárník, M.; Gadea, F. X. *J. Chem. Phys.* **2009**, *131*, 114306.
- [95] Peoux, G.; Monnerville, M.; Duhoo, T.; Pouilly, B. *J. Chem. Phys.* **1997**, *107*, 70.
- [96] Pouilly, B.; Monnerville, M. *Chem. Phys.* **1998**, *238*, 437.
- [97] Rakitzis, T. P.; Samartzis, P. C.; Toomes, R. L.; Kitsopoulos, T. N. *J. Chem. Phys.* **2004**, *121*, 7222.
- [98] Baumfalk, R.; Buck, U.; Frischkorn, C.; Nahler, N. H.; Hüwel, L. *J. Chem. Phys.* **1999**, *111*, 2595.
- [99] Baumfalk, R.; Nahler, N. H.; Buck, U.; Niv, M. Y.; Gerber, R. B. *J. Chem. Phys.* **2000**, *113*, 329.
- [100] Fárník, M.; Poterya, V.; Votava, O.; Ončák, M.; Slavíček, P.; Dauster, I.; Buck, U. *J. Phys. Chem. A* **2009**, *113*, 7322.
- [101] Zhong, Q.; Castleman, A. W. *Chem. Rev.* **2000**, *100*, 4039.
- [102] Slavíček, P.; Jungwirth, P.; Lewerenz, M.; Nahler, N. H.; Fárník, M.; Buck, U. *J. Chem. Phys.* **2004**, *120*, 4498.
- [103] Nahler, N. H.; Fárník, M.; Buck, U.; Vach, H.; Gerber, R. B. *J. Chem. Phys.* **2004**, *121*, 1293.

CHAPTER 6. BIBLIOGRAPHY

- [104] Fárník, M.; Nahler, N. H.; Buck, U.; Slavíček, P.; Jungwirth, P. *Chem. Phys.* **2005**, *315*, 161.
- [105] Schmidt, M.; Kusche, R.; von Issendorff, B.; Haberland, H. *Nature* **1998**, *393*, 238.
- [106] Slavíček, P.; Jungwirth, P.; Lewerenz, M.; Nahler, N. H.; Fárník, M.; Buck, U. *J. Phys. Chem. A* **2003**, *107*, 7743.
- [107] Baumfalk, R.; Nahler, N. H.; Buck, U. *Phys. Chem. Chem. Phys.* **2001**, *3*, 2372.
- [108] Sobolewski, A. L.; Domcke, W. *Phys. Chem. Chem. Phys.* **2002**, *4*, 4.
- [109] Sobolewski, A. L.; Domcke, W. *J. Phys. Chem. A* **2003**, *107*, 1557.
- [110] Sobolewski, A. L.; Domcke, W. *Phys. Chem. Chem. Phys.* **2005**, *7*, 970.
- [111] Sobolewski, A. L.; Domcke, W. *J. Chem. Phys.* **2005**, *122*, 184320.
- [112] Sobolewski, A. L.; Domcke, W. *Phys. Chem. Chem. Phys.* **2007**, *9*, 3818.
- [113] Nee, J. B.; Suto, M.; Lee, L. C. *J. Chem. Phys.* **1986**, *85*, 4919–4924.
- [114] Cheng, B. M.; Chung, C. Y.; Bahou, M.; Lee, Y. P.; Lee, L. C. *J. Chem. Phys.* **2002**, *117*, 4293–4298.
- [115] Ončák, M.; Slavíček, P.; Poterya, V.; Fárník, M.; Buck, U. *J. Phys. Chem. A* **2008**, *112*, 5344.
- [116] Poterya, V.; Fárník, M.; Slavíček, P.; Buck, U.; Kresin, V. V. *J. Chem. Phys.* **2007**, *126*, 071101.
- [117] Fárník, M.; Buck, U. *Phys. Scripta: Comm. At. Mol. Opt. Phys.* **2007**, *76*, 73.
- [118] Poterya, V.; Fárník, M.; Ončák, M.; Slavíček, P. *Phys. Chem. Chem. Phys.* **2008**, *10*, 4835.

CHAPTER 6. BIBLIOGRAPHY

- [119] Ashfold, M. N. R.; Cronin, B.; Devine, A. L.; Dixon, R. N.; Nix, M. G. D. *Science* **2006**, *312*, 1637–1640.
- [120] Devine, A. L.; Cronin, B.; Nix, M. G. D.; Ashfold, M. N. R. *J. Chem. Phys.* **2006**, *125*, 184302.
- [121] Schwell, M.; Jochims, H.-W.; Baumgärtel, H.; Leach, S. *Chem. Phys.* **2008**, *353*, 145.
- [122] Jagoda-Cwiklik, B.; Slavíček, P.; Cwiklik, L.; Nolting, D.; Winter, B.; Jungwirth, P. *J. Phys. Chem. A* **2008**, *112*, 3499.
- [123] Machado, F.; Davidson, E. *J. Chem. Phys.* **1992**, *97*, 1881.
- [124] Serrano-Andres, L.; Fulscher, M.; Roos, B.; Merchán, M. *J. Phys. Chem.* **1996**, *100*, 6484.
- [125] Su, M. D. *J. Phys. Chem. A* **2007**, *111*, 1567.
- [126] Barbatti, M.; Lischka, H.; Salzmann, S.; Marian, C. *J. Chem. Phys.* **2009**, *130*, 034305.
- [127] Poterya, V.; Profant, V.; Fárnik, M.; Slavíček, P.; Buck, U. *J. Chem. Phys.* **2007**, *127*, 064307.
- [128] Profant, V.; Poterya, V.; Fárnik, M.; Slavíček, P.; Buck, U. *J. Phys. Chem. A* **2007**, *111*, 12477.
- [129] Poterya, V.; Tkáč, O.; Fedor, J.; Fárnik, M.; Slavíček, P.; Buck, U. *Int. J. Mass Spec.* **2010**, *2010*, 85.
- [130] Rubio-Lago, L.; Zaouris, D.; Sakellariou, Y.; Sofikitis, D.; Kitsopoulos, T. N.; Wang, F.; Yang, X.; Cronin, B.; Devine, A. L.; King, G. A.; Nix, M. G. D.; Ashfold, M. N. R. *J. Chem. Phys.* **2007**, *127*, 064306.
- [131] Lipciuc, M. L.; Wang, F.; Yang, X.; Kitsopoulos, T. N.; Fanourgakis, G. S.; Xantheas, S. S. *Chem. Phys. Chem.* **2008**, *9*, 1838.
- [132] Poterya, V.; Profant, V.; Fárnik, M.; Šišťík, L.; Slavíček, P.; Buck, U. *J. Phys. Chem. A* **2009**, *113*, 14583.

CHAPTER 6. BIBLIOGRAPHY

- [133] Buck, U.; Fárník, M. *Int. Rev. Phys. Chem.* **2006**, *25*, 583.
- [134] Slavíček, P.; Ončák, M.; Poterya, V.; Fárník, M. *Chem. Listy* **2008**, *102*, 467.
- [135] Friedrich, B.; Herschbach, D. *J. Phys. Chem. A* **1999**, *103*, 10280.
- [136] Friedrich, B.; Herschbach, D. *J. Chem. Phys.* **1999**, *111*, 6157.
- [137] Khriachtchev, L.; Pettersson, M.; Runeberg, N.; Lundell, J.; Räsänen, M. *Nature* **2000**, *406*, 874.
- [138] Kumar, A.; Kolaski, M.; Kim, K. *J. Chem. Phys.* **2008**, *128*, 034304.
- [139] David, O.; Dedonder-Lardeux, C.; Jouvét, C.; Kang, H.; Martrenchard, S.; Ebata, T.; Sobolewski, A. *J. Chem. Phys.* **2004**, *120*, 10101.
- [140] David, O.; Dedonder-Lardeux, C.; Jouvét, C. *Int. Rev. Phys. Chem.* **2002**, *21*, 499.
- [141] Carrera, A.; Nielsen, I. B.; Carcabal, P.; Dedonder, C.; Broquier, M.; Jouvét, C.; Domcke, W.; Sobolewski, A. L. *J. Chem. Phys.* **2009**, *130*, 024302.
- [142] Frutos, L.; Markmann, A.; Sobolewski, A.; Domcke, W. *J. Phys. Chem. B* **2007**, *111*, 6110–6112.
- [143] Sanche, L. *Nature* **2009**, *461*, 358.
- [144] Whitaker, B. *Imaging in Molecular Dynamics*; Cambridge University Press: Cambridge, **2003**.

Appendix A

List of abbreviations

CCD	Charge-coupled device (camera)
CFC	Chlorofluorocarbon, freon
CI	Conical intersection
CICR	Cluster isolated chemical reaction
CM	Center-of-mass (system)
CTTS	Charge-transfer-to-solvent (electronic band)
FT	Fourier transformation
FTIR	Fourier transformation infrared (spectroscopy)
FWHM	Full width at half maximum
IR	Infrared (radiation, laser, etc.)
KED	Kinetic energy distribution
LAB	Laboratory (system, angle, etc.)
MC	Monte-Carlo (simulation)
PES	Potential energy surface
PSC	Polar stratospheric cloud
REMPI	Resonance-enhanced multiphoton ionization
SFM	Sum frequency mixing
SHG	Second harmonic generation
TFP	Thin film polarizer
TOF	Time-of-flight (spectrometer, spectrum, etc.)
UV	Ultraviolet (radiation, laser, etc.)
WMTOF	Time-of-flight spectrometer of Wiley-McLaren type

Appendix B

Thesis publications

4.1 Photodissociation of hydrogen halides in rare gas clusters

1. Slavíček, P.; Jungwirth, P.; Lewerenz, M.; Nahler, N. H.; Fárník, M.; Buck, U.: *Photodissociation of hydrogen iodide on the surface of large argon clusters: The orientation of the librational wave function and the scattering from the cluster cage*
J. Chem. Phys. **2004**, *120*, 4498 – 4511.
2. Nahler, N. H.; Fárník, M.; Buck, U.; Vach, H.; Gerber, R. B.: *Photodissociation of HCl and small (HCl)_m complexes in and on large Ar_n clusters*
J. Chem. Phys. **2004**, *121*, 1293 – 1302.
3. Fárník, M.; Nahler, N. H.; Buck, U.; Slavíček, P.; Jungwirth, P.: *Photodissociation of HBr on the surface of Ar_n clusters at 193 nm*
Chem. Phys. **2005**, *315*, 161 – 170.
4. Slavíček, P.; Jungwirth, P.; Lewerenz, M.; Nahler, N. H.; Fárník, M.; Buck, U.: *Pickup and Photodissociation of Hydrogen Halides in Floppy Neon Clusters*
J. Phys. Chem. A **2003**, *107*, 7743 – 7754.

4.2 Atmospherically relevant clusters

5. Fárník, M.; Buck, U.: *Photodissociation of HBr molecules in clusters:*

APPENDIX B. THESIS PUBLICATIONS

from rare gas clusters to water nanoparticles

Phys. Scripta: Comm. At. Mol. Opt. Phys. **2007**, 76, 73 – 78.

6. Poterya, V.; Fárník, M.; Slavíček, P.; Buck, U.; Kresin, V. V.: *Photodissociation of hydrogen halide molecules on free ice nanoparticles*
J. Chem. Phys. **2007**, 126, 071101.
7. Ončák, M.; Slavíček, P.; Poterya, V.; Fárník, M.; Buck, U.: *Emergence of charge-transfer-to-solvent band in the absorption spectra of hydrogen halides on ice nanoparticles: spectroscopic evidence for acidic dissociation*
J. Phys. Chem. A **2008**, 112, 5344–5353.
8. Poterya, V.; Fárník, M.; Ončák, M.; Slavíček, P.: *Water photodissociation in free ice nanoparticles at 243 nm and 193 nm*
Phys. Chem. Chem. Phys. **2008**, 10, 4835 – 4842.

4.3 Biomolecules in clusters

9. Poterya, V.; Profant, V.; Fárník, M.; Slavíček, P.; Buck, U.: *Experimental and theoretical study of the pyrrole clusters photochemistry: Closing the $\pi\sigma^*$ dissociation pathway by complexation*
J. Chem. Phys. **2007**, 127, 064307.
10. Profant, V.; Poterya, V.; Fárník, M.; Slavíček, P.; Buck, U.: *Fragmentation dynamics of size selected pyrrole clusters prepared by electron impact ionization*
J. Phys. Chem. A **2007**, 111, 12477 – 12486.
11. Poterya, V.; Profant, V.; Fárník, M.; Šišťík, L.; Slavíček, P.; Buck, U.: *Photoinduced Processes in Hydrogen Bonded System: Photodissociation of Imidazole Clusters*
J. Phys. Chem. A **2009**, 113, 14583 – 14590.
12. Poterya, V.; Tkáč, O.; Fedor, J.; Fárník, M.; Slavíček, P.; Buck, U.: *Mass spectrometry of hydrogen bonded clusters of heterocyclic molecules: Electron ionization vs. photoionization*
Int. J. Mass Spec. **290**, 2010, 85 – 93.

APPENDIX B. THESIS PUBLICATIONS

4.4 Novel rare gas molecules

13. Nahler, N. H.; Fárník, M.; Buck, U.: *Search for oriented HXeX molecules from the photolysis of HCl and HBr in xenon clusters*
Chem. Phys. **2004**, *301*, 173 – 183.
14. Buck, U.; Fárník, M.: *Oriented xenon hydride molecules in the gas phase*
Int. Rev. Phys. Chem. **2006**, *25*, 583 – 612.
15. Poterya, V.; Votava, O.; Fárník, M.; Ončák, M.; Slavíček, P.; Buck, U.; Friedrich, B.: *Generation and orientation of organoxenon molecule H-Xe-CCH in the gas phase*
J. Chem. Phys. **2008**, *128*, 104313.
16. Slavíček, P.; Ončák, M.; Poterya, V.; Fárník, M.: *Syntéza v létajících nanoreaktorech: Hydridy vzácných plynů*
Chem. Listy **2008**, *102*, 467 – 473.

Statement about the authorship of the presented publications: The research covered in this thesis represents a very complex, demanding and complicated experiment accompanied by theoretical interpretations based on state-of-the-art calculations. Therefore the presented publications resulted from the collaboration of several coauthors, and usually independent experimental and a theoretical groups were involved. However, it should be noted that in the majority of the presented publications the contribution of the author of these Thesis was pivotal. In most cases the author was responsible for making the experimental proposal, measuring and evaluating the experimental data, he was strongly involved in the experimental interpretations, and finally responsible for writing the publications themselves. This is reflected by the fact that he was the corresponding author of 8 publications and the lead author of further 2 publications from the 16 publications covered in this thesis. His role in the remaining 6 publications was also essential. This is further detailed in a separate document submitted with the application and signed by the coauthors.



Michal Fárník received his PhD at the Faculty of Mathematics and Physics, Charles University in Prague in 1995 studying experimentally ion molecular reactions in crossed molecular beams at the J. Heyrovský Institute of Physical Chemistry. He was awarded the Alexander von Humboldt postdoctoral Fellowship and spent three years 1995-98 at the MPI für Strömungsforschung in Göttingen, Germany studying large helium clusters (He-nanodroplets). In 1998 he moved to JILA in Boulder, Colorado, USA, where he studied vibrational spectroscopy and dynamics of small molecular cluster and ionic species. In 2002 he moved back to Göttingen to work on spectroscopy, dynamics and photodissociation of various molecular clusters at MPI and Göttingen University.

In 2005 he received J. E. Purkyně Fellowship of ASCR and returned back to the J. Heyrovský Institute of Physical Chemistry in Prague. From Göttingen he brought to Prague a unique experimental apparatus for investigation of clusters and nanoparticles in molecular beams in vacuum. He has founded a new "*Molecular and Cluster Dynamics Group*" around this experiment.

<http://www.jh-inst.cas.cz/~farnik/>

"...the monograph represents a nice introduction into the molecular beam methods ... the issue of physics and chemistry in molecular clusters is introduced to the reader in a lucid and didactic way ... I have read the monograph with interest and attention ... the text has a high scientific level and is written in a readable way..."

*Prof. RNDr. Petr Klán, Ph.D.,
Masaryk University, Brno*

"I consider the dissertation to be a nicely written monograph ... it is well arranged and neat work which is a pleasure to read ... the author has chosen English as the dissertation language and mastered it excellently..."

*RNDr. Zdeněk Havlas, DrSc.,
ÚOCH AV ČR, Praha*

